THEORY OF ALKALI HALIDES CONTAINING H^- IONS

OPTICAL ABSORPTION SPECTRA
IN
THE THEORY OF ALKALI HALIDES CONTAINING H^- IONS

By

TREVOR GETHINS, B.Sc.

A Thesis

Submitted to the Faculty of Graduate Studies

in Partial Fulfilment of the Requirements

for the Degree

Doctor of Philosophy

McMaster University

October 1968

DOCTOR OF PHILOSOPHY (1968) McMASTER UNIVERSITY
(Physics) Hamilton, Ontario.

TITLE: Optical Absorption Spectra in the Theory of Alkali Halides containing H^- ions

AUTHOR: Trevor Gethins, B.Sc.
(University of Birmingham, England)

SUPERVISOR: Professor E. J. Woll, Jr.

NUMBER OF PAGES: v, 111

SCOPE AND CONTENTS:

Optical absorption spectra of alkali halide crystals containing H^- ions (U-centres) are calculated using a two-parameter model to describe the defect. It is shown that this model gives a satisfactory account of the observed anharmonic sideband of the main U-centre absorption band in the infrared, and also of the impurity-induced far infrared absorption for the two host crystals considered, potassium bromide and potassium iodide. The broadening of localized modes and resonances is also discussed. In particular, the anharmonic broadening is calculated for the main U-centre line in KI and KBr and for a localized gap mode in KI:KH.

ACKNOWLEDGEMENTS

It is a pleasure to thank Dr. E. J. Woll for supervising this work. His many suggestions have always proved useful while his willingness to discuss every aspect of the problem has been invaluable in developing the physical ideas presented here. Furthermore, the enthusiasm which he has shown throughout has always been a source of encouragement for which I am grateful.

I should also like to thank Dr. T. Timusk for introducing Dr. Woll and myself to this problem. He has kept us constantly informed of experimental developments in the field and taken an active interest in their theoretical explanation.

I am indebted to McMaster University for giving me the opportunity to study in Canada and to the Ontario Government and the National Research Council of Canada for financial support.

My thanks go also to Miss C. Wivell for typing the final draft of this manuscript so efficiently and conscientiously.

Finally, I should like to thank my wife both for her continual encouragement and for typing a rough draft of this thesis.

TABLE OF CONTENTS

LIST OF TABLES

CHAPTER 1

INTRODUCTION

The possibility that lattice defects can lead to the appearance of vibrational modes whose frequency lies outside the continuous frequency spectrum of the perfect crystal was first discussed by Lifshitz (1943, 1944). He formulated the theoretical problem of calculating the properties (for example, the density of vibrational states) of the lattice with defects in such a way that its solution did not require that the size of the perturbation be small in the usual sense, but that it be localized in space. This formulation was therefore particularly suited to the theoretical study of crystal lattices containing a single defect, and the conditions governing the occurrence of localized modes of vibration associated with such a defect had been considered in detail before such a mode had been seen experimentally (Montroll and Potts 55; Maradudin et al. 58; Domb et al. 59). The first experimental evidence for localized modes was reported by Schaefer (1960). He observed an absorption band in the infrared spectra of alkali halides containing U-centres, which are negative hydrogen ion impurities substituted for halide ions of the

perfect crystal. The presence of such an absorption band was explained by Rosenstock and Klick (1960) and also by Wallis and Maradudin (1960). These workers showed that as a consequence of its light mass, the hydrogen ion impurity gives rise to a high frequency, localized vibrational mode which is optically active. Essentially only the hydrogen ion moves in this mode, which is often referred to as the "U-centre localized mode".

A description of the dynamics of the perfect host crystal is needed before the local mode frequency can be predicted theoretically. Early calculations employed a nearest neighbour force constant model to do this, and were able to explain the observed local mode frequency using the mass change as the only perturbation of the host crystal resulting from the impurity (Wallis and Maradudin 60; Takeno et al. 62). Similar calculations were subsequently carried out using models to describe the perfect crystal which take into account the long range electrostatic forces, as indeed a realistic model must. These were performed by Jaswal and Montgomery (1964) using the rigid-ion and deformation-dipole models, by Fieschi et al. (1965) using the shell model, and by Page and Strauch (1967) using the "breathing" shell model. In each case, the authors found that the predicted local mode frequency is in poor agreement with experiment unless a considerable decrease in the

central force constant connecting the H^- ion to its nearest neighbours, as well as the mass change, is included in the perturbation.

In addition to the main U-centre line, which corresponds to the creation of a single U-centre local mode phonon, Schaefer (1960) also observed sidebands corresponding to the creation of a local mode phonon plus a lattice phonon, which have since been studied in more detail by several workers (Brada and Mitra 64; Dötsch et al. 65; Fritz 65; Fritz et al. 65; Timusk and Klein 66). The existence of sidebands can be attributed to the anharmonic coupling of the local mode to other vibrational modes of the crystal, with the cubic anharmonic terms dominating (Fritz 65; Elliott et al. 65; Timusk and Klein 66; Nguyen 66; Bilz et al. 66). An alternative mechanism, requiring the second-order electric dipole interaction, has been considered in detail by Nguyen (1966, 1968) and by Page and Dick (1968), who conclude that the anharmonic interaction dominates.

The leading anharmonic terms giving rise to sideband contributions contain only the coordinates of the hydrogen ion and its nearest neighbours. By calculating with a simple form for this anharmonic interaction, Timusk and Klein (1966) were able to show that, as a consequence of the highly localized nature of the coupling, the sideband lineshape depends only on the vibrational spectra of

ions in the defect area. Therefore it is very important that perturbations caused by the presence of the impurity, both the mass change and force constant changes, be carefully taken into account in the calculation. They evaluated the decrease in the hydrogen ion-nearest neighbour force constant needed to predict the correct U-centre local mode frequency, and used this value in their calculation of the sideband lineshape. Their model leads to reasonable overall agreement with experiment. However, in the particular cases of KBr and KI, certain peaks in the sideband are predicted at very different frequencies from those observed experimentally. These peaks are interpreted as arising from the interaction of the H^- ion with vibrational modes in which the amplitudes of its nearest neighbours are large. Such modes are called resonances. Gethins et al. (1967) extended the model to include a force constant change between the first and fourth neighbours of the H^- ion. They showed that a decrease in this force constant reduced the frequencies of the resonances in the sideband, considerably improving agreement with experiment. In that calculation, the anharmonic coupling chosen by Timusk and Klein (1966) was again used.

Recently Kühner and Wagner (1968) have done a calculation similar to that of Gethins et al. (1967), using a more complete anharmonic coupling. Their results show

that this can also improve the agreement. However, these authors found it necessary to assign arbitrary values to the ratios of the anharmonic coupling constants involved. In chapter 4 of this work, less arbitrary procedures for evaluating these ratios are suggested and are used in a detailed calculation of the sideband lineshape.

The introduction of an impurity ion into a crystal also induces optical absorption in the far infrared, which has been studied experimentally by Sievers (1965) and by Timusk et al. (1968). This problem has been theoretically investigated by many authors (Lifshitz 43, 44; Dawber and Elliott 63a, 63b; Maradudin 63, 64a, 66; Rebane et al. 64; Benedek and Nardelli 67; Patnaik and Mahanty 67; Martin 67; Takeno 68; Timusk et al. 68; Woll et al. 68). The presence of the impurity removes the translational symmetry of the lattice. This lifts the requirement that the phonon and photon have the same wavelengths and allows all modes of appropriate point symmetry with respect to the defect site to contribute to the absorption. Therefore, in addition to the strong reststrahlen absorption characteristic of pure alkali halides, when U-centres are present absorption can also occur at other frequencies. This absorption can show considerable structure; for instance, resonances similar to those appearing in the sideband can occur. These have been interpreted by Woll et al.

(1968) as being due to absorption by optically active modes which have large amplitudes near the defect.

In his original work, Schaefer (1960) also studied the temperature dependence of the width of the U-centre local mode peak. This study has since been extended by Mirlin and Reshina (1964), by Fritz et al. (1965) and by Bauerle and Fritz (1967). It is found that the line has a small, non-zero width at very low temperatures, which increases with temperature. The residual width at zero temperature can be understood in terms of the possibility of anharmonic decay of the local mode phonon into lattice phonons (Elliott et al. 65). At non-zero temperatures it is necessary to consider a second anharmonic mechanism, in which thermally excited lattice phonons are scattered by the local mode phonon, as shown by Elliott et al. (1965), by Ivanov et al. (1966) and by Ipatova and Klotchichin (1966). These authors came to the conclusion that the "scattering" mechanism does in fact dominate the "decay" mechanism at high temperatures in many cases.

Although the qualitative aspects of this problem are well understood, apart from the work of Elliott et al. (1965) on CaF_2 containing H^- ions, almost no numerical estimates of the linewidths of U-centre local mode phonons have been made. This is probably due to the lack of information on the values of the anharmonic constants near

the impurity and the need to know the detailed vibrational spectra of ions in the defect area.

In the present work, the various properties described above for alkali halides containing U-centres are treated theoretically, using a model of the defect containing two parameters. This model was originally applied to calculation of the sideband spectrum for KI and KBr (Gethins et al. 67). It is shown that this model leads to a satisfactory explanation of the far infrared absorption as well as the sideband spectra, which implies that it provides an adequate description of the dynamics of ions near the defect. For this reason, the model is also applied to the calculation of the broadening of the main U-centre line for KI and KBr. In addition, the model is applied to calculation of the broadening of an A_{1g} symmetry mode which happens to be localized in the case of KI. This mode lies in the band gap of the KI crystal containing U-centres, and gives rise to a strong peak in the sideband spectrum.

In chapter 2, the Green's function treatment of the harmonic lattice containing a point defect is reviewed and the theory of thermodynamic Green's functions is presented in a form which is convenient for the problems under consideration. In chapter 3, the theoretical model used for the U-centre is described. In chapter 4, the

techniques and model are applied to the calculation of the sideband lineshape and in chapter 5 to the calculation of the far infrared absorption spectrum. In chapter 6, the anharmonic broadening of modes is considered. The broadening of the localized gap mode in KI:KH is calculated first, followed by calculation of the broadening of the main U-centre local mode peak. The application of similar techniques to anharmonic broadening of sharp resonances observed in the sideband and far infrared spectra is also discussed.

CHAPTER 2

GENERAL FORMALISM

A. THE PERFECT LATTICE

The vibration Hamiltonian H_o for an alkali halide crystal in the harmonic approximation can be written (Maradudin 63)

$$H_o = \frac{1}{2} \sum_{\underline{L}\alpha\kappa} M_\kappa \dot{x}_{\underline{L}}^{\alpha\kappa 2} + \frac{1}{2} \sum_{\substack{\underline{L}\alpha\kappa \\ \underline{L}'\alpha'\kappa'}} \Phi_{\underline{L},\underline{L}'}^{\alpha\kappa,\alpha'\kappa'} x_{\underline{L}}^{\alpha\kappa} x_{\underline{L}'}^{\alpha'\kappa'} \quad , \qquad (1)$$

where $x_{\underline{L}}^{\alpha\kappa}$ is the displacement from equilibrium of the ion on the site at position $\underline{L}$ in the α-direction and $\dot{x}_{\underline{L}}^{\alpha\kappa}$ is its time derivative. The label κ indicates the type of ion on site $\underline{L}$ and M_κ is its mass (κ = + and κ = -, indicating alkali and halide ions, respectively). $\Phi_{\underline{L},\underline{L}'}^{\alpha\kappa,\alpha'\kappa'}$ is the interionic force constant defined by

$$\Phi_{\underline{L},\underline{L}'}^{\alpha\kappa,\alpha'\kappa'} = \left(\frac{\partial^2 V}{\partial x_{\underline{L}}^{\alpha\kappa} \, \partial x_{\underline{L}'}^{\alpha'\kappa'}} \right)_{\underline{x} = 0} \quad . \qquad (2)$$

Here V is the potential energy of the crystal and the condition $\underline{x} = 0$ indicates that the second derivative is to be evaluated with every ion at its equilibrium position. Assuming a cyclic boundary condition for the displacements

and making the substitution

$$x_{\underline{L}}^{\alpha\kappa} = u_{\underline{L}}^{\alpha\kappa} \, e^{-i\omega t}/\sqrt{M_\kappa} \quad , \qquad (3)$$

where ω is the frequency of vibration and $u_{\underline{L}}^{\alpha\kappa}$ is a time-independent amplitude, the equation of motion for the $\underline{L}$ th ion can be reduced to the form (Maradudin 63)

$$\sum_{\underline{L}'\alpha'\kappa'} \left(\frac{\Phi_{\underline{L},\underline{L}'}^{\alpha\kappa,\alpha'\kappa'}}{\sqrt{M_\kappa \, M_{\kappa'}}} - \omega^2 \, \delta_{\underline{L},\underline{L}'} \, \delta_{\alpha,\alpha'} \, \delta_{\kappa,\kappa'} \right) u_{\underline{L}'}^{\alpha'\kappa'} = 0 \quad . \qquad (4)$$

Defining

$$A_{\underline{L},\underline{L}'}^{\alpha\kappa,\alpha'\kappa'} = \frac{\Phi_{\underline{L},\underline{L}'}^{\alpha\kappa,\alpha'\kappa'}}{\sqrt{M_\kappa \, M_{\kappa'}}} \qquad (5)$$

enables the equations of motion for all $\underline{L}$ to be combined into the matrix equation

$$(A - \omega^2 I)u = 0 \quad , \qquad (6)$$

where I is the unit matrix. The matrix A, for a crystal containing 2N ions, is diagonalized by making a unitary transformation, using the matrix U, whose elements are

$$U_{\underline{L}\alpha\kappa,\underline{k}j} = \frac{1}{\sqrt{N}} \, \varepsilon_\alpha^\kappa(\underline{k}j) e^{i\underline{k}\cdot\underline{L}} \quad , \qquad (7)$$

to the representation of plane waves denoted by $\underline{k}$ and j. The index j labels the six normal modes of vibration which correspond to each value of the wave vector $\underline{k}$ and which have characteristic frequencies $\omega_{\underline{k}j}$. $\underline{\varepsilon}(\underline{k}j)$ is an eigenvector whose elements $\varepsilon_\alpha^\kappa(\underline{k}j)$ give the relative vibrational amplitudes

of the two types of ion in the three Cartesian directions for the $(\underline{k}j)$th normal mode.

The Green's function matrix for the perfect crystal, $G(\omega^2)$, is defined by the equation

$$(A - \omega^2 I)\, G(\omega^2) = I \quad . \qquad (8)$$

In the $\{\underline{k}j\}$-representation, A is diagonal with elements $\omega_{\underline{k}j}{}^2$, and therefore in this representation the elements of G are

$$G(\omega^2;\underline{k}j,\underline{k}'j') = \frac{\delta_{\underline{k},\underline{k}'}\,\delta_{j,j'}}{\omega_{\underline{k}j}^2 - \omega^2} \equiv G(\omega^2;\underline{k}j) \quad . \qquad (9)$$

The normalized density of states for the crystal, defined by

$$\rho(\omega) = \frac{1}{6N} \sum_{\underline{k}j} \delta(\omega_{\underline{k}j} - \omega) \quad , \qquad (10)$$

can be written in terms of the Green's function matrix elements as

$$\rho(\omega) = \frac{2\omega}{\pi} \sum_{\underline{k}j} \mathrm{Im}\,\{G(\omega^2 + i0^+;\underline{k}j)\} \qquad (11)$$

using equation (9) and well-known properties of the Dirac δ-function. The small positive quantity 0^+ is needed to specify the sign of the imaginary part required in equation (11).

B. THE HARMONIC LATTICE CONTAINING A SUBSTITUTIONAL IMPURITY

The changes in mass and force constants caused by

the substitution of a single impurity into the crystal can be taken into account by replacing the matrix A in equation (8) by the matrix $\bar{A}$ given by

$$\bar{A}(\omega^2) = A + \Gamma(\omega^2) \quad . \tag{12}$$

The elements of Γ, the change in dynamical matrix, are defined in the $\{\underline{L}\alpha\kappa\}$-representation by

$$\frac{\Gamma^{\alpha\kappa,\alpha'\kappa'}_{\underline{L},\underline{L}'}(\omega^2)}{(M_\kappa M_{\kappa'})^{-1/2}} = \left(\frac{\partial^2 \Delta V}{\partial u^{\alpha\kappa}_{\underline{L}} \, \partial u^{\alpha'\kappa'}_{\underline{L}'}}\right)_{\underline{u}=0} + \lambda\omega^2 \delta_{\underline{L},0}\delta_{\underline{L},\underline{L}'}\delta_{\alpha,\alpha'}\delta_{\kappa,-}\delta_{\kappa,\kappa'} \tag{13}$$

where the impurity has been taken at a negative ion site which has also been chosen as the origin of coordinates. ΔV is the change in potential energy of the crystal resulting from force constant changes; the mass change has been taken into account explicitly by the term proportional to λ, given by

$$\lambda = (M_- - M_I) \; / \; M_- \tag{14}$$

where M_I is the mass of the impurity. The equation of motion for the perturbed harmonic crystal is therefore

$$(\bar{A}(\omega^2) - \omega^2 I)u = 0 \quad . \tag{15}$$

The elements of the vector u are again defined by equation (3); that is, in terms of the masses of the unperturbed crystal.

The perturbed Green's function matrix $\bar{G}(\omega^2)$ is

defined in the $\{\underline{L}\alpha\kappa\}$-representation by

$$\bar{G}(\omega^2;\underline{L}\alpha\kappa,\underline{L}'\alpha'\kappa') = (\bar{A}(\omega^2) - \omega^2 I)^{-1}_{\underline{L}\alpha\kappa,\underline{L}'\alpha'\kappa'} \quad . \qquad (16)$$

$\bar{G}$ is diagonal in the representation of perturbed phonons labelled by p (perturbed) and has elements

$$\bar{G}(\omega^2;p,p') = \frac{\delta_{p,p'}}{\omega_p^2 - \omega^2}$$

$$\equiv \bar{G}(\omega^2;p) \quad , \qquad (17)$$

where ω_p is the frequency of phonon p.

It is not possible to give a useful general expression for the elements $U_{\underline{L}\alpha\kappa,p}$ of the transformation matrix from the position to the perturbed phonon representation. However, in the particular case of the U-centre, elements corresponding to the local mode phonon are particularly simple since it can be assumed that only the H^- ion moves (Kagan and Iosilevskii 63). The local mode frequency Ω is then determined by a single element of the dynamical matrix and it follows from equation (16) that

$$\bar{G}(\omega^2;\underline{0}\alpha-,\underline{0}\alpha-) = (\bar{A}^{\alpha-,\alpha-}_{\underline{0},\underline{0}}(\omega^2)-\omega^2)^{-1} \quad . \qquad (18)$$

Using equations (12) and (13) with equation (17) gives

$$\bar{G}(\omega^2;\underline{0}\alpha-,\underline{0}\alpha-) = \frac{M_-}{M_H} \cdot \frac{1}{\Omega^2 - \omega^2}$$

$$= \frac{M_-}{M_H} \cdot \bar{G}(\omega^2;P_\alpha) \quad , \qquad (19)$$

where P_α labels the local mode phonon polarized in the

direction α. M_I has been set equal to the H^- ion mass M_H, and Ω^2 is given by

$$\Omega^2 = \frac{M_-}{M_H}\left[A^{\alpha-,\alpha-}_{\underline{0},\underline{0}} + \left(\frac{\partial^2 \Delta V}{\partial u^{\alpha-}_{\underline{0}} \partial u^{\alpha-}_{\underline{0}}} \right)_{\underline{u} = 0} \right] . \qquad (20)$$

It follows from equation (19) that

$$U_{\underline{0}\alpha-,P_\alpha} = \sqrt{\frac{M_-}{M_H}} \quad . \qquad (21)$$

$\overline{G}(\omega^2)$ can be written in terms of $G(\omega^2)$ using equation (16) with equations (8) and (12). The result is the Dyson equation

$$\begin{aligned} \overline{G} &= (I + G\Gamma)^{-1} G \\ &= G - G\Gamma G + G\Gamma G\Gamma G - .... \end{aligned} \quad . \qquad (22)$$

Defining the T-matrix (Klein 63) by

$$\begin{aligned} T &= \Gamma(I + G\Gamma)^{-1} \\ &= \Gamma - \Gamma G\Gamma + \Gamma G\Gamma G\Gamma - .... \end{aligned} \quad , \qquad (23)$$

equation (22) can be rewritten

$$\overline{G} = G - GTG \quad . \qquad (24)$$

Equations (22) and (24) are the two forms for $\overline{G}$ most suited to taking full advantage of the space localization of the perturbation described by Γ. In particular, the expression (22) will be useful when only elements of $\overline{G}$ are required which correspond to the vicinity of the impurity, while the expression (24) will be used when other elements of $\overline{G}$ are required.

C. ANHARMONIC EFFECTS IN THE PERTURBED LATTICE

The complete vibrational Hamiltonian H for a lattice containing a mass defect can be written

$$H = H_o + H_{imp} + H_A$$
$$\equiv H_o' + H_A \qquad (25)$$

where H_{imp} is the correction to H_o, defined in equation (1), resulting from the addition of the impurity. Their sum, H_o', is thus the Hamiltonian for the perturbed lattice in the harmonic approximation. H_A consists of the anharmonic terms in the crystal potential and will be treated as a perturbation to H_o'. This is conveniently done using the method of thermodynamic Green's functions (Kadanoff and Baym 62) as discussed by Maradudin and Fein (1962) and by Cowley (1963) , who consider anharmonic effects in the perfect lattice. A slightly modified form of the theory given by Maradudin (1963) will be used here.

The phonon thermodynamic Green's function of the variable $v = it/\hbar$ is defined by

$$G^A(v;\underline{L}\alpha\kappa,\underline{L}'\alpha'\kappa') = \langle T\, u_{\underline{L}}^{\alpha\kappa}(v)\, u_{\underline{L}'}^{\alpha'\kappa'}(0)\rangle_H$$
$$= \frac{1}{Z}\,\text{trace}\,(e^{-\beta H}\{T\, u_{\underline{L}}^{\alpha\kappa}(v)\, u_{\underline{L}'}^{\alpha'\kappa'}(0)\}) \qquad (26)$$

where $u_{\underline{L}}^{\alpha\kappa}(v)$ is the Heisenberg operator defined by

$$u_{\underline{L}}^{\alpha\kappa}(v) = e^{vH}\, u_{\underline{L}}^{\alpha\kappa}(0)\, e^{-vH} \quad . \qquad (27)$$

Z is the crystal's partition function and β is $1/k_B T$ where k_B is Boltzmann's constant and T is the absolute temperature. The superscript A simply indicates that this Green's function includes anharmonic effects, and the time-ordering operator T orders the operators which follow it so that their arguments decrease from left to right. An expression such as that in equation (26) can be evaluated by exploiting the similarity between the dependence on temperature and that on complex time (Alekseev 61; Kadanoff and Baym 62). In fact, using the cyclic property of the trace, equation (26) can be rearranged to show that $G^A(v)$ is periodic along the v-axis (in the direction of complex time) with period β. This suggests expanding G^A in a Fourier series:

$$G^A(v;\underline{L}\alpha\kappa,\underline{L}'\alpha'\kappa') = \frac{1}{\beta} \sum_{\ell=-\infty}^{\infty} G_\ell^A(\underline{L}\alpha\kappa,\underline{L}'\alpha'\kappa') e^{2\pi i \ell v/\beta} \qquad (28)$$

where

$$G_\ell^A(\underline{L}\alpha\kappa,\underline{L}'\alpha'\kappa') = \int_0^\beta G^A(v;\underline{L}\alpha\kappa,\underline{L}'\alpha'\kappa') e^{-2\pi i \ell v/\beta} dv \quad . \qquad (29)$$

Before proceding with the perturbation theory which enables the Fourier coefficients defined in equation (29) to be calculated, it is worthwhile to clarify their importance

in the theory of optical absorption. The (x,x)-component of the optical absorption constant at frequency ω can be written (Maradudin 63)

$$\alpha_{xx}(\omega) = - \frac{8\pi}{\hbar V c} \cdot \frac{\omega}{\eta(\omega)} \cdot \mathrm{Im} \int_0^\infty e^{-0^+ t} \cdot \sin \omega t \cdot \langle M_x(t) M_x(0) \rangle_H dt \tag{30}$$

where V is the crystal's volume, $\eta(\omega)$ its refractive index and c is the velocity of light. The x-component of the crystal's electric dipole moment, $M_x(t)$, is given by

$$M_x(t) = \sum_{\underline{L}} \frac{e_\kappa}{\sqrt{M_\kappa}} \cdot u_{\underline{L}}^{x\kappa}(t) \tag{31}$$

where e_κ is the charge on the κ th ion. Using equations (26), (28) and (30), together with results derived by Maradudin and Fein (1962), the absorption constant can be rewritten

$$\alpha_{xx}(\omega) = \frac{4\pi\omega}{Vc\eta(\omega)} \sum_{\substack{\underline{L}\kappa \\ \underline{L}'\kappa'}} \frac{e_\kappa e_{\kappa'}}{\sqrt{M_\kappa M_{\kappa'}}} \mathrm{Im}\{G^A(\omega + i0^+; \underline{L}x\kappa, \underline{L}'x'\kappa')\} \tag{32}$$

where $G^A(\omega; \underline{L}x\kappa, \underline{L}'x'\kappa')$ is obtained from $G_\ell^A(\underline{L}x\kappa, \underline{L}'x'\kappa')$ by making the transition to the continuous variable ω using the identification (Maradudin and Fein 62)

$$\frac{2\pi i \ell}{\beta\hbar} \equiv i\omega_\ell = \omega \quad . \tag{33}$$

The problem is thus essentially solved when the Fourier coefficients G_ℓ^A have been determined.

Starting from equation (26), the thermodynamic Green's

function can be written (Matsubara 55)

$$G^A(v;\underline{L}\alpha\kappa,\underline{L}'\alpha'\kappa') = \langle T\ \tilde{u}^{\alpha\kappa}_{\underline{L}}(v)\ \tilde{u}^{\alpha'\kappa'}_{\underline{L}'}(0)\ \sum_{n=0}^{\infty} \frac{(-1)^n}{n!} \quad x$$

$$x \int_0^\beta \cdots \int_0^\beta dv_1 \cdots dv_n\ \tilde{H}_A(v_1) \cdots \tilde{H}_A(v_n) \rangle_{H'_o} \tag{34}$$

where $\tilde{O}(v)$ is an operator in the interaction represention,

$$\tilde{O}(v) = e^{vH'_o}\ O(0)\ e^{-vH'_o} \quad . \tag{35}$$

The n = 0 term in equation (34) is the harmonic Green's function defined by

$$\bar{G}(v;\underline{L}\alpha\kappa,\underline{L}'\alpha'\kappa') = \langle T\ \tilde{u}^{\alpha\kappa}_{\underline{L}}(v)\ \tilde{u}^{\alpha'\kappa'}_{\underline{L}'}(0) \rangle_{H'_o} \quad , \tag{36}$$

which, in complete analogy to equation (28), can be expanded in a Fourier series:

$$\bar{G}(v;L\alpha\kappa,L'\alpha'\kappa') = \frac{1}{\beta} \sum_{\ell=-\infty}^{\infty} \bar{G}_\ell(\underline{L}\alpha\kappa,\underline{L}'\alpha'\kappa') e^{2\pi i \ell v/\beta} \tag{37}$$

where

$$\bar{G}_\ell(\underline{L}\alpha\kappa,\underline{L}'\alpha'\kappa') = \int_0^\infty dv\ \bar{G}(v;\underline{L}\alpha\kappa,\underline{L}'\alpha'\kappa') e^{-2\pi i \ell v/\beta} . \tag{38}$$

The general procedure for obtaining the required coefficients G^A_ℓ in terms of the coefficients $\bar{G}_\ell$ starting from equation (34) and using the "diagram" technique is well established (e.g. Maradudin and Fein 62), but is usually specialized

to the case where the unperturbed system is the one described by H_o and not by H'_o. However, this simply means that instead of labelling single lines in the diagram by $\underline{k}$ and j, which characterize the normal modes of the perfect crystal, they are to be labelled as perturbed phonons by p (Maradudin 64b). Each line therefore represents a factor $\overline{G}_\ell(p)$, which is shown to be given by

$$\overline{G}_\ell(p) = \frac{1}{\omega_p^2 + \omega_\ell^2} \tag{39}$$

in appendix 1. G^A_ℓ is represented diagrammatically by a double line which must have two labels in the {p}-representation since G^A_ℓ is not diagonal. The Dyson equation for $G^A_\ell(p,p')$ is shown schematically in figure 1. In that figure, the "bubble", which represents the sum of all linked proper diagrams (Cowley 63) containing at least one anharmonic vertex, is called the proper self-energy, and represents a factor $M_\ell(p,p_1)$. Thus the equation can be written

$$G^A_\ell(p,p') = \overline{G}_\ell(p)\ \delta_{p,p'} + \overline{G}_\ell(p) \sum_{p_1} M_\ell(p,p_1)\ G^A_\ell(p_1,p') \tag{40}$$

It has been shown by Maradudin and Fein (1962) that if only diagonal elements of $G^A_\ell(p,p')$ are required, then it is a good approximation to neglect off-diagonal terms of the proper self-energy. In that case $G^A_\ell(p,p)$ can be

written

$$G_\ell^A(p,p) = \frac{1}{\bar{G}_\ell^{-1}(p) - M_\ell(p)}$$

$$\equiv G_\ell^A(p) \qquad (41)$$

where

$$M_\ell(p) \equiv M_\ell(p,p) \quad .$$

The general rules for the drawing of diagrams and their evaluation have been given by many authors (e.g. Cowley 63). For the applications considered in this work, it is convenient to use the position representation to label internal lines in M_ℓ. Such lines require two labels, of course, since it is not the representation in which $\bar{G}_\ell$ is diagonal. The modified rules for evaluating diagrams labelled in this way are given in appendix 1.

CHAPTER 3

A THEORETICAL MODEL OF THE U-CENTRE

It was pointed out in the introduction that, when a realistic model is used to represent the host crystal, it is necessary to introduce force constant changes as well as the mass change to account for the observed U-centre local mode frequency. There is no reason to expect that any of the short-range force constants involving the H^- ion are the same as those of the perfect crystal; however, it is reasonable to argue that the most pronounced difference will be the change Δf, in the longitudinal force constant f, between the H^- ion and its nearest neighbours. If Δf is the only such change considered, as in the model of Timusk and Klein (1966), its value can be determined from the observed local mode frequency and is found to represent a large decrease in f.

The shapes of some of the absorption spectra characteristic of the U-centre, for instance the sidebands, are largely determined by the vibrational spectra of the neighbours of the H^- ion (Timusk and Klein 66). In fact, to explain the sideband lineshape in some detail, it has been found necessary to extend the model described above (Gethins et al. 67). The considerable decrease in the force

constant f suggests that the equilibrium distance between the H^- ion and its nearest neighbour will be less than the perfect crystal value. Such a shift in equilibrium position will cause a weakening in the force constant g between nearest and fourth nearest neighbours of the H^- ion. This effect is included in the present model as a change Δg in g. The force constants which are considered to be perturbed in this model are shown schematically in figure 2.

The change in the crystal's potential energy due to Δf and Δg can be written

$$\Delta V = \sum_{\substack{\alpha=x,y,z \\ s=\pm 1}} \left\{ \frac{\Delta f}{2} \left(M_+^{-\frac{1}{2}} u_{s\bar{\alpha}}^{\alpha+} - M_-^{-\frac{1}{2}} u_{\underline{0}}^{\alpha-} \right)^2 + \right.$$

$$\left. + \frac{\Delta g}{2} \left(M_-^{-\frac{1}{2}} u_{2s\bar{\alpha}}^{\alpha-} - M_+^{-\frac{1}{2}} u_{s\bar{\alpha}}^{\alpha+} \right)^2 \right\} \qquad (1)$$

where $\bar{\alpha}$ is a vector in direction α whose magnitude is equal to the interionic spacing 'a'. Therefore, using the definition given in equation (13) of chapter 2, the non-zero elements of the matrix Γ are

$$\Gamma_{\underline{0},\underline{0}}^{\alpha-,\alpha-} = \frac{2\Delta f}{M_-} + \lambda\omega^2$$

$$\Gamma_{\pm\bar{\alpha},\pm 2\bar{\alpha}}^{\alpha\pm\ \alpha-} = -\frac{\Delta g}{\sqrt{M_+ M_-}}$$

$$\Gamma_{\pm\bar{\alpha},\pm\bar{\alpha}}^{\alpha+,\alpha+} = \frac{\Delta f + \Delta g}{M_+}$$

$$\Gamma^{\alpha^-,\alpha^-}_{\pm 2\bar{\alpha},\pm 2\bar{\alpha}} = \frac{\Delta g}{M_-}$$

$$\Gamma^{\alpha+,\alpha-}_{\pm\bar{\alpha},\underline{0}} = -\frac{\Delta f}{\sqrt{M_+ M_-}} \quad , \quad \alpha = x,y,z \; . \qquad (2)$$

Because the presence of the impurity leaves the point symmetry of its site unchanged, it proves convenient to choose, as a basis for the non-zero part of the matrix Γ, coordinates which transform according to the irreducible representations of the octahedral group. A suitable choice is

$$Q_n(E_g) = \sqrt{M_n/6}\ (2q_n(x) - q_n(y) - q_n(z))$$

$$Q_n(E'_g) = \sqrt{M_n/2}\ (q_n(y) - q_n(z))$$

$$Q_n(A_{1g}) = \sqrt{M_n/3}\ (q_n(x) + q_n(y) + q_n(z))$$

$$Q_n(T^{\alpha}_{1u}) = \sqrt{1/2}\ (u^{\alpha\kappa}_{n\bar{\alpha}} + u^{\alpha\kappa}_{-n\bar{\alpha}})$$

$$Q_{n=0}(T^{\alpha}_{1u}) = u^{\alpha-}_{\underline{0}} \quad , \quad \begin{matrix} n = 1,2 \\ \alpha = x,y,z \end{matrix} \qquad (3)$$

where

$$q_n(\alpha) = \frac{1}{\sqrt{M_n}}\ (u^{\alpha\kappa}_{n\bar{\alpha}} - u^{\alpha\kappa}_{-n\bar{\alpha}}) \quad ,$$

and

$$M_1 \equiv M_+$$

$$M_2 \equiv M_- \; .$$

This basis defines a 15 x 15 subspace outside of which the elements of Γ are all zero. Let the elements of Γ be those of the small matrix γ in this subspace, which will be referred to as the "space of γ" (Klein 63). Then, γ has the block diagonal form

$$\gamma = \begin{bmatrix} \gamma(E_g) & & & & & & \\ & \gamma(E_g') & & & & & \\ & & \gamma(A_{1g}) & & & & \\ & & & \gamma(T^x_{1u}) & & & \\ & & & & \gamma(T^y_{1n}) & & \\ & & & & & \gamma(T^z_{1u}) & \end{bmatrix} \quad (4)$$

where, for example, the elements of the 2 x 2 matrix $\gamma(E_g)$ will be labelled $\gamma_{nn'}(E_g)$ as suggested by the notation of equation (3). The non-zero elements of γ are

$$\gamma_{11}(S) = \frac{\Delta f + \Delta g}{M_+}$$

$$\gamma_{22}(S) = \frac{\Delta g}{M_-}$$

$$\gamma_{12}(S) = \gamma_{21}(S) = -\frac{\Delta g}{\sqrt{M_+ M_-}}$$

$$\gamma_{00}(T^{\alpha}_{1u}) = \frac{2\Delta f}{M_-} + \lambda\omega^2$$

$$\gamma_{10}(T^{\alpha}_{1u}) = \gamma_{01}(T^{\alpha}_{1u}) = -\Delta f\sqrt{\frac{2}{M_+M_-}}\,, \qquad \begin{matrix} S = A_{1g}, E_g, E'_g, T_{1u} \\ \alpha = x,y,z \end{matrix}$$

. (5)

If $g(\omega^2)$ and $\bar{g}(\omega^2)$ are written for the parts of $G(\omega^2)$ and $\bar{G}(\omega^2)$ respectively, in the space of γ, then from equation (22) of chapter 1 it readily follows (Klein 63) that

$$\bar{g} = (I + g\gamma)^{-1}g = \frac{(I + g\gamma)^{+}g}{\det\,(I + g\gamma)} \quad , \qquad (6)$$

where the notation M^+ has been used to denote the adjoint matrix of a matrix M. The condition for the occurrence of a local mode is (Klein 63) the existence of a solution of the equation

$$\det\,(I + g\gamma) = 0 \qquad (7)$$

outside the frequency range of the eigenmodes of the perfect crystal. In the representation defined by equation (3), like γ, g is also block diagonal and therefore so is $(I + g\gamma)$. Thus equation (7) reduces to the condition that the product of the determinants of each of the "blocks" is equal to zero. Since the H^- ion only moves in modes of T_{1u} symmetry, as can be seen from equation (3), the frequency Ω of the triply degenerate U-centre local mode

is given by

$$\det \left(I + g(\Omega^2)\gamma(\Omega^2)\right)_{T_{1u}^{\alpha}} = 0 \quad . \qquad (8)$$

Because $\Omega >> \omega_m$, the maximum phonon frequency in the unperturbed lattice, it is a good approximation (Klein 68) to consider simply

$$1 + g_{00}(\Omega^2)\ \gamma_{00}(\Omega^2) + g_{01}(\Omega^2)\ \gamma_{01}(\Omega^2) = 0 \quad , \qquad (9)$$

where all the matrix elements refer to the T_{1u}^{α}-block. Since Ω is known from experiment, equation (9), which is independent of Δg, can be used to determine Δf. The matrix g is real at frequency Ω and its elements can be calculated as described in appendix 3. The computed values of those required in equation (9) are

$$g_{00}(\Omega^2) = -\ 0.14683 \times 10^{-28}\ (\text{rad/sec})^{-2}$$
$$g_{01}(\Omega^2) = \quad 0.34387 \times 10^{-30}\ (\text{rad/sec})^{-2} \qquad \text{for KBr,}$$

and

$$g_{00}(\Omega^2) = -\ 0.19767 \times 10^{-28}\ (\text{rad/sec})^{-2}$$
$$g_{01}(\Omega^2) = \quad 0.45255 \times 10^{-30}\ (\text{rad/sce})^{-2} \qquad \text{for KI,}$$

and the results for Δf are

$$\Delta f = -\ 8860 \ \text{dyne/cm} \qquad \text{for KBr}$$
$$= -\ 8660 \ \text{dyne/cm} \qquad \text{for KI} \quad . \qquad (10)$$

These values will be used throughout this work.

CHAPTER 4

SIDEBANDS OF THE U-CENTRE LOCALIZED MODE

A. FORMULA FOR THE LINESHAPE

The expression for the absorption constant given in equation (32) of chapter 2 can be approximately written

$$\alpha_{xx}(\nu) = \frac{4\pi e^2 \nu}{Vc' M_-} \mathrm{Im}\{G^A(\nu + i0^+; \underline{0}x-, \underline{0}x-)\} \qquad (1)$$

for frequency ν near the U-centre local mode frequency. c' is the velocity of light in the crystal near that frequency. If it is assumed that in the local mode only the hydrogen ion moves, then equation (1) can be written

$$\alpha_{xx}(\nu) = \frac{4\pi e^2 \nu}{Vc' M_H} \mathrm{Im}\{G^A(\nu + i0^+; P_x)\} \quad . \qquad (2)$$

The form given in equation (21) of chapter 2 has been used for the eigenvector of the local mode phonon,

$$U_{\underline{L}\alpha\kappa, P_x} = \delta_{\kappa,-}\delta_{\underline{L},\underline{0}}\delta_{\alpha,x}\sqrt{\frac{M_-}{M_H}} \quad . \qquad (3)$$

Absorption can occur at frequencies both above and below Ω (upper and lower sidebands), since the local mode can interact anharmonically either to create a "lattice phonon" (a perturbed phonon other than P_α) or to destroy one that has been thermally excited. The anharmonic terms

giving rise to such interactions must therefore contain the square of the H^- ion coordinate. The most important terms of this type result from cubic anharmonic interactions between the hydrogen ion and its nearest neighbours and are given in equation (3) of appendix 2. These interactions can be treated using the perturbation theory discussed in chapter 2. The diagram to be considered (Bilz et al. 66) is shown in figure 3 with all internal labellings which are allowed by the anharmonic terms and which do not contain off-diagonal elements of $\bar{G}$ for coordinates of different symmetry, since these elements are zero. The contribution of the diagram to the self-energy $M_\ell^{(s)}(P_x)$ for the sideband is evaluated using the rules given in appendix 1. A factor two must be associated with the diagram to account for topologically equivalent diagrams, and a factor $\sqrt{M_-/M_H}$ arises at each vertex from the expansion of $Q_o(T^x_{lu})$ in the $\{p\}$-representation. The labellings shown in figures 3a and 3b have an additional factor two at each vertex since the pair of coordinates $Q_o(T^x_{lu})$ are interchangeable. The total contribution of the diagram is therefore

$$M_\ell^{(s)}(P_x) \equiv M_\ell^{(a)}(P_x) + M_\ell^{(b)}(P_x) + 2M_\ell^{(c)}(P_x)$$

$$= \frac{2}{3M_{-}M_{+}M_{H}\beta} \sum_{\ell_1=-\infty}^{\infty} \bar{G}_{\ell_1}(Q_o(T^x_{1u})) \times$$

$$\times \{ (\bar{V}_3 + 2\bar{V}_2)^2 \bar{G}_{\ell-\ell_1}(Q_1(A_{1g})) + 2(\bar{V}_3 - \bar{V}_2)^2 \bar{G}_{\ell-\ell_1}(Q_1(E_g)) +$$

$$+ 12\bar{V}_2^2 \bar{G}_{\ell-\ell_1}(Q_1(T^{xy}_{2g})) \} \qquad (4)$$

where $M^{(a)}$, $M^{(b)}$ and $M^{(c)}$ are the contributions from the labellings shown in figures 3a, 3b and 3c respectively. The symmetry coordinate $Q_1(T^{xy}_{2g})$ is defined in appendix 2. An abbreviated notation has been used to denote the diagonal elements of $\bar{G}$ and the definitions

$$\bar{V}_3 = \left.\frac{\partial^3 \bar{V}}{\partial r^3}\right|_{\bar{r}_o} ,$$

$$\bar{V}_2 = \frac{1}{\bar{r}_o}\left.\left(\frac{\partial^2 \bar{V}}{\partial r^2}\right)\right|_{\bar{r}_o} \qquad (5)$$

have been used, where $\bar{r}_o$ is the perturbed hydrogen ion-nearest neighbour distance and $\bar{V}$ is the perturbed potential. The elements of $\bar{G}$ can now be formally expanded in the $\{p\}$-representation. Using equation (39) of chapter 2 and equation (3), the contribution $M^{(a)}_{\ell}(P_x)$ given by equation (4) becomes

$$M^{(a)}_{\ell}(P_x) = \frac{2(\bar{V}_3 + 2\bar{V}_2)^2}{3M_{+}M_H^2\beta} \sum_p \sum_{\ell_1} \frac{1}{\Omega^2 + \omega^2_{\ell_1}} \cdot \frac{U_{Q_1(A_{1g}),p} U_{p,Q_1(A_{1g})}}{\omega_p^2 + \omega^2_{\ell-\ell_1}} \qquad (6)$$

where ω_p is the frequency of the phonon p. The sum over ℓ_1 can be performed using the results of appendix 1. At low temperatures, the Bose-Einstein factors can be set equal to zero, giving

$$M^{(a)}(\nu;P_x) = \frac{(\bar{V}_3 + 2\bar{V}_2)^2\hbar}{3M_+M_H^2\Omega} \sum_p U_{Q_1(A_{1g}),p} \times$$

$$\times \frac{1}{2\omega_p}\left\{\frac{1}{\nu + \Omega + \omega_p} - \frac{1}{\nu - \Omega - \omega_p}\right\} U_{p,Q_1(A_{1g})} \qquad (7)$$

where the continuous variable ν has been introduced using equation (33) of chapter 2. The imaginary part of this equation essentially gives

$$\mathrm{Im}\{M^{(a)}(\omega + i0^+)\} = \frac{(\bar{V}_3 + 2\bar{V}_2)^2\hbar}{3M_+M_H^2\Omega} \sum_p U_{Q_1(A_{1g}),p} \times$$

$$\times \frac{\pi}{2\omega_p}\delta(\omega - \omega_p)\, U_{p,Q_1(A_{1g})}$$

$$= \frac{(\bar{V}_3 + 2\bar{V}_2)^2\hbar}{3M_+M_H^2\Omega} \cdot \mathrm{Im}\{\bar{G}(\omega^2 + i0^+; Q_1(A_{1g}))\} \qquad (8)$$

which follows from the definition of $\bar{G}$ given in equation (17) of chapter 2. The symbol ω, defined by

$$\omega \equiv \nu - \Omega \quad ,$$

has been used to indicate the frequency measured with respect to the local mode frequency.

Now, from equations (17) and (41) of chapter 2,

$$G^A(\nu;P_x) = \frac{1}{\overline{G}^{-1}(\nu;P_x) - M(\nu;P_x)}$$

$$= \frac{1}{\Omega^2 - \nu^2 - M(\nu;P_x)} \quad . \qquad (9)$$

Taking imaginary parts gives

$$\mathrm{Im}\{G^A(\nu + i0^+;P_x)\} = \frac{\mathrm{Im}\{M(\nu + i0^+;P_x)\}}{(\Omega^2 - \nu^2 - \mathrm{Re}\{M(\nu,P_x)\})^2 + (\mathrm{Im}\{M(\nu;P_x)\})^2} \qquad (10)$$

$$\approx \frac{\mathrm{Im}\{M(\nu + i0^+;P_x)\}}{(\Omega^2 - \nu^2)^2} \quad , \qquad (11)$$

which is a good approximation if the perturbation is sufficiently small. Using equation (8) and analogous expressions for the contributions $M^{(b)}$ and $M^{(c)}$, together with equations (2) and (11), the optical absorption constant for the upper sideband at low temperature can be written

$$\alpha_{xx}(\omega) = \frac{\pi e^2 \hbar \overline{v}_3^2}{Vc' M_H^3 M_+ \Omega^2} \cdot \ell(\omega) \quad . \qquad (12)$$

The function $\ell(\omega)$ is the lineshape, defined by

$$\ell(\omega) = \frac{(1 + \frac{\omega}{\Omega})}{(1 + \frac{\omega}{2\Omega})^2 \omega^2} \mathrm{Im} \left\{ \frac{(1 + 2\xi)^2}{3} \overline{G}(\omega^2 + i0^+;Q_1(A_{1g})) + \right.$$

$$\left. + \frac{2(1 - \xi)^2}{3} \overline{G}(\omega^2 + i0^+;Q_1(E_g)) + 4\xi^2 G(\omega^2 + i0^+;Q_1(T_{2g})) \right\} ,$$

$$\equiv \frac{\pi}{2} \left\{ \frac{(1 + 2\xi)^2}{3} L(\omega;A_{1g}) + \frac{2(1 - \xi)^2}{3} L(\omega;E_g) + \right.$$

$$\left. + 4\xi^2 L(\omega;T_{2g}) \right\} \qquad (13)$$

where $\xi = \bar{V}_2/\bar{V}_3$. The value of ξ (which is negative) determines the relative weights of the A_{1g}, E_g and T_{2g} parts in the sideband, which are described by the functions $L(\omega;A_{1g})$, $L(\omega;E_g)$ and $L(\omega;T_{2g})$, respectively. It should be pointed out that the elements of $\bar{G}$ having T_{2g} symmetry are equal to those of G when the model of the defect described in chapter 3 is used.

B. CALCULATION OF THE SIDEBAND SPECTRA

The calculation of the matrix elements of $\bar{G}$ required in equation (13) is described in appendix 3. The Dyson equation has been used to express elements of $\bar{G}$ corresponding to A_{1g} and E_g symmetries in terms of the elements of G and Γ of corresponding symmetry. Elements of G have been calculated using shell model phonons derived from neutron diffraction data (Cowley et al. 63; Dolling et al. 66) using a modification of the method introduced by Gilat and Raubenheimer (1966). The required elements of $\bar{G}$ refer to the nearest neighbours of the H^- ion, and depend through the Dyson equation on the perturbation parameters Δf and Δg, while the mixture of symmetry types called for in equation (13) depends on the ratio ξ.

The choice $\Delta g = 0$, $\xi = 0$ corresponds to the model of Timusk and Klein (1966). This model leads to satisfactory agreement with the lineshape observed at low frequencies, but the detailed agreement at higher frequencies is rather poor. Considerable improvement can be effected by taking non-zero values for Δg and ξ.

The positions and intensities of peaks in the calculated sideband spectrum are determined by the behaviour of the complex determinants $D(E_g)$ and $D(A_{1g})$, defined in appendix 3, which arise in the matrix inversions required by the Dyson equation. In particular, a resonance or antiresonance occurs whenever the real part of these determinants has a zero. If this zero occurs at a frequency where the imaginary part of the corresponding determinant is zero, for instance in the band gap of the unperturbed density of states, then the resonance becomes a pole. This indicates the existence of a perturbed phonon which is largely localized on the nearest neighbours of the H^- ion.

The Timusk and Klein model predicts a pole of E_g symmetry in the band gap of both KI and KBr and resonances of A_{1g} symmetry are predicted in their optical bands (Timusk and Klein 66; Gethins et al. 67). Comparison with experiment shows that, in KBr, no peak is observed in the band gap, while in KI, although a peak is present in the gap, it is at a considerably higher frequency than that

predicted by this model. Furthermore, considerable structure is observed near the top of the acoustic band which is not explained by the simple model.

The effect of giving Δg a negative value, that is, weakening the force constant g, is to lower the frequencies of the poles and resonances. This improves the agreement to such an extent that it becomes possible to establish a correspondence between the various resonances in the theory and peaks in the experimental sideband spectra (Gethins et al. 67). Thus the peaks at 79 cm^{-1} and 111 cm^{-1} in KBr are associated with resonances in the E_g and A_{1g} component parts, respectively, of the lineshape. In KI, the peak at 65.5 cm^{-1} is a resonance of E_g symmetry and the peak in the gap at 93 cm^{-1} has A_{1g} symmetry.

The A_{1g} and E_g parts of the sideband were therefore calculated using several values of Δg and the predicted positions of the resonances were compared to those observed. The results are shown in figure 4. The values $\Delta g = -5000$ dyne/cm and -4400 dyne/cm, for KI and KBr respectively, were found to fit the positions of both resonances in each case to within 3 cm^{-1}, which is comparable to anharmonic frequency shifts which have been neglected. In the case of KI, the position of the E_g resonance relative to the peak predicted at 61.5 cm^{-1} was also considered in choosing Δg. This peak at 61.5 cm^{-1}

arises from an off-symmetry van Hove singularity in the density of states of the unperturbed crystal (see figure 14) and therefore results from phonons not measured directly in the neutron diffraction experiments. Its position could therefore be in error by the 3 cm^{-1} necessary to align it with the peak observed at 58 cm^{-1} in the KI sideband. Far infrared results discussed in the next chapter also seem to suggest that this is the case. Since the position of the resonance in the theory is to some extent determined by the position of this critical point, it is reasonable that some weight be given to the relative positions of the resonance and critical point peaks in assigning a value to Δg.

The contributions of the A_{1g} and E_g parts of the sideband lineshape for the values of Δg given above, together with the T_{2g} contribution, are shown in figures 5 and 6 for KI and KBr respectively, and the resonance denominators $D(A_{1g})$ and $D(E_g)$ are plotted in figure 7. The results for KI:KH and KBr:KH are shown in figures 8 and 9. The value $\xi = -0.15$, which is discussed in appendix 4, was used in both cases. The results are in good agreement with the experimental curves shown in the same figures. It should be pointed out that the most noticeable difference, that peaks associated with the resonances in the theoretical curves are predicted too narrow, is a result of neglecting

the anharmonic broadening of the perturbed phonons in the final state of the sideband process. This broadening is discussed in detail in chapter 6. Also, the agreement for the relative intensities of corresponding peaks in the theory and experiment is improved by the considerations of the next section.

C. CORRECTIONS TO THE LINESHAPE

As can be seen from equation (12), the intensity of the sideband depends on the square of the anharmonic constant $\bar{V}_3$. Although this intensity cannot be measured absolutely, the ratio of the area under the upper sideband to the area under the peak at frequency Ω, which at low temperatures is equal to the Huang-Rhys factor s, has been measured (Fritz et al. 65). This provides a means of estimating $\bar{V}_3$. Since the values of $\bar{V}_3$ and other anharmonic constants in the defect area are needed to estimate the contributions of higher-order processes to absorption in the sideband region, their determination is of considerable importance. The intensity I_o of the local mode peak can be obtained from equation (2) by replacing G^A by $\bar{G}$ and using equation (17) of chapter 2. Integration of the absorption constant over frequency then gives

$$I_o = \frac{2\pi^2 e^2}{\bar{V} c' M_H} \quad . \qquad (14)$$

Using this value with equation (12) enables s to be written

$$s = \frac{\hbar \bar{V}_3^2}{2\pi M_H^2 M_+ \Omega^2} \int_0^{\omega_m} \ell(\omega) d\omega \quad , \qquad (15)$$

where the integral extends over the upper sideband to the maximum phonon frequency ω_m.

It has been pointed out by Bilz et al. (1967) that the approximation made in going from equation (10) to equation (11) is not justified in the case of strong impurity effects, and can considerably affect the intensities of peaks in the original sideband spectrum. The more exact lineshape $\ell'(\omega)$ which would result from using equation (10) can be calculated from $\ell(\omega)$ using (Bilz et al. 67)

$$\ell'(\omega) = \ell(\omega) \cdot \frac{(\Omega^2 - \nu^2 - \mathrm{Re}\{M^{(s)}(0;P_x)\})^2}{(\Omega^2 - \nu^2 - \mathrm{Re}\{M^{(s)}(\omega;P_x)\})^2 + (\mathrm{Im}\{M^{(s)}(\omega;P_x)\})^2} \quad , \qquad (16)$$

where it can be seen from equations (8) and (13) that

$$\mathrm{Im}\, M^{(s)}(\omega;P_x) = \frac{\hbar \bar{V}_3^2}{M_+ M_H^2 \Omega} \cdot \frac{(1 + \omega/2\Omega)^2 \omega^2}{(1 + \omega/\Omega)} \cdot \ell(\omega) \quad . \qquad (17)$$

The real part of $M^{(s)}$ is obtained from its imaginary part using an equation analogous to equation (6) of appendix 3. The corrected lineshape was calculated from $\ell(\omega)$ for various values of $\bar{V}_3$, and in each case the value of s given by

$$s = \frac{\hbar \bar{V}_3^2}{2\pi M_H^2 M_+ \Omega^2} \int_0^{\omega_m} \ell'(\omega) d\omega \qquad (18)$$

was evaluated. The values of $\bar{V}_3$ corresponding to the experimental values of s were thus found to be

$$\bar{V}_3 = -0.9 \times 10^{12} \text{ dyne/cm}^2 \qquad \text{for KI (using } s = 0.22)$$

and

$$\bar{V}_3 = -1.15 \times 10^{12} \text{ dyne/cm} \qquad \text{for KBr (using } s = 0.17) \qquad (19)$$

It should be noted that the value of the integral required in equation (18) can only be evaluated following a calculation of the sideband lineshape and therefore $\bar{V}_3$ obtained in this way is dependent on details of the model used. In addition, since $\ell(\omega)$ varies with ξ, the value of $\bar{V}_3$ also shows a slight dependence on ξ. However, at this time there is no reason to expect either that the present model of the U-centre is not a reasonable one or that the values of ξ which have been used are very much in error, and therefore it seems probable that the values of $\bar{V}_3$ quoted are reliable estimates.

The corrected lineshape for KI is compared to $\ell(\omega)$ in figure 10. The magnitude and relative intensities of peaks in the sideband are affected, resulting in an overall improvement in the agreement with experiment. The corrections obtained in the present calculation seem to be smaller than those estimated by Bilz et al. (1967), probably due to differing values of $\bar{V}_3$; however, direct comparison is

difficult since the correction was applied in a different way.

It is interesting to consider replacing the H^- ion by a D^- ion. Since the ions are electronically identical the values of $\bar{V}_3$ and ξ are unaffected; however from equations (16) and (17) it can be seen that the changes in mass and local mode frequency result in the correction factor of that equation being of less importance in the case of D^- than in the case of H^-, a result which is explained by the fact that anharmonic interactions are less important for the D^- ion because of its smaller amplitude. This effect, together with similar effects arising in evaluating the contributions to absorption in this frequency range of other anharmonic processes (for instance, contributions to the two-phonon sideband spectrum), should lead to observable differences in the relative intensities of corresponding peaks in the sideband spectra of the H^- and D^- local mode.

CHAPTER 5

FAR INFRARED ABSORPTION

It has been ovserved experimentally that the far infrared absorption of alkali halides, which is normally restricted to the reststrahlen absorption, is modified by the presence of an impurity. For instance, in the case of crystals containing U-centres, considerable absorption is induced at frequencies near the top of the acoustic band. This absorption can be calculated using the model developed in the preceding chapters without the introduction of new parameters.

A convenient form for the optical absorption constant for this problem has been given recently by Klein (1968):

$$\alpha_{xx}(\omega) = \frac{(\eta^2(\infty) + 2)^2}{9\eta(\omega)} \cdot \frac{4\pi N e^2 \omega}{cV\mu} \operatorname{Im}\{\bar{G}_{R_x,R_x}(\omega^2 + i0^+)\} \tag{1}$$

where ω is now the actual absorption frequency, $\eta(\infty)$ is the index of refraction in the high frequency limit (taken equal to unity in previous expressions for $\alpha(\omega)$) and μ is the reduced mass of the alkali and halide pair, given by $\mu = M_+M_-/(M_+ + M_-)$. The matrix element of $\bar{G}$ required is defined in the plane wave representation discussed in

chapter 2, and is the diagonal element corresponding to the phonon with $\underline{k} = 0$ in the transverse optical branch, polarized in the x-direction, that is, the "Reststrahlen" phonon, R_x. Equation (1) can be derived from equation (32) of chapter 2 by expanding the matrix element of G^A in that equation in terms of its elements in the $\{\underline{k},j\}$-representation, using the transformation matrix defined by equation (7) of chapter 2. The summation on $\underline{L}$ and $\underline{L}'$ can then be performed essentially giving equation (1). (Anharmonic effects have been neglected.)

The matrix element of $\overline{G}$ needed in equation (1) is most easily evaluated using equation (24) of chapter 2, which expresses $\overline{G}$ in terms of the T-matrix. Since G is diagonal in the $\{\underline{k},j\}$-representation with elements defined in equation (9) of chapter 2, the required element of $\overline{G}$ can be written

$$\overline{G}_{R_x,R_x}(\omega^2) = (\omega_{R_x}^2 - \omega^2)^{-1} - (\omega_{R_x}^2 - \omega^2)^{-2}\, T_{R_x,R_x}(\omega^2), \quad (2)$$

and for $\omega \neq \omega_{R_x}$, equation (1) becomes

$$\alpha_{xx}(\omega) = -\frac{(\eta^2(\infty) + 2)^2}{9\eta(\omega)} \cdot \frac{4\pi\omega e^2}{cV\mu} \cdot \frac{\mathrm{Im}\{T_{R_x,R_x}(\omega^2 + i0^+)\}}{(\omega_{R_x}^2 - \omega^2)^2} \quad . \quad (3)$$

It can be seen from equation (23) of chapter 2 that in the $\{\underline{L}\alpha\kappa\}$-representation, T is only non-zero in the space of γ,

and a matrix t can be defined such that the elements of T are equal to those of t in this subspace. Expanding T_{R_x,R_x} in the $\{\underline{L}\alpha\kappa\}$-representation then gives

$$T_{R_x,R_x}(\omega^2) = \frac{1}{N} \sum'_{\substack{\underline{L}\alpha\kappa \\ \underline{L}'\alpha'\kappa'}} \varepsilon_\alpha^\kappa(R_x)\ \varepsilon_{\alpha'}^{\kappa'}(R_x)\ t(\omega^2;\underline{L}\alpha\kappa,\underline{L}'\alpha'\kappa') \qquad (4)$$

where the summation is restricted to the space of γ. $\varepsilon_\alpha^\kappa(R_x)$ is an element of the polarization vector for the mode R_x, and is determined by normalization and by the requirement that the centre of mass of the alkali and halide ions remains fixed. It has the value

$$\varepsilon_\alpha^\pm(R_x) = \pm\, \delta_{\alpha,x} \left(\frac{\mu}{M_\pm}\right)^{\frac{1}{2}} \qquad . \qquad (5)$$

It is convenient to rewrite the summation of equation (4) using the symmetry coordinates defined in equation (3) of chapter 3. The result involves only "odd" matrix elements of t, and using equation (5) can be written

$$T_{R_x,R_x} = \frac{\mu}{N} \left\{ \frac{1}{M_-}(t_{00}(T_{1u}^x) + 2\sqrt{2} \cdot t_{02}(T_{1u}^x) + 2t_{22}(T_{1u}^x)) + \right.$$

$$\left. + \frac{2}{M_+} t_{11}(T_{1u}^x) - 2\sqrt{\frac{2}{M_+M_-}} (t_{01}(T_{1u}^x) + 2t_{12}(T_{1u}^x)) \right\}, \qquad (6)$$

where the notation $t_{nn'}(T_{1u}^x)$ is analogous to that used for the elements of γ and g in chapter 3. The elements of the matrix $t(T_{1u}^x)$ can be obtained from the T_{1u}^x part of equation

(23) of chapter 2, that is,

$$t(T_{1u}^{x}) = \gamma(T_{1u}^{x}) \quad (I + g(T_{1u}^{x})\ \gamma(T_{1u}^{x}))^{-1} \quad . \qquad (7)$$

The elements of $\gamma(T_{1u}^{x})$ are defined in equation (5) of chapter 3, and the calculation of the real and imaginary parts of the matrix elements of $g(T_{1u}^{x})$ as a function of frequency is described in appendix 3. Since the matricies involved are of small dimension (3 x 3), the inversion required in equation (7) can be easily performed. Formally, the result can be written

$$t(T_{1u}^{x}) = \frac{D^{*}(T_{1u}^{x})}{|D(T_{1u}^{x})|^{2}} \cdot \gamma(T_{1u}^{x}) \cdot (I + g(T_{1u}^{x})\ \gamma(T_{1u}^{x}))^{\dagger} \qquad (8)$$

where the quantity $D(T_{1u}^{x})$ and its complex conjugate $D^{*}(T_{1u}^{x})$ are defined by

$$D(T_{1u}^{x}) = \det(I + g(T_{1u}^{x})\ \gamma(T_{1u}^{x})) \qquad . \qquad (9)$$

$D(T_{1u}^{x})$ plays the same role in this problem as that played by $D(A_{1g})$ and $D(E_{g})$ in the sideband calculation; that is, zeroes of its real part determine the frequencies of resonances or antiresonances (depending on the slope of $\mathrm{Re}\{D\}$ at its zero) which appear in the spectrum. The important difference is that while resonances in "even" modes of ions in the defect area are observed in the one-phonon sideband spectra, resonances of "odd" modes are seen in far infrared measurements. $D(T_{1u}^{x})$ is plotted in figure

11 for KBr and KI. The zeroes of Re{D} marked with arrows give resonances, whereas the unmarked zeroes give anti-resonances.

The absorption constant was calculated from equation (3) using equations (6) and (8) with the results shown in figures 12 and 13 for KI and KBr, respectively. Experimental curves (Timusk et al. 68) are also plotted there for comparison.

The most striking contribution to the infrared absorption curve is the pole at the reststrahlen frequency ω_{R_x}. This pole occurs in the first term of equation (2) and is the only contribution of this term. The second term of equation (2) modifies the absorption near ω_{R_x}, and in addition gives rise to the absorption observed at other frequencies. In particular, this absorption is strong close to the frequency of the resonance which occurs at the top of the acoustic band, and reflects some details of the frequency distribution in that region. (The index of refraction has been assumed to be constant over this frequency region.) It is remarkable that the force constant model developed in chapters 2 and 3, whose parameters were chosen to reproduce features of the sideband extending over most of the frequency distribution, should lead to such close agreement with experiment for the position and general shape of the narrow band of structure observed in the far

infrared absorption curves.

The resonances which are predicted in the theoretical curves are very much narrower than any of the experimental peaks, probably due to neglect of anharmonic broadening effects. Other peaks in the theoretical curves arise from van Hove singularities in the total densities of states which can be seen in figure 14. The critical points involved are the ones giving the high peaks at 83.5 cm^{-1} in KBr and 61.5 cm^{-1} in KI, which in each case arise from a saddle-point of the dispersion surfaces in an off-symmetry direction in the (001) plane of wave-vector space, (referred to subsequently as the "off-symmetry saddle"), together with the ones producing the shoulders on the high-frequency sides of these peaks (at 88 cm^{-1} and 64 cm^{-1}, in KBr and KI respectively), which arise from saddle-points falling on directions of high-symmetry (referred to as "on-symmetry saddles").

A detailed discussion of the correspondence between the experimental peaks and peaks in the theoretical curves has been given by Woll et al. (1968). In KBr, the following tentative identification is suggested: the shoulder at 86.5 cm^{-1} in the experimental curve corresponds to the peak at 83.5 cm^{-1} in the theory. The peak at 89 cm^{-1} in both the experimental and theoretical curves is the resonance. Any contribution from the shoulder at 88 cm^{-1} must coincide

with the resonance. In KI, the small peak at 64 cm^{-1} in the experiment corresponds to the shoulder at the same frequency in the theoretical curve. The peak at 58 cm^{-1} in the experiment probably corresponds to the one predicted at 61 cm^{-1} in the theory, and the remaining peak, at 61 cm^{-1}, can then be identified with the resonance.

This interpretation suggests that although the on-symmetry saddles occur at the observed frequencies, the off-symmetry saddle is predicted at a frequency 3 cm^{-1} low in KBr and 3 cm^{-1} high in KI. This point also arose in the discussion of the position of the corresponding peak in the sideband spectrum of KI (see chapter 3). It is probable that the error arises from use of the shell model to predict off-symmetry dispersion surfaces not directly observed in neutron experiments. Such effects have also been suggested in other contexts (Dynes et al. 68).

In concluding this chapter, it can be said that calculations of far infrared absorption spectra of KI and KBr containing U-centres based on the present model of the defect, show satisfactory agreement with experimental results and have helped to explain how such spectra should be interpreted.

CHAPTER 6

ANHARMONIC BROADENING OF LOCALIZED MODES AND RESONANCES IN THE PERTURBED CRYSTAL

A. GENERAL REMARKS

The appearance in theoretical spectra of peaks which are much narrower than those observed experimentally, as discussed in chapters 4 and 5, is probably a consequence of neglecting anharmonic effects in the final states of the process under consideration. These effects lead to lifetime broadening of the perturbed phonons which can be treated in the theory by replacing the harmonic Green's function matrix $\overline{G}$ by G^A in the expressions for the absorption constant given in equation (13) of chapter 4 and equation (1) of chapter 5. The contribution of each perturbed phonon p to the absorption spectra is governed by the element $\mathrm{Im}\{G^A(\omega + i0^+;p)\}$, which is, roughly speaking, a Lorentzian function of finite width. For phonons not appreciably localized near the defect site, this width will be approximately equal to that of phonons of similar wave vector and polarization in the perfect crystal. However, the widths of phonons which are appreciably localized will be determined in part by

perturbed anharmonic coefficients and by perturbed vibrational spectra of ions in the vicinity of the defect. Calculation of the broadening of such phonons, including the high frequency localized mode, will be discussed in this chapter.

B. BROADENING OF THE GAP MODE IN KI:KH

The perturbed phonon of A_{1g} symmetry occurring in the band gap of KI:KH will be labelled p_A, with corresponding frequency ω_A. The phonon is localized on the nearest neighbours of the H^- ion to an extent determined by the transformation matrix element $U_{Q_1(A_{1g}),p_A}$. This element can be calculated as follows: the projection $\bar{\rho}_{11}(\omega;A_{1g})$ of the density of states, which is plotted in figure 15, is given by

$$\bar{\rho}_{11}(\omega;A_{1g}) = \sum_p U_{Q_1(A_{1g}),p}\, \delta(\omega_p - \omega)\, U_{p,Q_1(A_{1g})} \quad , \qquad (1)$$

with normalization such that

$$\int_0^{\omega_m} \rho_{11}(\omega;A_{1g})\,d\omega = 1 \quad . \qquad (2)$$

The area under the pole at ω_A, which is equal to the square of $U_{Q_1(A_{1g}),p_A}$, can therefore be estimated. The result is

$$U_{Q_1(A_{1g}),p_A} = 0.91 \quad . \qquad (3)$$

Other elements of the transformation matrix for the mode p_A, whose values fall (in magnitude) exponentially with increasing distance from the defect, can be estimated similarly or calculated using the method of Dawber and Elliott (1963a). In the present calculation the approximate value

$$U_{Q_1(A_{1g}),p_A} = 1 \qquad (4)$$

will be used; that is, it will be assumed that the mode is completely localized on the nearest neighbours of the H^- ion. This assumption simplifies the calculation, and is sufficiently realistic to yield meaningful results.

The lowest order processes contributing to the broadening of the phonon p_A are cubic anharmonic processes. At low temperatures the "decay" mechanism dominates, in which the phonon p_A decays into two phonons having frequencies in the acoustic band. At higher temperatures, a thermally excited acoustic phonon can interact with p_A to leave a phonon with frequency corresponding to the optical band. The leading cubic anharmonic terms required for these processes, which must contain the coordinate $Q_1(A_{1g})$ at least once, are given in equation (7) of appendix 2. Terms with transverse anharmonic coefficients have been neglected.

The self-energy, $M_\ell(p_A)$, of p_A is determined by evaluating the diagram shown in figure 17 using the rules

given in appendix 1. The result is

$$M_{\ell}(p_A) = \frac{1}{\beta} \sum_{\substack{Q_1 Q_1' \\ Q_2 Q_2'}}{}' C(Q_1 Q_2; Q_1' Q_2') \; \Sigma_{\ell_1} \bar{G}_{\ell_1}(Q_1, Q_1') \; \bar{G}_{\ell - \ell_1}(Q_2, Q_2') \; . \tag{5}$$

Here the primed summation indicates that Q_1, Q_1', Q_2 and Q_2' take all values of the symmetry coordinates, defined in equation (3) of chapter 3, which occur in the anharmonic terms under consideration, excluding combinations in which any phonon line is labelled with coordinates of different symmetry, and excluding combinations which do not yield a "distinct" set of labels. Labellings which differ only by the interchange of the two phonon lines are not "distinct" in this context. The factor $C(Q_1 Q_2; Q_1' Q_2')$ results from application of the rules (iv) and (v) of appendix 1; its values for all sets of labels which need to be considered are given in Table 1. The values quoted include factors which account for labellings giving equal contributions; for example, whenever two labellings occur which differ only by interchange of the two vertices, the contributions are equal and have been taken into account simply by listing only one of the combinations and multiplying the value of 'C' quoted by two. Similarly, the total contributions of labellings containing coordinates of E_g symmetry and those with E_g' symmetry are equal. Therefore only the labels of E_g symmetry have been listed, and the values of 'C' include

TABLE 1

VALUES OF THE COMBINATORIAL FACTOR $C(Q_1\ Q_2;\ Q_1'\ Q_2')^*$

Q_1	Q_2	Q_1'	Q_2'	$C(Q_1\ Q_2;\ Q_1'\ Q_2')$
A_1	A_1	A_1	A_1	$(\bar{V}_3 - V_3)^2/12M_+^3 \equiv c_1$
A_1	A_1	A_2	A_2	$-V_3(\bar{V}_3 - V_3)/6M_-M_+^2 \equiv c_2$
A_1	A_1	A_1	A_2	$V_3(\bar{V}_3 - V_3)/3M_-^{1/2}M_+^{5/2} \equiv c_3$
A_2	A_2	A_2	A_2	$V_3^2/12M_-^2M_+ \equiv c_4$
A_1	A_2	A_2	A_2	$-V_3^2/3M_-^{3/2}M_+^{3/2} \equiv c_5$
A_1	A_2	A_1	A_2	$V_3^2/6M_-M_+^2 \equiv c_6$
A_1	A_2	A_2	A_1	c_6
E_1	E_1	E_1	E_1	$2c_1$
E_1	E_1	E_2	E_2	$2c_2$
E_1	E_1	E_1	E_2	$2c_3$
E_2	E_2	E_2	E_2	$2c_4$

TABLE 1

VALUES OF THE COMBINATORIAL FACTOR $C(Q_1\ Q_2;\ Q_1'\ Q_2')^*$ (cont'd)

Q_1	Q_2	Q_1'	Q_2'	$C(Q_1\ Q_2;\ Q_1'\ Q_2')$
E_1	E_2	E_2	E_2	$2c_5$
E_1	E_2	E_1	E_2	$2c_6$
E_1	E_2	E_2	E_1	$2c_6$
T_0	T_0	T_0	T_0	$\bar{v}_3^{\,2}/M_+M_-^{\,2}$
T_0	T_0	T_0	T_1	$-\bar{v}_3^{\,2}2\sqrt{2}/M_+^{\,3/2}M_-^{\,3/2}$
T_0	T_0	T_1	T_1	$\bar{v}_3(\bar{v}_3 - v_3)/M_+^{\,2}M_-$
T_0	T_0	T_2	T_2	$-v_3\bar{v}_3/M_-^{\,2}M_+$
T_0	T_0	T_1	T_2	$2v_3\bar{v}_3/M_+^{\,3/2}M_-^{\,3/2}$
T_0	T_1	T_0	T_1	$\bar{v}_3^{\,2}/M_-M_+^{\,2}$
T_0	T_1	T_1	T_0	$\bar{v}_3^{\,2}/M_-M_+^{\,2}$
T_0	T_1	T_1	T_1	$-\bar{v}_3(\bar{v}_3 - v_3)\sqrt{2}/M_+^{\,5/2}M_-^{\,1/2}$

TABLE 1

VALUES OF THE COMBINATORIAL FACTOR $C(Q_1\ Q_2;\ Q_1'\ Q_2')$* (cont'd)

Q_1	Q_2	Q_1'	Q_2'	$C(Q_1\ Q_2;\ Q_1'\ Q_2')$
T_0	T_1	T_2	T_2	$\bar{V}_3 V_3 \sqrt{2}/M_-^{3/2} M_+^{3/2}$
T_0	T_1	T_1	T_2	$-\bar{V}_3 V_3 \sqrt{2}/M_+^{2} M_-$
T_0	T_1	T_2	T_1	$-\bar{V}_3 V_3 \sqrt{2}/M_+^{2} M_-$
T_1	T_1	T_1	T_1	$3c_1$
T_1	T_1	T_2	T_2	$3c_2$
T_1	T_1	T_1	T_2	$3c_3$
T_2	T_2	T_2	T_2	$3c_4$
T_1	T_2	T_2	T_2	$3c_5$
T_1	T_2	T_1	T_2	$3c_6$
T_1	T_2	T_2	T_1	$3c_6$

*See footnotes to table 2.

a factor two. In an analogous way, the factors 'C' containing T^x_{1u} symmetry coordinates have been multiplied by three to take into account T^y_{1u} and T^z_{1u} terms. The factor arising from rule (v), which is included in 'C', was calculated in the following way. It includes a factor equal to the number of times $Q_1(A_{1g})$ occurs at each vertex (since there is a choice in selecting which of these will be transformed to give the external label p_A) together with a factor two if the remaining two coordinates at either vertex are identical (since these are then interchangeable). Equation (5) can be reduced to a form suitable for calculation by following the procedure used in chapter 4. The elements of $\overline{G}$ can be formally expanded in the $\{p\}$-representation and the summation on ℓ_1 performed. Taking the imaginary part of the result gives

$$\mathrm{Im}\{M(\omega + i0^+;p_A)\} = \pi\hbar \sum'_{\substack{Q_1Q_1' \\ Q_2Q_2'}} C(Q_1Q_2;Q_1'Q_2') \sum_{p_1,p_2} U_{Q_1,p_1} U_{Q_2,p_2} \times$$

$$\times \frac{1}{4\omega_{p_1}\omega_{p_2}} \{ (1 + n_1 + n_2)\, \delta(\omega_{p_1} + \omega_{p_2} - \omega) + (n_1 - n_2) \times$$

$$\delta(\omega_{p_2} - \omega_{p_1} - \omega) - \delta(\omega_{p_1} - \omega_{p_2} - \omega) \} U_{p_2,Q_2'} U_{p_1,Q_1'} \,. \qquad (6)$$

The notation,

$$n_i \equiv n(\omega_{p_i}) = (e^{\beta\hbar\omega_{p_i}} - 1)^{-1} \quad , \quad i = 1,2 \quad , \qquad (7)$$

has been used for the Bose-Einstein distribution function. The δ-functions in equation (6) can be rewritten, using

$$\delta(\omega_2 \pm \omega_1 - \omega) = \int_0^\omega d\omega' \; \delta(\omega_1 - \omega') \; \delta(\omega_2 - \omega \pm \omega') \quad , \qquad (8)$$

which is valid for positive frequencies, and the summations on p_1 and p_2 can be performed to give a result in the form

$$\mathrm{Im}\{M(\omega + i0^+;p_A)\} = \frac{\hbar}{\pi} \sum_{\substack{Q_1Q_1' \\ Q_2Q_2'}} C(Q_1Q_2;Q_1'Q_2') \; \{ \; I_1(\omega) + I_2(\omega) \; \}. \qquad (9)$$

Here

$$I_1(\omega) \equiv \int_0^\omega d\omega' \; \{ \; 1 + n(\omega') + n(\omega - \omega') \; \} \; \mathrm{Im}\, \bar{G}(\omega'^2 + i0^+;Q_1,Q_1') \; x$$

$$x \; \mathrm{Im}\, \bar{G}((\omega - \omega')^2 + i0^+;Q_2,Q_2') \qquad (10)$$

gives the contribution of the "decay" mechanism, while

$$I_2(\omega) \equiv \int_0^\omega d\omega' \; \{ \; n(\omega') - n(\omega + \omega') \} \; \{ \; \mathrm{Im}\, \bar{G}(\omega'^2 + i0^+;Q_1,Q_1') \; x$$

$$x \; \mathrm{Im}\, \bar{G}((\omega + \omega')^2 + i0^+;Q_2,Q_2') \; \mathrm{Im}\, \bar{G}(\omega'^2 + i0^+;Q_2,Q_2')$$

$$x \; \mathrm{Im}\, \bar{G}((\omega + \omega')^2 + i0^+;Q_1,Q_1') \; \} \qquad (11)$$

gives the contribution due to absorption of an acoustic

phonon.

The required width can be related to the quantity $\mathrm{Im}\{M(p_A)\}$ using equation (41) of chapter 2. The imaginary part of that equation gives, using equation (17) of chapter 2,

$$\mathrm{Im}\, G^A(\omega + i0^+;p_A) = \frac{\mathrm{Im}\, M(\omega + i0^+;p_A)}{(\omega_A^2 - \omega^2)^2 + (\mathrm{Im}\, M(\omega + i0^+;p_A))^2} \quad . (12)$$

Here the frequency shift due to anharmonic processes has been neglected. If the imaginary part of the self-energy is approximately constant for ω near ω_A, equation (12) describes a Lorentzian peak whose full width at half maximum, (half-width), $W(p_A)$, is given by

$$W(p_A) = \frac{1}{\omega_A} \cdot \mathrm{Im}\, M(\omega_A + i0^+;p_A) \quad . \quad (13)$$

The width $W(p_A)$ has been determined from this equation with equation (9) for various temperatures. The elements of $\bar{G}$ were calculated, as before, using the method described in appendix 3, and the values used for the anharmonic coefficients were

$$\bar{V}_3 = 0.9 \times 10^{12} \text{ dyne/cm}^2 \qquad \text{(see chapter 4)} \qquad (14)$$

$$V_3 = 6.2 \times 10^{12} \text{ dyne/cm}^2 \qquad \text{(see appendix 4).} \qquad (15)$$

The results for $W(p_A)$ are plotted in figure 18, together with some experimental values of Klein (1966) for the width

of the gap mode in the sideband spectrum. To allow a meaningful comparison to be made, $W(p_A)$ must be corrected for the half-width, W(P), of the high frequency local mode phonon P. The corrected value $W'(p_A)$ is approximately given by the sum of the two widths since the peaks are approximately Lorentzian. The half-width W(P) for KI:KH has been measured as 14.5 cm^{-1} at $90^{o}K$ by Fritz et al. (1965) and its value at other temperatures was estimated by assuming a T^2-dependence (the results of the next section indicate that this is a good approximation for the present purpose). The results for $W'(p_A)$ are also shown in figure 18. It can be seen that its behaviour at high temperatures is largely determined by that of the high frequency local mode, whereas as low temperatures, W(P) can be neglected and a useful comparison of the present results with experiment is possible. The theoretical estimates are smaller than experimental results, by a factor approximately two at low temperatures. This disagreement may arise from several sources; the likliest source is neglected terms in the anharmonic Hamiltonian. The most important group of such terms is the group of terms proportional to the transverse cubic anharmonic coefficient. Although this coefficient is smaller than V_3, it gives rise to a large number of terms, namely, those connecting the motion of each of the ions involved in the A_{1g} localized mode with

the motions of its six nearest neighbours. Inclusion of these terms would require, in addition to $\overline{V}_2$, which can be estimated using equation (6) of appendix 4, knowledge of the corresponding quantity in the perfect lattice, which can be determined using the shell model parameters referred to in appendix 4. However, the large number of added terms would greatly complicate the computational task of evaluating the broadening; for this reason, they have been neglected in the present treatment. It should be pointed out, however, that a similar effect, depending on transverse cubic anharmonic coefficients between the impurity and its nearest neighbours, considerably influenced the shape of the sideband spectrum. Therefore, it may be expected that including similar terms in the broadening can produce a significant improvement in agreement with experiment.

A second possible source of the discrepancy is the approximate form, given in equation (4), for the displacement corresponding to the A_{1g} localized mode. However, it does not seem likely that the error introduced by this approximation, which is of order 10%, could account for the factor of two discrepancy between theory and experiment.

In order to demonstrate the importance of calculating with perturbed phonons, the half-width $W(p_A)$ was also calculated from equation (13) using unperturbed phonons (i.e.

replacing $\bar{G}$ by G in equations (10) and (11)). The theoretical results obtained in this way were approximately a factor two smaller than those obtained using perturbed phonons, at low temperatures. Since the perturbation weakens the force constants near the defect, the amplitudes of vibration of ions close to the impurity are, roughly speaking, larger at lower frequencies than they would be in the unperturbed system, as can be seen from figure 15. This has the effect of increasing the density of states available for decay of the gap mode into acoustic phonons, thus increasing its broadening. Such an effect is also important in evaluating the probability of decay for the high frequency local mode, which is discussed in the next section.

C. BROADENING OF THE U-CENTRE LOCAL MODE PHONON

At low temperatures, the anharmonic broadening of the U-centre local mode is determined by the "decay" mechanism. For the H^- ion case, the lowest order process that can occur is decay of the local mode phonon into three lattice phonons, whereas, in the D^- ion case, decays into both two and three phonons are important (Elliott et al. 65). At higher temperatures another mechanism, the "scattering" mechanism, (called by Klein (1968) the "Raman" mechanism) becomes increasingly important, and strong

arguments have been given to predict that it eventually dominates (Elliott et al. 65; Ivanov et al. 66). The results of the present calculation confirm this prediction for KBr and KI. The leading anharmonic terms for the decay mechanism are cubic and quartic anharmonic interactions between the H^- or D^- ion and its nearest neighbours, and are given in equations (4) and (5) of appendix 2. The contributions to the self-energy resulting from decay into two or three phonons will be denoted by M^{II} and M^{III}, respectively, and can be found by evaluating the diagrams shown in figure 19. Applying the rules of appendix 1 gives

$$M_{\ell}^{II}(P_x) = \frac{1}{\beta} \sum_{\substack{Q_1 Q_1' \\ Q_2 Q_2'}}{}' C^{II}(Q_1 Q_2; Q_1' Q_2') \sum_{\ell_1} \bar{G}_{\ell_1}(Q_1, Q_1') \times$$

$$\times \bar{G}_{\ell-\ell_1}(Q_2, Q_2') \qquad (16)$$

$$M_{\ell}^{III}(P_x) = \frac{1}{\beta} \sum_{\substack{Q_1 Q_1' \\ Q_2 Q_2' \\ Q_3 Q_3'}} C^{III}(Q_1 Q_2 Q_3; Q_1' Q_2' Q_3') \times$$

$$\times \sum_{\ell_1 \ell_2} \bar{G}_{\ell_1}(Q_1, Q_1') \, \bar{G}_{\ell_2}(Q_2, Q_2') \, \bar{G}_{\ell-\ell_1-\ell_2}(Q_3, Q_3') \, . \qquad (17)$$

The quantities $C^{II}(Q_1 Q_2; Q_1' Q_2')$ and $C^{III}(Q_1 Q_2 Q_3; Q_1' Q_2' Q_3')$ contain anharmonic constants and combinatorial factors as

TABLE 2

VALUES OF COMBINATORIAL FACTOR $C^{II}(Q_1\ Q_2;\ Q_1'\ Q_2')$*†

Q_1	Q_2	Q_1'	Q_2'	$C(Q_1\ Q_2;\ Q_1'\ Q_2')/\overline{V}_3^{\,2}$
T_0	A_1	T_0	A_1	$2/3M_-M_+M_D$
T_0	A_1	T_1	A_1	$-2\sqrt{2}/3M_-^{1/2}M_+^{3/2}M_D$
T_1	A_1	T_1	A_1	$1/3M_DM_+^{\,2}$
T_0	E_1	T_0	E_1	$4/3M_-M_+M_D$
T_0	E_1	T_1	E_1	$-4\sqrt{2}/3M_-^{1/2}M_+^{3/2}M_D$
T_1	E_1	T_1	E_1	$2/3M_DM_+^{\,2}$

* NOTE The following notation has been used: $A_i \equiv Q_i(A_{1g})$

$E_i \equiv Q_i(E_g)$

$T_i \equiv Q_i(T_{1u})$

† NOTE The factors have been adjusted so that only the listed labellings should be used.

TABLE 3

VALUES OF THE COMBINATORIAL FACTOR $C^{III}(Q_1\ Q_2\ Q_3;\ Q_1'\ Q_2'\ Q_3')$*

Q_1	Q_2	Q_3	Q_1'	Q_2'	Q_3'	$C^{III}(Q_1\ Q_2\ Q_3;\ Q_1'\ Q_2'\ Q_3')/\bar{V}_4^2$
T_0	T_0	T_0	T_0	T_0	T_0	$2/3M_-^3M_{H,D}$
T_0	T_0	T_0	T_0	T_0	T_1	$-2\sqrt{2}/M_-^{5/2}M_+^{1/2}M_{H,D}$
T_0	T_0	T_0	T_0	T_1	T_1	$2/M_-^2M_+M_{H,D}$
T_0	T_0	T_0	T_1	T_1	T_1	$-\sqrt{2}/3M_-^{3/2}M_+^{3/2}M_{H,D}$
T_0	T_0	T_1	T_0	T_0	T_1	$1/M_-^2M_+M_{H,D}$
T_0	T_1	T_0	T_0	T_0	T_1	$2/M_-^2M_+M_{H,D}$
T_0	T_0	T_1	T_0	T_1	T_1	$-2\sqrt{2}/M_-^{3/2}M_+^{3/2}M_{H,D}$
T_1	T_0	T_0	T_0	T_1	T_1	$-\sqrt{2}/M_-^{3/2}M_+^{3/2}M_{H,D}$
T_0	T_0	T_1	T_1	T_1	T_1	$1/M_-M_+^2M_{H,D}$
T_0	T_1	T_1	T_0	T_1	T_1	$1/2M_-M_+^2M_{H,D}$
T_1	T_0	T_1	T_0	T_1	T_1	$1/M_-M_+^2M_{H,D}$
T_0	T_1	T_1	T_1	T_1	T_1	$-1/\sqrt{2}\ .\ M_+^{5/2}M_-^{1/2}M_{H,D}$

TABLE 3

VALUES OF THE COMBINATORIAL FACTOR $C^{III}(Q_1\ Q_2\ Q_3;\ Q_1'\ Q_2'\ Q_3')^*$ (cont'd)

Q_1	Q_2	Q_3	Q_1'	Q_2'	Q_3'	$C^{III}(Q_1\ Q_2\ Q_3;\ Q_1'\ Q_2'\ Q_3')/\bar{V}_4^2$
T_1	T_1	T_1	T_1	T_1	T_1	$1/12M_+^3M_{H,D}$
T_0	A_1	A_1	T_0	A_1	A_1	$1/18M_-M_+^2M_{H,D}$
T_0	A_1	A_1	T_1	A_1	A_1	$-\sqrt{2}/18M_+^{5/2}M_-^{1/2}M_{H,D}$
T_0	A_1	E_1	T_0	A_1	E_1	$2/9M_+^2M_-M_{H,D}$
T_0	A_1	E_1	T_1	A_1	E_1	$-2\sqrt{2}/9M_+^{5/2}M_-^{1/2}M_{H,D}$
T_0	E_1	E_1	T_0	E_1	E_1	$2/9M_+^2M_-M_{H,D}$
T_0	E_1	E_1	T_1	E_1	E_1	$-2\sqrt{2}/9M_+^{5/2}M_-^{1/2}M_{H,D}$
T_1	A_1	A_1	T_1	A_1	A_1	$1/36M_+^3M_{H,D}$
T_1	A_1	E_1	T_1	A_1	E_1	$1/9M_+^3M_{H,D}$
T_1	E_1	E_1	T_1	E_1	E_1	$1/9M_+^3M_{H,D}$

*See footnotes to table 2.

before, and are given in Table 2 and Table 3, respectively. Their values have been adjusted to account for labellings leading to equal contributions, and therefore, only the listed labellings should be used. It should be noted that both quantities contain the factor $M_-/M_{H,D}$ where $M_{H,D}$ is the mass of the hydrogen or deuterium impurity. This factor results from transformation of a displacement coordinate $Q_0(T^x_{1u})$ at each vertex to give the external label P_x, using the matrix element given in equation (3) of chapter 4.

Applying the procedure of the previous section allows reduction of the imaginary parts of M^{II} and M^{III} to the forms

$$\text{Im } M^{II}(\omega + i0^+;P_x) = \frac{\hbar}{\pi}\,\theta(\omega - \omega_m) \sum_{\substack{Q_1Q_1' \\ Q_2Q_2'}} C^{II}(Q_1Q_2;Q_1'Q_2') \times$$

$$\times \int_{\omega-\omega_m}^{\omega_m} d\omega' \{ 1 + n(\omega') + n(\omega - \omega') \} \text{ Im } \bar{G}(\omega'^2 + i0^+;Q_1,Q_2) \times$$

$$\times \text{ Im } \bar{G}((\omega - \omega')^2 + i0^+;Q_2,Q_2') \qquad (18)$$

for the broadening due to decay into two phonons, and

$$\text{Im } M^{III}(\omega + i0^+;P_x) = \frac{\hbar^2}{\pi^2} \sum_{\substack{Q_1Q_1' \\ Q_2Q_2' \\ Q_3Q_3'}} C^{III}(Q_1Q_2Q_3;Q_1'Q_2'Q_3') \times$$

$$x \int_0^{\omega_m} d\omega' \int_0^{\omega_m} d\omega'' \, \theta(\omega - \omega' - \omega'') \{ (1 + n(\omega'))(1 + n(\omega'')) \, x$$

$$x \, (1 + n(\omega - \omega' - \omega'')) - n(\omega') \, n(\omega'') \, n(\omega - \omega' - \omega'') \, x$$

$$x \, \mathrm{Im} \, \bar{G}((\omega - \omega' - \omega'')^2 + i0^+; Q_1, Q_1')$$

$$x \, \mathrm{Im} \, \bar{G}(\omega'^2 + i0^+; Q_2, Q_2') \cdot \mathrm{Im} \, \bar{G}(\omega''^2 + i0^+; Q_3, Q_3') \qquad (19)$$

for the broadening due to decay into three phonons. In these expressions, the function $\theta(\omega)$ is the step function, defined by

$$\theta(\omega) = 1 \qquad \text{for } \omega \geq 0$$

$$= 0 \qquad \text{for } \omega < 0 \; . \qquad (20)$$

The scattering mechanism broadens the local mode by scattering a thermally excited lattice phonon into another state of the same frequency. This process requires interaction of four phonons, and can therefore occur directly through the quartic anharmonic interaction or indirectly through two successive cubic anharmonic interactions. In the present calculation, the truncated cubic anharmonic Hamiltonian introduced by Elliott et al. (1965) is used, which contains only terms in which two of the three phonons interacting are local mode phonons. The anharmonic terms which have been considered in evaluating the contribution of the scattering mechanism are given in

equation (6) of appendix 2.

The largest non-vanishing contributions arise from the processes shown schematically in figure 20a (Elliott et al. 65). It can be seen from the anharmonic terms that the lines referring to lattice phonons must be labelled by symmetry coordinates which are either even for both lines or odd for both lines, and that the indirect transition process occurs only when both lines refer to even symmetry. The effect of the indirect processes can be included in the contribution of the direct processes simply by replacing the anharmonic constant $\bar{V}_4$ by $\tilde{V}_4$, where

$$\begin{aligned} \tilde{V}_4 &= \bar{V}_4 && \text{both lines of odd symmetry} \\ &= \bar{V}_4 - \frac{\bar{V}_3^{\,2}}{4M_{H,D}\Omega^2_{H,D}} && \text{both lines of even symmetry.} \end{aligned} \tag{21}$$

The quantity $\Omega_{H,D}$ is equal to the local mode frequency of a hydrogen or deuterium U-centre, as appropriate. This result for $\tilde{V}_4$, given by Elliott et al. (1965), can be seen to be correct by comparing the matrix elements for the direct and indirect transitions.

The contribution of the scattering process to the self-energy of the local mode can be obtained by evaluating the diagram in figure 20b. Labelling this contribution M^s and following the procedure of the previous section,

leads to the result

$$\text{Im } M^s(\omega = \Omega_{H,D}; P_x) = \frac{\hbar^2 M_-}{\pi \Omega_{H,D} M_{H,D}} \sum_{\substack{Q_1 Q_1' \\ Q_2 Q_2'}} C^s(Q_0(T_{1u}^x) Q_1 Q_2; Q_0(T_{1u}^x) Q_1' Q_2') \times$$

$$\times \int_0^{\omega_m} d\omega' \; n(\omega') \{ 1 + n(\omega') \} \cdot \text{Im } \bar{G}(\omega'^2 + i0^+; Q_1, Q_1') \times$$

$$\times \text{Im } \bar{G}(\omega'^2 + i0^+; Q_2, Q_2') \qquad . \qquad (22)$$

This equation, as well as equations (18) and (19), have been obtained in a slightly different form by Ipatova and Klotchichin (66). The values of C^s, which contain the constants $\tilde{V}_4$, are given in Table 4. They have been adjusted, as before, so that only the labellings listed must be considered.

The contributions to the self-energy of the high frequency local mode given by equations (18), (19) and (22) have been separately evaluated for both hydrogen and deuterium U-centres at several temperatures, again calculating the matrix elements of $\bar{G}$ as described in appendix 3. The values of $\bar{V}_3$ given in equation (19) of chapter 4 were used together with the following values of $\bar{V}_4$:

$$\bar{V}_4 = 1.95 \times 10^{20} \text{ dyne/cm}^3 \quad \text{for KI}$$

$$= 2.45 \times 10^{20} \text{ dyne/cm}^3 \quad \text{for KBr} \qquad (23)$$

which are discussed in appendix 4. The half-width $W(P_x)$

TABLE 4

VALUES OF THE COMBINATORIAL FACTOR $C^S(Q_0(T^x_{1u})\ Q_1\ Q_2;\ Q_0(T^x_{1u})\ Q'_1\ Q'_2)$*

Q_1	Q_2	Q'_1	Q'_2	$C^S(Q_0(T^x_{1u})\ Q_1\ Q_2;\ Q_0(T^x_{1u})\ Q'_1\ Q'_2)/\tilde{V}_4^2$
T_0	T_0	T_0	T_0	$2/M_-^3 M_{H,D}$
T_0	T_0	T_1	T_1	$2/M_-^2 M_+ M_{H,D}$
T_0	T_0	T_0	T_1	$-4\sqrt{2}/M_-^{5/2} M_+^{1/2} M_{H,D}$
T_1	T_1	T_1	T_1	$1/2M_- M_+^2 M_{H,D}$
T_1	T_1	T_0	T_1	$-2\sqrt{2}/M_-^{3/2} M_+^{3/2} M_{H,D}$
T_0	T_1	T_0	T_1	$2/M_-^2 M_+ M_{H,D}$
T_0	T_1	T_1	T_0	$2/M_-^2 M_+ M_{H,D}$
A_1	A_1	A_1	A_1	$1/18M_+^2 M_- M_{H,D}$
E_1	E_1	E_1	E_1	$2/9M_+^2 M_- M_{H,D}$
A_1	E_1	A_1	E_1	$2/9M_+^2 M_- M_{H,D}$

*See footnotes to table 2.

was then evaluated using

$$W(P_x) = \frac{1}{\Omega_{H,D}} \text{Im } M(\Omega_{H,D} + i0^+; P_x) \quad , \qquad (24)$$

where

$$M = M^{II} + M^{III} + M^{S} \quad . \qquad (25)$$

The results for both hydrogen and deuterium U-centres are plotted in figures 21 and 22 for KBr and KI respectively, together with some experimental results of Mirlin and Reshina (1964), of Schaefer (1960) and of Fritz et al. (1965). The calculations indicate that $W(P_x)$ is essentially determined by the scattering mechanism above about $10^{o}K$ for hydrogen U-centres in both KBr and KI, and above $50^{o}K$ and $30^{o}K$ for deuterium U-centres in KBr and KI respectively. This is in general agreement with the conclusions of Elliott et al. (1965), based on numerical estimates in $CaF:H^-$ and $CaF:D^-$, and also those of Ivanov et al. (1966) and of Ipatova and Klotchichin (1966).

Comparison between theory and experiment is at present restricted to temperatures above $50^{o}K$ by the available data, that is, to the range in which the theoretical result is almost independent of the contributions of the decay mechanism. Therefore, while the general, low temperature, behaviour of $W(P_x)$ for hydrogen and deuterium U-centres in KBr and KI corresponds qualitatively to results of experimental measurements in other alkali

halides (Fritz et al. 65; Bauerle and Fritz 67), a quantitative comparison must await further experimental investigation. At higher temperatures, where data are available for comparison, it can be seen that the theoretical values are too small by a factor close to ten. This error probably results either from the use of an incorrect value for the anharmonic constant $\bar{V}_4$ of from the use of the truncated Hamiltonian in calculating the second order cubic anharmonic contributions to the scattering process. If an underestimate of $\bar{V}_4$ is assumed to be the dominating error, then, since the contribution of the scattering process to the self energy is essentially proportional to $\bar{V}_4^2$, the value of $\bar{V}_4$ used must be in error by a factor of order three. Since the value used depends directly on the parameter ξ, whose estimation is discussed in appendix 4, it is possible that such a large error has been made. It should be noted that where this parameter has been used before in the work, for calculating sideband spectrum shape and evaluating $\bar{V}_3$ from the sideband area, the results have been insensitive to the value of ξ. However, the truncation of the cubic anharmonic Hamiltonian may also have influenced the magnitude of the result. Until the validity of this truncation has been fully investigated, the value of $\bar{V}_4$ should not be adjusted to fit the experimental results. The situation would be clearer if comparison between theory

and experiment at lower temperatures, where the decay mechanism is dominant, could be achieved. Since corrections to the contribution of the decay process, the most important of which result from neglect of terms in the Hamiltonian proportional to the transverse anharmonic coupling, should not be large, such a comparison would reveal any errors in $\overline{V}_3$ and $\overline{V}_4$.

Experimental values for the half-width at low temperatures are available in other alkali halides (Fritz et al. 65; Bauerle and Fritz 67). However, before broadening calculations are attempted in these crystals, it is important that any force constant model used to describe the U-centre should adequately reproduce experimental defect spectra, such as the sideband and far infrared lineshapes. The importance of using such a model in estimating the broadening of localized modes can be demonstrated by repeating the present calculations using unperturbed densities of states, that is, replacing $\overline{G}$ by G in equations (18), (19) and (22). The elements of $\mathrm{Im}\{G\}$ and $\mathrm{Im}\{\overline{G}\}$ occurring in those equations are shown in figures 15 and 16 for KI and KBr, respectively. The results show that the use of unperturbed phonons leads to results which differ widely from those presented above, especially at low temperatures where the decay mechanism is dominant. For example, $W(P_x)$ was found to be larger by a factor of order

four for KI:KD at 10°K when unperturbed spectra were used. The reason for this dependence is that the broadening resulting from the decay process is determined by the amplitudes of vibration of ions near the defect at optical frequencies. Since the force constants near the impurity have been weakened, these amplitudes are smaller and, consequently, there is less broadening. The contribution of the scattering mechanism, which is negligible at very low temperature, is, in fact, smaller when unperturbed phonons are used. This is understandable since there are always more thermally excited acoustic than optical phonons, and their contribution to the scattering part of the broadening is smaller in the unperturbed crystal.

Before closing this discussion, one other result of the calculations should be mentioned. The contribution of the two-phonon decay process to the broadening of the deuterium peaks was found to be smaller by an order of magnitude than that of the three-phonon decay process. This is a consequence of the fact that the two phonons in the final state of the cubic process must be high frequency optical phonons, whereas the three phonons in the final state of the quartic process are essentially unrestricted in frequency. This has been pointed out by Ivanov et al. (1966) in discussing measurements on KBr:KD. It is interesting to speculate that, since the final

three-phonon state is similarly restricted in the case of hydrogen impurity, it might be necessary to include processes of one higher order to account for the residual width of such U-centres.

D. BROADENING OF RESONANCES

It has been shown in chapters 4 and 5 that some of the peaks observed in optical absorption spectra are resonances resulting from local perturbations associated with the impurity. The peaks predicted theoretically are in every case narrower than those observed experimentally, and are, in fact, narrower than the observed A_{1g} local mode peak observed in the gap in KI:KH. It is therefore likely that observed peak widths, for resonances as well as for the A_{1g} local mode in KI:KH, are due to anharmonic broadening.

The methods of this chapter allow calculation of the broadening in cases where a peak is due to a single mode whose frequency is outside the continuous frequency spectrum and which is therefore truly localized. However, the predicted resonances lie in the continuum and involve many modes which, though they have enhanced amplitude near the impurity, are not truly localized (Klein 63). Therefore, two questions must be answered to produce a theory of anharmonic broadening of resonance peaks: first, how are

the continuum spectra to be expressed in terms of broadened continuum modes, and second, how is the broadening to be calculated for modes which are neither truly localized nor modes of the perfect lattice?

The first question can be answered by considering the displacement corresponding to a particular mode of the perturbed lattice. For continuum modes, this displacement is given by Klein (1963)

$$U_{\underline{L}\alpha\kappa,p(\underline{k}j)} = U_{\underline{L}\alpha\kappa,\underline{k}j} -$$

$$- \sum_{\substack{\underline{L}'\alpha'\kappa' \\ \underline{L}''\alpha''\kappa''}} G(\omega^2_{\underline{k}j} + i0^+;\underline{L}\alpha\kappa,\underline{L}\alpha'\kappa') \; T(\omega^2_{\underline{k}j} + i0^+;\underline{L}'\alpha'\kappa',\underline{L}''\alpha''\kappa'') \; x$$

$$x \; U_{\underline{L}''\alpha''\kappa'',\underline{k}j} \qquad . \qquad (26)$$

Here $p(\underline{k}j)$ is the eigenmode of the perturbed lattice corresponding to the $(\underline{k}j)$th mode of the unperturbed lattice. The elements of the T matrix, and therefore the non-zero terms in the sums, are restricted to the space of γ. The elements of $\mathrm{Im}\{G^A\}$ in the $\{\underline{L}\alpha\kappa\}$-representation, for frequencies in the continuum, are given by

$$\mathrm{Im}\; G^A(\omega^2 + i0^+;\underline{L}\alpha\kappa,\underline{L}'\alpha'\kappa')$$

$$= \sum_{\underline{k}j} U_{\underline{L}\alpha\kappa,p(\underline{k}j)} \frac{\mathrm{Im}\; M(\omega + i0^+;p(\underline{k}j)}{(\omega^2 - \omega^2_{\underline{k}j})^2 + (\mathrm{Im}\; M(\omega + i0^+;p(\underline{k}j))^2} \; x$$

$$x \; U_{p(\underline{k}j),\underline{L}'\alpha'\kappa'} \qquad . \qquad (27)$$

For the sideband calculation, only a few elements of G^A are required in the $\{\underline{L}\alpha\kappa\}$-representation, and these can be found from equation (27) using equation (26). In the far infrared calculation, the quantity required is

$$\sum_{\substack{\underline{L}\kappa \\ \underline{L}'\kappa'}} \frac{e_\kappa e_{\kappa'}}{\sqrt{M_\kappa M_{\kappa'}}} \operatorname{Im} G^A(\omega^2 + i0^+; \underline{L}x\kappa, \underline{L}'x'\kappa')$$

$$= \sum_{\underline{k}j} \left| \sum_{\underline{L}\kappa} \frac{e_\kappa}{\sqrt{M_\kappa}} U_{\underline{L}x\kappa, p(\underline{k}j)} \right|^2 \frac{\operatorname{Im} M(\omega + i0^+; p(\underline{k}j))}{(\omega^2 - \omega^2_{\underline{k}j})^2 + (\operatorname{Im} M(\omega + i0^+; p(\underline{k}j)))^2} \quad . \qquad (28)$$

This can be reduced to a from suitable for calculation using the result

$$\sum_{\underline{L}\kappa} \frac{e_\kappa}{\sqrt{M_\kappa}} U_{\underline{L}x\kappa, p(\underline{k}j)} = \frac{e}{\sqrt{\mu}} \left[\delta_{\underline{k}j, R_x} \right.$$

$$- \sum_{\substack{\underline{L}'\alpha'\kappa' \\ \underline{L}''\alpha''\kappa''}} G(\omega^2_{\underline{k}j} + i0^+; R_x, \underline{L}'\alpha'\kappa') \, T(\omega^2_{\underline{k}j} + i0^+; \underline{L}'\alpha'\kappa', \underline{L}''\alpha''\kappa'') \, x$$

$$\left. x \, U_{\underline{L}''\alpha''\kappa'', \underline{k}j} \right] \quad , \qquad (29)$$

which follows from the same considerations used in deriving equation (1) of chapter 5, and is easily calculable because of the restriction of the sums to the space of γ.

In results (27) and (28), the required spectra have been written as sums on individual phonons, whose frequencies are the same as those of the unperturbed crystal. The contribution of each phonon is a broadened

phonon peak with projection factors calculated correctly for the perturbed crystal. Calculation of the broadening of the phonon peaks would answer the second question; unfortunately, this calculation cannot be carried out using either the techniques used here for purely localized phonons, or those developed elsewhere (e.g. Maradudin and Fein 62) for unperturbed phonons. It is expected that the broadening of modes near the resonance will lie between the values appropriate to a completely localized mode of the same symmetry and the values appropriate to the corresponding unperturbed modes. For the present, no quantitative calculation of that broadening will be attempted.

CHAPTER 7

CONCLUSION

The extended force constant model which has been developed for the defect has led to a considerably improved understanding of both the sideband absorption and the far infrared absorption associated with U-centres in KI and KBr. The symmetries of the resonance peaks observed in the sideband spectra have been predicted from the theory and these predictions have been partially verified experimentally by observing the behaviour of the peaks under uniaxial stress (Fritz et al. 67). Also, one of the peaks in the impurity-induced far infrared spectra of both KI and KBr has been shown to arise from a resonance mode (of T_{1u} symmetry) while other absorption maxima have been related to sharp peaks in the unperturbed density of states. However, the precise correspondence between the theoretical and experimental peaks in that calculation is not yet well-defined. The difficulty lies in the fact that the exact peak positions are determined both by the model used for the defect and also by the positions of sharp maxima in the perfect densities of states, which in the present case are determined from the shell model. Since some of these maxima arise from regions of $\underline{k}$-space where the phonons

have not been directly measured by neutron diffraction, their positions could be in error by a few wavenumbers. Further experimental investigation of both the perfect and perturbed crystals should allow a positive identification of peaks in the far infrared spectra to be made. Since this gives an additional experimental resonance frequency, it should be considered together with the local mode frequency and the two resonance frequencies of the sideband in evaluating the parameters of future models of the U-centre.

Apart from effects resulting from the neglect of anharmonic broadening in the calculations of these spectra, essentially two differences remain between theory and experiment. These are first, that the relative intensities of peaks (especially in the sideband calculations) are not correctly given, and second, that the positions of some of the resonance peaks in the theory are in error by a few wavenumbers (possibly as many as 9 cm^{-1} in the far infrared calculation for KI:KH). While the first error must be largely due to the neglect of higher-order processes which can contribute to absorption in the sideband region, both errors may result in part from using an oversimplified model. A more realistic model of the impurity would allow for many changes of force constant; the strongest being those connecting the impurity to its nearest neighbours, and a

series of smaller changes associated with relaxation of the lattice about the impurity. The present theory attempts to describe these effects with the two parameters Δf and Δg. It is therefore not surprising that the fitting of all resonance frequencies is not perfect, nor would it be surprising to find that the description of vibrational amplitudes of ions near the defect proved to be only approximate. However, that a single choice of Δf and Δg fits so many data so closely suggests that the most significant force constant changes for the problems studied are indeed the ones which have been included.

The perturbations associated with the impurity are such that some phonons become localized, or in some cases approximately localized, near the defect. A method was presented in chapter 6 which shows how the broadening of such phonons can be calculated by taking advantage of their localized nature. The method was applied to the calculation of the half-width of the high frequency U-centre local mode in KI and KBr, and also to that of the localized gap mode in KI:KH. The results of those calculations were discussed in detail in chapter 6, but it is worthwhile emphasising two of the conclusions here. First, it was shown that especially at low temperatures, where the "decay" mechanism is dominant, it is important to use perturbed phonons in the calculation. The decrease in force constants around

the defect considerably increases the effective density of states for decay into acoustic phonons, while the effective density of states for decay into high frequency phonons is decreased. The effect of this is to reduce the residual width of the high-frequency local mode (since it can only decay into optical phonons), whereas the width of the gap mode in KI:KH is considerably increased (since it decays only into acoustic phonons).

The second conclusion of chapter 6 is that the half-widths depend critically on the values of anharmonic constants near the defect. Since only the determination of the constant $\overline{V}_3$ is at all reliable (see chapter 4 and appendix 4), it seems sensible to use $\overline{V}_4$ and V_3 as parameters in future calculations. The values obtained in that way could then be used to determine details of the forces near the defect. Before this can be done however, the importance of the corrections suggested in chapter 6 should be carefully examined and, if necessary, they should be incorporated into the theory.

In summary, the present theory of the sideband absorption, and to a lesser extent, the far infrared absorption, leads to satisfactory overall agreement with experiment, which suggests that the vibrational spectra of ions near the defect are reasonably well explained by the force constant model which has been developed. These

spectra can therefore be used with some confidence in calculations of the anharmonic broadening of localized modes using extensions of procedures discussed in chapter 6. This should lead to a more precise knowledge of the anharmonic constants, and hence the form of the interactions, near the impurity.

APPENDIX 1

EVALUATION OF DIAGRAMS

A. EVALUATION OF THE FOURIER COEFFICIENT $\bar{G}_{\ell}(p)$

Creation and destruction operators (in the interaction representation) for the perturbed phonon p, $\tilde{a}_p^+(v)$ and $\tilde{a}_p(v)$ respectively, can be defined such that (Maradudin 64b)

$$\tilde{u}_L^{\alpha\kappa}(v) = \sum_p U_{L\alpha\kappa,p} \left[\tilde{a}_p^+(v) + \tilde{a}_p(v) \right] \quad . \qquad (1)$$

Using this expansion, it follows from equation (36) of chapter 2 that

$$\bar{G}(v;\underline{L}\alpha\kappa,\underline{L}'\alpha'\kappa') = \sum_{p,p'} U_{\underline{L}\alpha\kappa,p} < T \left(\tilde{a}_p^+(v) + \tilde{a}_p(v) \right) x$$

$$x \left(\tilde{a}_{p'}^+(0) + \tilde{a}_{p'}(0) \right) >_{H_o'} U_{p',\underline{L}'\alpha'\kappa'} \quad . \qquad (2)$$

Therefore,

$$\bar{G}(v;p,p') = < T(\tilde{a}_p^+(v) + \tilde{a}_p(v)(\tilde{a}_{p'}^+(0) + \tilde{a}_{p'}(0)) >_{H_o'} . \qquad (3)$$

The thermal average can be evaluated using the eigenstates of H_o' (the perturbed phonons), with the result

$$\bar{G}(v;p,p') = \delta_{p,p'} \cdot \frac{\hbar}{2\omega_p} \{ n_p e^{|v|\hbar\omega_p} + (1 + n_p) e^{-|v|\hbar\omega_p} \}$$

, (4)

where

$$n_p = (e^{\beta\hbar\omega_p} - 1)^{-1}$$

and the values

$$\langle a_p^+ a_{p'} \rangle_{H_o'} = \delta_{p,p'} \frac{\hbar n_p}{2\omega_p} \quad ,$$

$$\langle a_p a_{p'}^+ \rangle_{H_o'} = \delta_{p,p'} \frac{\hbar}{2\omega_p} (1 + n_p) \qquad (5)$$

have been used. Now, $\bar{G}_\ell(p,p')$ can be written in terms of $\bar{G}(v;p,p')$ using equation (38) of chapter 2 as

$$\bar{G}_\ell(p,p') = \int_0^\beta dv\, \bar{G}(v;p,p') e^{-2\pi i \ell v/\beta} \quad . \qquad (6)$$

Substituting the value of $\bar{G}(v;p,p')$ from equation (4) and integrating gives

$$\bar{G}_\ell(p,p') = \delta_{p,p'} \cdot \frac{1}{\omega_p^2 + \omega_\ell^2} \quad . \qquad (7)$$

Therefore,

$$\bar{G}_\ell(p) \equiv \bar{G}_\ell(p,p)$$

$$= \frac{1}{\omega_p^2 + \omega_\ell^2} \quad . \qquad (8)$$

B. RULES FOR THE EVALUATION OF DIAGRAMS

The internal lines of diagrams contributing to the self-energy $M_\ell(p)$ have been labelled in the $\{\underline{L}\alpha\kappa\}$-representation. The modified rules for their evaluation are:

(i) Include a factor $\overline{G}_\ell(\underline{L}\alpha\kappa,\underline{L}'\alpha'\kappa')$ for a line whose end-points are labelled by $(\underline{L}\alpha\kappa)$ and $(\underline{L}'\alpha'\kappa')$.

(ii) Include a factor $\beta^{n-m-1}(-1)^n/n!$ for a diagram with n vertices and m phonon lines.

(iii) Include a factor equal to the number of topologically equivalent diagrams.

(iv) Include an anharmonic coupling constant at each vertex.

(v) Having chosen a time-ordering, include a combinatorial factor which gives the number of pairing schemes to which a particular labelling corresponds (this must be separately evaluated for each set of end-point labels, as described in the main text).

(vi) Sum over the labels at each vertex in a way that is consistent with the anharmonic terms (this point is also clarified in the main text).

(vii) Conserve the quantity 'ℓ' at each vertex and sum over intermediate ℓ's. The following results, which are obtained using a contour integral for

each series, as described, for example, by Kadanoff and Baym (1962), are assumed in the main text:

$$\sum_{\ell_1=-\infty}^{\infty} \frac{1}{\omega_1^2 + \omega_{\ell_1}^2} \cdot \frac{1}{(\omega_{\ell_1} - \omega_\ell)^2 + \omega_2^2} = \frac{\beta\hbar}{4\omega_1\omega_2} \left\{ \frac{1 + n_1 + n_2}{i\omega_\ell + \omega_1 + \omega_2} - \right.$$

$$\left. - \frac{1 + n_1 + n_2}{i\omega_\ell - \omega_1 - \omega_2} + \frac{n_1 - n_2}{i\omega_\ell + \omega_2 - \omega_1} - \frac{n_1 - n_2}{i\omega_\ell - \omega_2 + \omega_1} \right\}, \quad (9)$$

$$\sum_{\ell_1=-\infty}^{\infty} \sum_{\ell_2=-\infty}^{\infty} \frac{1}{\omega_{\ell_1}^2 + \omega_1^2} \cdot \frac{1}{\omega_{\ell_2}^2 + \omega_2^2} \cdot \frac{1}{(\omega_\ell - \omega_{\ell_1} - \omega_{\ell_2})^2 + \omega_3^2}$$

$$= \frac{\beta^2\hbar^2}{8\omega_1\omega_2\omega_3} \left\{ \frac{(1 + n_2 + n_3)(1 + n_1) + n_2 n_3}{i\omega_\ell + \omega_1 + \omega_2 + \omega_3} - \right.$$

$$- \frac{n_1(1 + n_2 + n_3) + (1 + n_2)(1 + n_3)}{i\omega_\ell - \omega_1 - \omega_2 - \omega_3} +$$

$$+ \frac{(n_3 - n_2)(1 + n_1) + n_2(1 + n_3)}{i\omega_\ell + \omega_1 + \omega_2 - \omega_3} +$$

$$+ \frac{(n_2 - n_3)(1 + n_1) + n_3(1 + n_2)}{i\omega_\ell + \omega_1 + \omega_3 - \omega_2} +$$

$$+ \frac{(n_1 - n_2)(1 + n_3) + n_2(1 + n_1)}{i\omega_\ell - \omega_1 + \omega_2 + \omega_3} +$$

$$+ \frac{n_1(n_3 - n_2) - n_2(1 + n_3}{i\omega_\ell - \omega_1 + \omega_2 - \omega_3} +$$

$$+ \frac{n_1(n_2 - n_3) - n_3(1 + n_2)}{i\omega_\ell - \omega_1 - \omega_2 + \omega_3} +$$

$$\left. + \frac{n_2(n_3 - n_1) - n_1(1 + n_3)}{i\omega_\ell + \omega_1 - \omega_2 - \omega_3} \right\} . \quad (10)$$

APPENDIX 2

THE ANHARMONIC HAMILTONIAN, H_A

The anharmonic Hamiltonian for the crystal, H_A, has been derived assuming that anharmonic terms arise from nearest neighbour interactions through the short-range part of the interionic force (assumed to be central). These assumptions have been discussed by Cowley (1963). Furthermore, only those terms in the Taylor expansion of the crystal potential proportional to third and fourth powers of ionic displacements have been considered.

The following notation has been used for derivatives of the two-particle interactions:

$$\bar{V}_4 = \frac{\partial^4 \bar{V}}{\partial r^4} \Bigg|_{\bar{r}_o}$$

$$\bar{V}_3 = \frac{\partial^3 \bar{V}}{\partial r_3} \Bigg|_{\bar{r}_o}$$

$$\bar{V}_2 = \frac{1}{\bar{r}_o} \frac{\partial^2 \bar{V}}{\partial r^2} \Bigg|_{\bar{r}_o}$$

$$V_3 = \frac{\partial^3 V}{\partial r^3} \Bigg|_{r_o} \quad , \qquad (1)$$

where $\bar{V}$ is the potential for the short-range force between

the H^- (or D^-) impurity and its nearest neighbours, and $\bar{r}_o$ is their equilibrium separation. Similarly, V is the potential for the short-range force between the first and fourth neighbours of the impurity, and r_o their equilibrium separation. The numerical values used for the constants defined in equation (1) are given and discussed in appendix 4. Terms of the anharmonic Hamiltonian have been written using the symmetry coordinates defined in equations (3) of chapter 3, together with the coordinate $Q_1(T_{2g})$, defined by

$$Q_1(T_{2g}^{\alpha\beta}) = \frac{1}{2}(u_{\beta}^{\alpha+} - u_{-\beta}^{\alpha+} + u_{\alpha}^{\beta+} - u_{-\alpha}^{\beta+}), \quad \alpha = x,y,z, \quad \beta\neq\alpha. \quad (2)$$

The decomposition into symmetry coordinates is similar to that of Kühner and Wagner (1967).

In addition to the basic assumptions referred to above, additional assumptions have been made for each process treated. These are discussed at appropriate points in the main text. The relevant anharmonic terms for each process are listed below.

(1) The terms of H_A which have been used in the sideband calculation, $H_A^{(s)}$, are given by

$$H_A^{(s)} = \frac{Q_0^2(T_{1u}^x)}{M_-\sqrt{6M_+}}\{(\bar{V}_3 + 2\bar{V}_2)Q_1(A_{1g}) + \sqrt{2}(\bar{V}_3 - \bar{V}_2)Q_1(E_g)\} + \frac{2\bar{V}_2 Q_0(T_{1u}^x)}{M_-\sqrt{M_+}}\{Q_0(T_{1u}^y)Q_1(T_{2g}^{xy}) + Q_0(T_{1u}^z)Q_1(T_{2g}^{xz})\}. \quad (3)$$

(2) The terms of H_A which have been used in calculating the contribution to the self-energy of the U-centre local mode arising from decay into two phonons, decay into three phonons and the scattering mechanism, denoted by H_A^{II}, H_A^{III} and H_A^{s} respectively, are given by

$$H_A^{II} = \frac{\bar{V}_3 Q_0(T^x_{1u})}{\sqrt{6M_+M_-}} \{ Q_1(A_{1g}) + \sqrt{2}\, Q_1(E_g) \} \{ \frac{Q_0(T^x_{1u})}{\sqrt{M_-}} - \sqrt{\frac{2}{M_+}}\, Q_1(T^x_{1u}) \} \quad , \qquad (4)$$

$$H_A^{III} = \frac{\bar{V}_4 Q_0(T^x_{1u})}{12M_-^{1/2}} \{ \frac{Q_0^3(T^x_{1u})}{M_-^{3/2}} - \frac{2\sqrt{2}}{M_-M_+^{1/2}} Q_0^2(T^x_{1u}) Q_1(T^x_{1u}) + \frac{Q_0(T^x_{1u})}{M_+M_-^{1/2}} \left[3Q_1^2(T^x_{1u}) + (Q_1(A_{1g}) + \sqrt{2}\, Q_1(E_g))^2 \right] -$$

$$- \frac{Q_1(T^x_{1u})}{M_+^{3/2}} \cdot \sqrt{2} \left[Q_1^2(T^x_{1u}) + (Q_1(A_{1g}) + \sqrt{2}\, Q_1(E_g))^2 \right] \}, \qquad (5)$$

$$H_A^{s} = \frac{Q_0^2(T^x_{1u})\bar{V}_4}{12M_-} \{ \frac{Q_0^2(T^x_{1u})}{M_-} - \frac{2\sqrt{2}}{\sqrt{M_+M_-}} Q_0(T^x_{1u}) Q_1(T^x_{1u}) + \frac{1}{M_+} \left[3Q_1^2(T^x_{1u}) + (Q_1(A_{1g}) + \sqrt{2}\, Q_1(E_g))^2 \right] \} +$$

$$+ \frac{Q_0^2(T^x_{1u})\bar{V}_3}{M_-\sqrt{6M_+}} \{ Q_1(A_{1g}) + \sqrt{2}\, Q_1(E_g) \} \quad . \qquad (6)$$

(3) The terms of H_A used in calculating the self-energy of the gap mode in KI:KH, H_A^g, are given by

$$H_A^g = \frac{Q_1(A_{1g})}{6\sqrt{6M_+}} \{ \frac{(\bar{V}_3 - V_3)}{M_+} \left[Q_1^2(A_{1g}) + 3(Q_1^2(E_g) + \right.$$

$$\left. + Q_1^2(E_g') + \sum_{\alpha=x,y,z} Q_1^2(T_{1u})) \right] +$$

$$+ 3V_3 \left[\frac{Q_1(A_{1g})Q_2(A_{1g})}{M_+^{1/2}M_-^{1/2}} - \frac{Q_2^2(A_{1g})}{M_-} + \right.$$

$$+ \frac{2}{M_+^{1/2}M_-^{1/2}} (Q_1(E_g)Q_2(E_g) + Q_1(E_g')Q_2(E_g')) -$$

$$\left. - \frac{1}{M_-} \left(Q_2^2(E_g) + Q_2^2(E_g') + \sum_\alpha (Q_2^2(T_{1u}^\alpha) - 2Q_1(T_{1u}^\alpha)Q_2(T_{1u}^\alpha))\right) \right] +$$

$$+ \frac{6\bar{V}_3}{\sqrt{M_-}} \sum_\alpha Q_0(T_{1u}^\alpha) \left[\frac{Q_0(T_{1u}^\alpha)}{\sqrt{M_-}} - \sqrt{\frac{2}{M_+}} Q_1(T_{1u}^\alpha) \right] \} \quad . \qquad (7)$$

APPENDIX 3

CALCULATION OF GREEN'S FUNCTION MATRIX ELEMENTS

A. ELEMENTS OF $\bar{G}$.

Elements of the matrix $\bar{G}$ are related to elements of G by the Dyson equation, which is equation (22) of chapter 2. Since the elements required in the calculations of chapters 4, 5 and 6 are all in the space of γ, they can be written

$$\bar{G}(\omega^2;Q_n(A_{1g}),Q_{n'}(A_{1g})) = \bar{g}_{nn'}(\omega^2;A_{1g})$$

$$\bar{G}(\omega^2;Q_n(E_g),Q_{n'}(E_g)) = \bar{g}_{nn'}(\omega^2;E_g)$$

$$\bar{G}(\omega^2;Q_{n_1}(T^x_{1u}),Q_{n_1'}(T^x_{1u})) = \bar{g}_{n_1n_1'}(\omega^2;T^x_{1u}) \quad , \qquad (1)$$

$$n,n' = 1,2$$

$$n_1,n_1' = 0,1,2$$

where the symmetry coordinates are defined in equation (3) of chapter 3. The notation used for $\bar{g}$ is analogous to that used for g and γ in chapter 3. It follows from the definition of $\bar{g}$ (equation (6) of chapter 3) that its submatrices have the form (suppressing the frequency

variable ω)

$$\bar{g}(A_{1g}) = \frac{\left[I + g(A_{1g})\ \gamma(A_{1g}) \right]^{\dagger} g(A_{1g})}{\det\left(I + g(A_{1g})\ \gamma(A_{1g}) \right)}$$

$$\equiv \left[I + g(A_{1g})\ \gamma(A_{1g}) \right]^{\dagger} g(A_{1g}) \cdot \frac{D^*(A_{1g})}{|D(A_{1g})|^2} ,$$

$$\bar{g}(E_g) = \left[I + g(E_g)\ \gamma(E_g) \right]^{\dagger} g(E_g) \cdot \frac{D^*(E_g)}{|D(E_g)|^2} ,$$

$$\bar{g}(T^x_{1u}) = \left[I + g(T^x_{1u})\ \gamma(T^x_{1u}) \right]^{\dagger} g(T^x_{1u}) \cdot \frac{D^*(T^x_{1u})}{|D(T^x_{1u})|^2} , \quad (2)$$

where

$$D(A_{1g}) \equiv \det \left[I + g(A_{1g})\ \gamma(A_{1g}) \right]$$

and $D^*(A_{1g})$ is its complex conjugate. $D(E_g)$ and $D(T^x_{1u})$ are similarly defined. The required elements of $\bar{G}$ have been calculated from equations (1) and (2) using the elements of γ defined by equation (5) of chapter 3. The elements of g were calculated as described below.

B. ELEMENTS OF G

The elements of g required by equation (2), together with the diagonal element $G(\omega^2;Q(T_{2g}))$ called for in equation (13) of chapter 4, are calculated by making

an expansion in the $\{\underline{k}j\}$-representation:

$$g_{nn'}(\omega^2;Q_n(A_{1g}),Q_{n'}(A_{1g}))$$

$$= \frac{1}{N} \sum_{\underline{k}j} U_{Q_n(A_{1g}),\underline{k}j} (\omega^2_{\underline{k}j} - \omega^2)^{-1} U_{\underline{k}j,Q_{n'}(A_{1g})} , \qquad (3)$$

where equation (9) of chapter 2 has been used. Analogous expressions hold for elements of E_g, T_{2g} and T_{1u} symmetry. Using equation (7) of chapter 2, it can be seen that

$$U_{Q_n(A_{1g}),\underline{k}j} = i \sqrt{\frac{2}{3N}} \sum_{\alpha=x,y,z} \varepsilon_\alpha^{\kappa_n}(\underline{k}j) \sin nk_\alpha a,$$

$$U_{Q_n(E_g),\underline{k}j} = i \sqrt{\frac{1}{3N}} \sum_{\alpha=x,y,z} (3\delta_{\alpha,x} - 1)\varepsilon_\alpha^{\kappa_n}(\underline{k}j) \sin nk_\alpha a,$$

$$U_{Q_1(T^{x\beta}_{2g}),\underline{k}j} = i \sqrt{\frac{1}{N}} (\varepsilon_x^+(\underline{k}j) \sin k_\beta a + \varepsilon_\beta^+(\underline{k}j) \sin k_x a)$$

$$U_{Q_n(T^x_{1u}),\underline{k}j} = i \sqrt{\frac{2}{N}} \varepsilon_x^{\kappa_n}(\underline{k}j) \cos nk_x a$$

$$\beta = y,z,$$

$$U_{Q_0(T^x_{1u}),\underline{k}j} = i \sqrt{\frac{1}{N}} \varepsilon_x^-(\underline{k}j) , \quad n = 1,2, \qquad (4)$$

$$\kappa_1 \equiv + ,$$

$$\kappa_2 \equiv - .$$

The imaginary parts of the Green's function matrix elements were computed from the equation

$$\mathrm{Im}\{g_{nn'}(\omega^2 + i0^+;A_{1g})\} = \frac{\pi}{N} \sum_{kj} U_{Q_n(A_{1g}),\underline{k}j} \times$$

$$\times \delta(\omega^2_{\underline{k}j} - \omega^2) U_{\underline{k}j,Q_{n'}(A_{1g})}$$

which follows from equation (3), and analogous expressions for the matrix elements of E_g, T_{2g} and T_{1u} symmetry. The summation over $\underline{k}$ was performed using an effective 32,000 points uniformly distributed throughout the first Brillouin zone of reciprocal space. The eigenfrequencies and eigenvectors for each $\underline{k}$ were calculated using the neutron-determined shell model VI of Cowley et al. (1963) for KBr and of Dolling et al. (1966) for KI. The method of Gilat and Raubenheimer (1966) was used to obtain the elements of Im{G} in histogram form using 'bins' of size 0.5 cm^{-1}. The total density of states has also been calculated from equation (10) of chapter 2.

The elements of Re{G} are written in terms of corresponding elements of Im{G} using the Cauchy relations. For instance, the elements of $Re\{g(A_{1g})\}$ are given by

$$\text{Re } g_{nn'}(\omega^2;A_{1g}) = \frac{1}{\pi} \int_0^\infty \frac{\text{Im } g_{nn'}(\omega_1^2 + i0^+;A_{1g})}{\omega_1^2 - \omega^2} \, d\omega_1^2$$

where the principal part of the integral is required. This integral was performed numerically using a procedure suggested by Sievers er al. (1965).

APPENDIX 4

THE ANHARMONIC FORCE CONSTANTS

It has been assumed that the anharmonicity arises from nearest-neighbour, short-range forces which are described by a Born-Mayer potential. For the interaction between the H^- ion and its nearest neighbours, this potential will be written, following Cowley (1963),

$$\bar{V}(r) = \lambda e^{-r/\rho} \quad . \qquad (1)$$

Since $\bar{V}(r)$ describes the interaction between an H^- ion and a K^+ ion, the parameters λ and ρ are likely to be considerably different from the corresponding parameters in the potential for the interaction between nearest neighbours of the perfect crystal. In fact, their values should be fairly close to those found in a perfect potassium hydride crystal, and even to those in the KH molecule. Experimental data are limited to the molecular system. The value of ρ determined from that data, ρ_{mol}, is (Varshni and Shukla 63)

$$\rho_{mol} = 0.4724 \text{ Å} \quad . \qquad (2)$$

The equilibrium distance in the molecule, r_{mol}, has the value

$$r_{mol} = 2.85 \text{ Å} \quad . \qquad (3)$$

From the form of the potential and the definitions of $\bar{V}_4$, $\bar{V}_3$ and $\bar{V}_2$ given in appendix 2, the following relationships can be derived:

$$\bar{V}_3 = - \frac{\bar{r}_o}{\rho} \bar{V}_2 \qquad (4)$$

and

$$\bar{V}_4 = - \frac{1}{\rho} \bar{V}_3 \quad . \qquad (5)$$

Furthermore, the parameter ξ, which plays an important part in determining the sideband lineshape (see equation (13) of chapter 4), has also been defined as

$$\xi \equiv \frac{\bar{V}_2}{\bar{V}_3} \quad . \qquad (6)$$

From equation (4), ξ can be written

$$\xi = - \frac{\rho}{\bar{r}_o} \quad . \qquad (7)$$

A rough value for ξ can be obtained from this equation by using the approximate values (MacDonald 66)

$$\bar{r}_o = a$$

$$\rho = \rho_{mol} \quad , \qquad (8)$$

where 'a' is the lattice spacing of the host lattice. Experimental results (Hilsch and Pohl 38) indicate that the first of these approximations represents a small over-estimate of $\bar{r}_o$. The second approximation is justified

only if the value of ρ at distance 'a' is close to that describing the short-range force in the KH molecule at distance r_{mol}. At present there seems to be no way of estimating the dependability of this assumption. The values obtained for ξ were

$$\xi = -0.13 \qquad \text{for KI}$$

and

$$\xi = -0.14 \qquad \text{for KBr} \qquad . \qquad (9)$$

Equation (6) offers another possible way of estimating ξ. By definition (see appendix 2), $\bar{V}_2$ is given by

$$\bar{V}_2 = \frac{1}{\bar{r}_o} \frac{\partial^2 \bar{V}}{\partial r^2} \Big|_{\bar{r}_o}$$

$$\simeq \frac{1}{a} \frac{\partial^2 \bar{V}}{\partial r^2} \Big|_{\bar{r}_o} \qquad . \qquad (10)$$

The corresponding quantity in the perfect crystal is known from model calculations. Using the shell model notation of Cowley et al. (1963) in which the longitudinal and transverse force constants between nearest neighbours are A and B, respectively, $\bar{V}_2$ can be written

$$\bar{V}_2 \simeq \frac{1}{a}(A + \Delta A) \qquad (11)$$

where ΔA is the change in force constant resulting from replacing the potential of the perfect crystal by $\bar{V}$ and by changing the equilibrium distance from 'a' to $\bar{r}_o$. Although

the value of ΔA is related to that obtained for Δf, they are not equal since Δf is the change in total effective short-range force constant, which is given by A + 2B in the shell model (in the approximation that second neighbour forces may be neglected). An estimate of ΔA is given by

$$\frac{\Delta A}{A} = \frac{\Delta f}{A + 2B} \quad , \qquad (12)$$

assuming that A and B have suffered the same fractional change. Equation (10) then becomes

$$\bar{V}_2 \approx \frac{1}{a}(A + 2B + \Delta f) \quad . \qquad (13)$$

Using values of $\bar{V}_3$ already determined from the sideband area, (which are slightly dependent on the value assumed for ξ, as discussed in chapter 4) together with the shell model parameters, equation (6) gives the following estimates of ξ:

$$\xi = -0.17 \qquad \text{for KI} \quad ,$$

$$\xi = -0.21 \qquad \text{for KBr} \quad . \qquad (14)$$

Considering the nature of the approximations made in obtaining the independent estimates of ξ given in equations (9) and (14), the agreement is surprisingly good. It should be pointed out, however, that the situation is by no means satisfactory. For example, neglect of B in equation (13) would lead to values of ξ greater by about 50% than those given in equation (14). The two sets of values for ξ

would then differ by a factor close to two. Fortunately, even a crude estimate of ξ is sufficient to determine both the sideband lineshape and the value of $\bar{V}_3$ (see chapter 4) reasonably accurately. The value $\xi = -0.15$ has therefore been used in this determination for both KI and KBr.

However, higher-order anharmonic constants required in other calculations, for instance $\bar{V}_4$, can at present only be determined from equations like equations (4) and (5), and therefore depend on ξ (using equation (7)). In the present calculations, $\bar{V}_4$ was calculated from equation (5) using $\rho = \rho_{mol}$, and, for that reason, may not be a reliable estimate. The values obtained were

$$\bar{V}_4 = 1.95 \times 10^{20} \text{ dyne/cm for KI}$$

$$= 2.4 \times 10^{20} \text{ dyne/cm for KBr} \quad . \qquad (15)$$

The situation is slightly less complicated when the interaction between the first and fourth nearest neighbours of the H^- (or D^-) impurity is considered, since this interaction is probably adequately described by the Born-Mayer potential for the perfect lattice. Even so, it is likely that the equilibrium separation has been changed and at present there seems to be no dependable way of estimating the magnitude of the change. In the broadening calculation for the A_{1g} gap mode, the approximation $r_o = a$ was made. The value of V_3 for KI, which is the only

constant required, was then calculated using the shell model parameters of Dolling et al. (1966). The result was

$$V_3 = 6.2 \times 10^{12} \text{ dyne/cm}^2 \quad \text{for KI} \quad . \qquad (16)$$

BIBLIOGRAPHY

(1) A. I. Alekseev, Usp. Fiz. Nauk., 73 (1961) 41
(Soviet Phys. - Uspekhi, 4 (1961) 23)

(2) D. Bauerle and B. Fritz, phys. stat. sol.,
24 (1967) 207

(3) G. Benedek and B. F. Nardelli, Phys. Rev.,
155 (1967) 1004

(4) H. Bilz, D. Strauch and B. Fritz, J. Phys. Radium,
Suppl. 27 (1966) C2 - 3

(5) H. Bilz, R. Zeyher and R. K. Wehner, phys. stat. sol.,
20 (1967) K167

(6) Y. Brada and S. S. Mitra, Bull. Am. Phys. Soc.,
9 (1964) 644

(7) R. A. Cowley, Adv. in Phys., 12 (1963) 421

(8) R. A. Cowley, W. Cochran, B. N. Brockhouse and
A. B. Woods, Phys. Rev., 131 (1963) 1030

(9) P. G. Dawber and R. J. Elliott, Proc. Roy. Soc. (London),
A273 (1963a) 222

(10) P. G. Dawber and R. J. Elliott, Proc. Phys. Soc. (London),
81 (1963b) 453

(11) G. A. Dolling, R. A. Cowley, C. Schittenhelm and
I. M. Thorson, Phys. Rev., 147 (1966) 577

(12) C. Domb, A. A. Maradudin, E. W. Montroll and
G. H. Weiss, Phys. Rev., 155 (1959) 18, 21

(13) H. Dötsch, W. Gebhardt and C. Martius, Solid State Commun., 3 (1965) 297

(14) R. C. Dynes, J. P. Carbotte and E. J. Woll Jr., Solid State Commun., 6 (1968) 101

(15) R. J. Elliott, W. Hayes, G. D. Jones, H. F. MacDonald and C. T. Sennett, Proc. Roy. Soc. (London), A289 (1965) 1

(16) R. Fieschi, G. F. Nardelli and N. Terzi, Phys. Rev., 138 (1965) A203

(17) B. Fritz, in "Proceedings of the 1963 International Conference on Lattice Dynamics", R. F. Wallis, editor; Pergamon Press, London, 1965

(18) B. Fritz, J. Gerlach and U. Gross, in "Localized Excitations in Solids", R. F. Wallis, editor; Plenum Press, New York, 1968

(19) B. Fritz, U. Gross and D. Bäuerle, phys. stat. sol., 11 (1965) 231

(20) T. Gethins, T. Timusk and E. J. Woll Jr., Phys. Rev., 157 (1967) 744

(21) G. Gilat and L. J. Raubenheimer, Phys. Rev., 144 (1966) 390

(22) R. Hilsch and R. W. Pohl, Trans. Faraday Soc., 34 (1938) 883

(23) J. P. Ipatova and A. A. Klotchichin, J E T P (U. S. S. R.), 50 (1966) 1603
(Soviet Phys. - J E T P, 23 (1966) 1068)

(24) M. A. Ivanov, M. A. Krivoglaz, D. N. Mirlin and I. I. Reshina, Fizika Tverdogo Tela, 8 (1966) 192 (Soviet Phys. - Solid State, 8 (1966) 150)

(25) S. S. Jaswal and D. J. Montgomery, Phys. Rev., 135 (1964) A1257

(26) L. P. Kadanoff and G. Baym, "Quantum Statistical Mechanics"; Benjamin, New York, 1962

(27) Y. Kagan and Y. A. Iosilevskii, J E T P (U. S. S. R.), 44 (1963) 284 (Soviet Phys. - J E T P, 17 (1963) 1965)

(28) M. V. Klein, Phys. Rev., 131 (1963) 1500

(29) M. V. Klein, 1966, Private Communication to T. Timusk

(30) M. V. Klein, in "Physics of Color Centers", W. B. Fowler, editor; Academic Press, New York, 1968

(31) D. Kühner and M. Wagner, Z. Phys., 207 (1968) 111

(32) I. M. Lifshitz, J. Phys. (U. S. S. R.), 7 (1943) 211, 249

(33) I. M. Lifshitz, J. Phys. (U. S. S. R.), 8 (1944) 89

(34) R. A. MacDonald, Phys. Rev., 150 (1966) 597

(35) A. A. Maradudin, P. Mazur, E. W. Montroll and G. H. Weiss, Rev. Mod. Phys., 30 (1958) 175

(36) A. A. Maradudin and A. E. Fein, Phys. Rev., 128 (1962) 2589

(37) A. A. Maradudin, in "Astrophysics and the Many-Body Problem"; Benjamin, New York, 1963

(38) A. A. Maradudin, Rev. Mod. Phys., 36 (1964a) 417

(39) A. A. Maradudin, Annals of Phys., 30 (1964b) 371

(40) A. A. Maradudin, in "Solid State Physics", vols. 18 and 19, F. Seitz and D. Turnbull, editors; Academic Press, New York, 1966

(41) T. P. Martin, Phys. Rev., 160 (1967) 686

(42) T. Matsubara, Prog. Theor. Phys., 14 (1955) 351

(43) D. N. Mirlin and I. I. Reshina, Fizika Tverdogo Tela, 6 (1964) 3078
(Soviet Phys. - Solid State, 6 (1965) 2454)

(44) E. W. Montroll and R. B. Potts, Phys. Rev., 100 (1955) 525

(45) X. X. Nguyen, Solid State Commun., 4 (1966) 9

(46) X. X. Nguyen, Phys. Rev., 163 (1968) 896

(47) J. B. Page, Jr. and D. Strauch, phys. stat. sol., 24 (1967) 419

(48) J. B. Page, Jr. and B. G. Dick, Phys. Rev., 163 (1968) 910

(49) K. Patnaik and J. Mahanty, Phys. Rev., 155 (1967) 987

(50) K. K. Rebane, N. N. Kristofel, G. D. Trifonov and V. V. Khyzhnyakov, Izv. Akad. Nauk. Estonian S S R, 13 (1964) 87

(51) H. Rosenstock and C. Klick, Phys. Rev., 119 (1960) 1198

(52) G. Schaefer, J. Phys. Chem. Solids, 2 (1960) 233

(53) A. J. Sievers, in "Low Temperature Physics", J. G. Daunt et al., editors; Plenum Press, New York, 1965, vol. LT9, part B

(54) A. J. Sievers, A. A. Maradudin and S. S. Jaswal, Phys. Rev., 138 (1965) A272

(55) S. Takeno, S. Kashirvamura and E. Tenamoto, Prog. Theor. Phys. Suppl., 23 (1962) 124

(56) S. Takeno, Progr. Theor. Phys., 38 (1968) 995

(57) T. Timusk and M. V. Klein, Phys. Rev., 141 (1966) 664

(58) T. Timusk, E. J. Woll, Jr. and T. Gethins, in "Localized Excitations in Solids", R. F. Wallis, editor; Plenum Press, New York, 1968

(59) Y. P. Varshni and R. C. Shukla, Rev. Mod. Phys., 35 (1963) 130

(60) R. F. Wallis and A. A. Maradudin, Prog. Theor. Phys., 24 (1960) 1055

(61) E. J. Woll, Jr., T. Gethins and T. Timusk, 1968, submitted for publication in Canad. J. Phys.

FIGURE CAPTIONS

Figure 1. The Dyson equation for the anharmonic Green's function G_ℓ^A is shown. G_ℓ^A is represented by a double line and $\bar{G}_\ell$, the harmonic Green's function, by a single line. The "bubble" represents the proper self-energy M_ℓ.

Figure 2. The force constants which are considered to be perturbed by introduction of the H^- ion. The ion at the centre is the H^-. Its first neighbour (alkali) ions are represented, as well as its fourth neighbour (halide) ions. Δf and Δg are the changes in the force constants f and g, respectively, of the perfect crystal.

Figure 3. The diagram considered in the calculation of the U-centre sideband spectrum is shown with the three "labellings" consistent with the anharmonic potential $H_A^{(s)}$. In each case one of the internal lines, indicated by the label (P), is the high frequency local mode phonon. The contribution of (c) is to be doubled to account for the equivalent labelling in which y is replaced by z.

Figure 4. The computed A_{1g} and E_g resonance frequencies are plotted for various values of Δg. The experimental resonance positions are marked with arrows. The arrow labelled "(E_g)" for KI indicates the frequency of the resonance relative to that of the van Hove singularity. The dashed lines are drawn at the selected values of Δg. It should be noted that the figures have been drawn on an expanded scale and that the experimental accuracy is only ± 1.0 cm^{-1}.

Figure 5. The A_{1g}, E_g and T_{2g} sideband lineshapes are given for KI:KH. The values $\Delta f = -8660$ dyne/cm and $\Delta g = -5000$ dyne/cm were used. The dashed line in the band gap for the A_{1g} component represents a localized gap mode of A_{1g} symmetry. It should be noted that the T_{2g} component is independent of Δf and Δg.

Figure 6. The A_{1g}, E_g and T_{2g} sideband lineshapes are given for KBr:KH. The values $\Delta f = -8860$ dyne/cm and $\Delta g = -4400$ dyne/cm were used. It should be noted that the T_{2g} component is independent of both Δf and Δg.

Figure 7. The complex resonance denominators for A_{1g} and E_g symmetries are plotted for KI and KBr. Resonances occur where $Re\{D\}$ passes through zero with negative slope. The height of the resonance

is determined by the value of Im{D} (for the same symmetry) at the zero.

Figure 8. The results of the sideband calculation for KI:KH are compared with the experimental results of Timusk and Klein (see Gethins et al. 67). The sharp peak at 68 cm^{-1} in the theory is a resonance of E_g symmetry while the dashed line at 90 cm^{-1} indicates a pole of A_{1g} symmetry. (Background has not been subtracted from the experimental results.)

Figure 9. The results of the sideband calculation for KBr:KH are compared with experimental results of Timusk and Klein (1966). The sharp peak at 79 cm^{-1} in the theory is a resonance of E_g symmetry while the peak at 108 cm^{-1} is a resonance of A_{1g} symmetry. (Background has not been subtracted from the experimental results.)

Figure 10. The "uncorrected" and "corrected" sideband lineshapes, $\ell(\omega)$ and $\ell'(\omega)$ respectively, are compared for KI:KH. The position of the first maximum in the corrected curve is shifted by about $2cm^{-1}$ to higher frequencies. The intensities of peaks are also changed by the correction leading to better overall agreement with the experimental results shown in figure 8.

Figure 11. The real and imaginary parts of the resonance denominator for T_{1u} symmetry modes, $D(T_{1u})$, are plotted for KBr and KI. The zeroes of $Re\{D(T_{1u})\}$ marked with arrows give rise to resonances in the far infrared absorption spectra.

Figure 12. The results of the far infrared calculation for KI:KH are compared with the experimental results of Timusk et al. (1968). The peak at 77 cm^{-1} in the experimental curve is due to Cl^- impurities. The sharp peak at 68.5 cm^{-1} in the theory is a resonance of T_{1u} symmetry. (The unit A is $4\pi e^2 q\{(\eta^2(\infty) + 2)^2/9\eta(\omega)\mu c\} \times 10^{-12}$ sec, where q is the relative density of H^- ions.)

Figure 13. The results of the far infrared calculation for KBr:KH are compared with experimental results of Timusk et al. (1968). The peak at 95 cm^{-1} in the experimental curve is due to Cl^- impurities. The sharp peak at 89.5 cm^{-1} in the theory is a resonance of T_{1u} symmetry. (See caption of figure 12 for unit A.)

Figure 14. The total densities of states for KI and KBr, calculated from the shell model. The van Hove singularities occurring at 83.5 cm^{-1} and 88 cm^{-1}

in KBr at 61.5 cm^{-1} and 64 cm^{-1} in KI lead to peaks in the far infrared absorption spectra.

Figure 15. Projections of the perturbed and unperturbed densities of states of KI are compared. The dashed line represents a pole of A_{1g} symmetry predicted in the band gap at 90 cm^{-1}. The sharp peaks in the perturbed densities of states are resonances of E_g and T_{1u} symmetries.

Figure 16. Projections of the perturbed and unperturbed densities of states for KBr are compared. The sharp resonances in the perturbed densities of states appear in the sideband and far infrared absorption spectra.

Figure 17. The diagram considered in calculating the broadening of the gap mode in KI:KH is shown. The internal lines are labelled in the position representation.

Figure 18. The calculated results for the half-width $W(p_A)$ of the gap mode in KI:KH are shown as a function of temperature in a log-log plot. Also shown are some experimental measurements of Klein (1966) of the half-width of the gap mode in the sideband spectrum. The calculated quantity which should be compared to these

experimental values is $W'(p_A)$, which is obtained from $W(p_A)$ by correcting for the width of the main U-centre line. (The error bars on the experimental points have been estimated by T. Timusk.)

Figure 19. The two diagrams considered in calculating the broadening of the high frequency local mode are shown. The cubic process can only occur for deuterium U-centres whereas the quartic process is possible for both hydrogen and deuterium U-centres.

Figure 20. The three scattering processes which have been considered in evaluation of the broadening of the high frequency local mode are shown schematically in figure (a). In each case the initial and final states consist of a local mode phonon P and a lattice phonon, p or p'. The transition can procede either directly through the quartic anharmonic interaction or indirectly through two successive cubic interactions. In the calculation, evaluation of diagram (b) takes into account all of these processes when the renormalized quartic anharmonic coefficient $\tilde{V}_4$ is used.

Figure 21. The calculated values of the half-width W(P) of the high frequency local mode for hydrogen and deuterium U-centres in KBr are shown as a function of temperature in a log-log plot, together with some experimental results of (a) Mirlin and Reshina (1964) and (b) Fritz et al. (1965). Solid lines have been drawn through the theoretical points, dashed lines through the experimental ones. Note the change in scale at low temperatures.

Figure 22. The calculated values of the half-width W(P) of the high frequency local mode for hydrogen and deuterium U-centres in KI are shown as a function of temperature in a log-log plot. Some experimental results of (b) Fritz et al. (1965) and (c) Schaefer (1960) for KI:KH are also plotted. Solid lines have been drawn through the theoretical points and a dashed line through the experimental ones. Note the change in scale at low temperatures.

FIGURE 1. THE DYSON EQUATION FOR $G^A_\iota(p,p')$

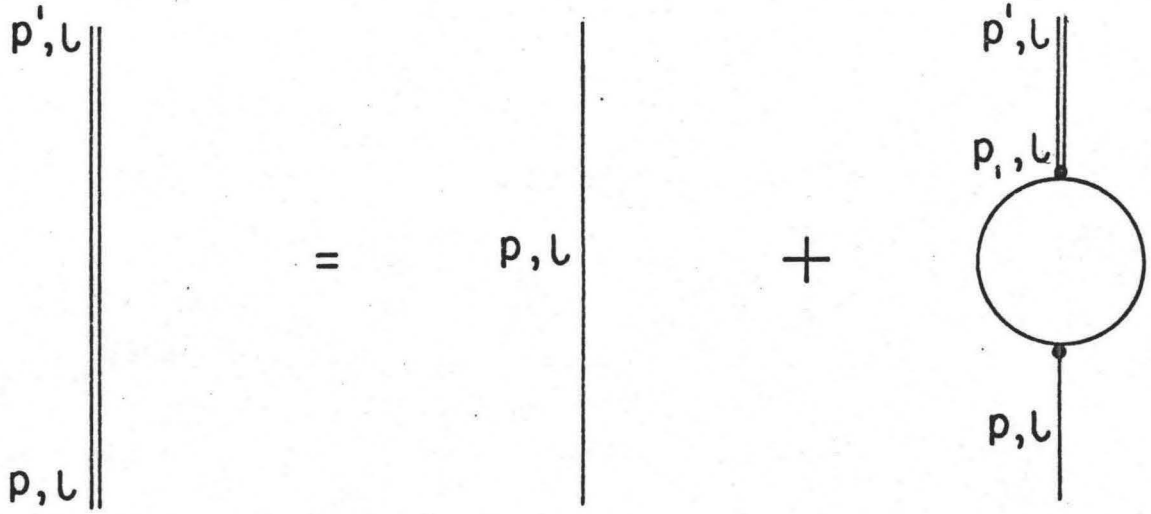

$$G^A_\iota(p,p') = \bar{G}_\iota(p)\,\delta_{p,p'} + \bar{G}_\iota(p) \sum_{p_1} M_\iota(p,p_1)\, G^A_\iota(p_1,p')$$

FIGURE 2. THE PERTURBED FORCE CONSTANTS.

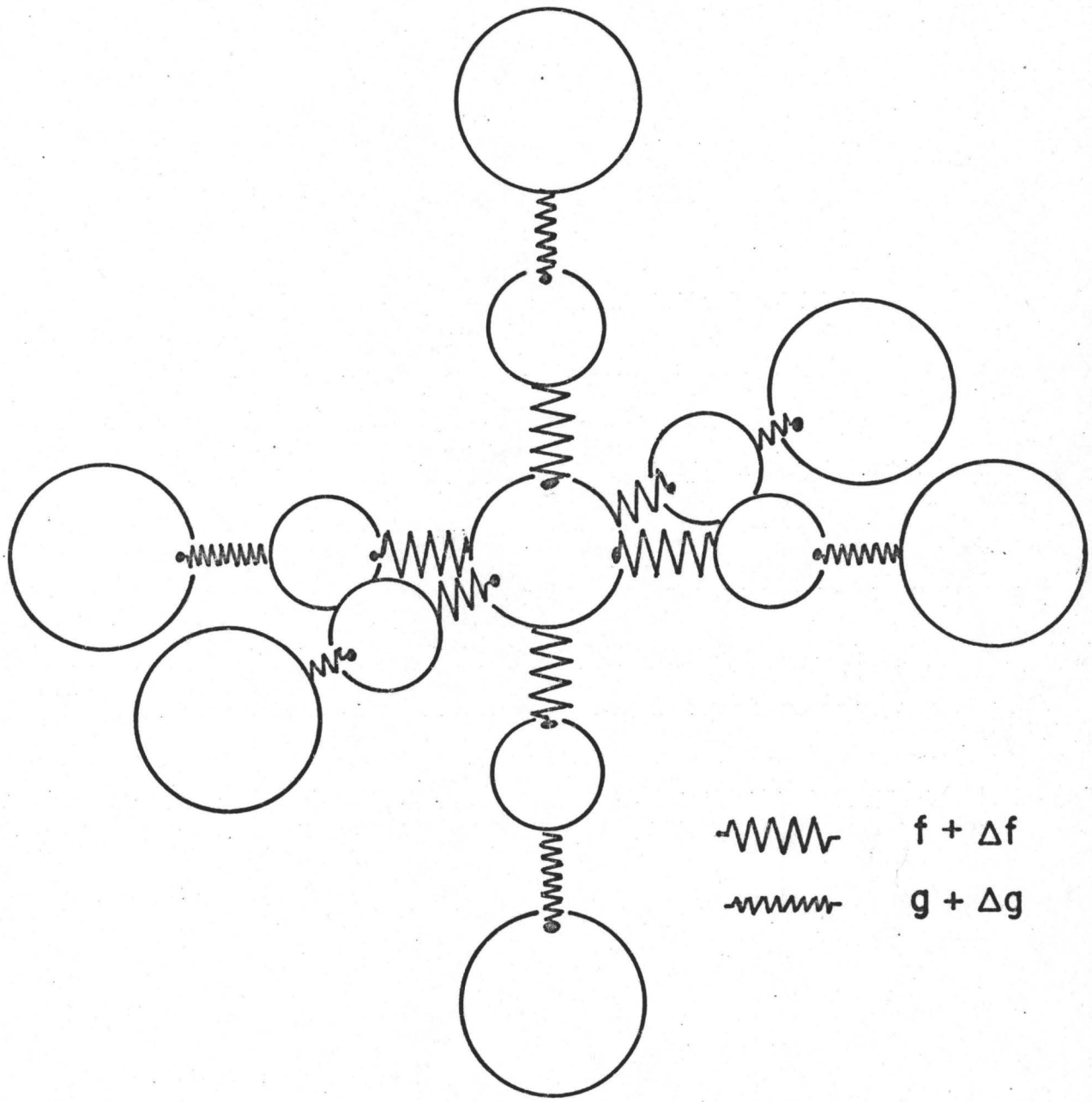

FIGURE 3. DIAGRAM CONTRIBUTING TO $M_l^{(s)}(P_x)$

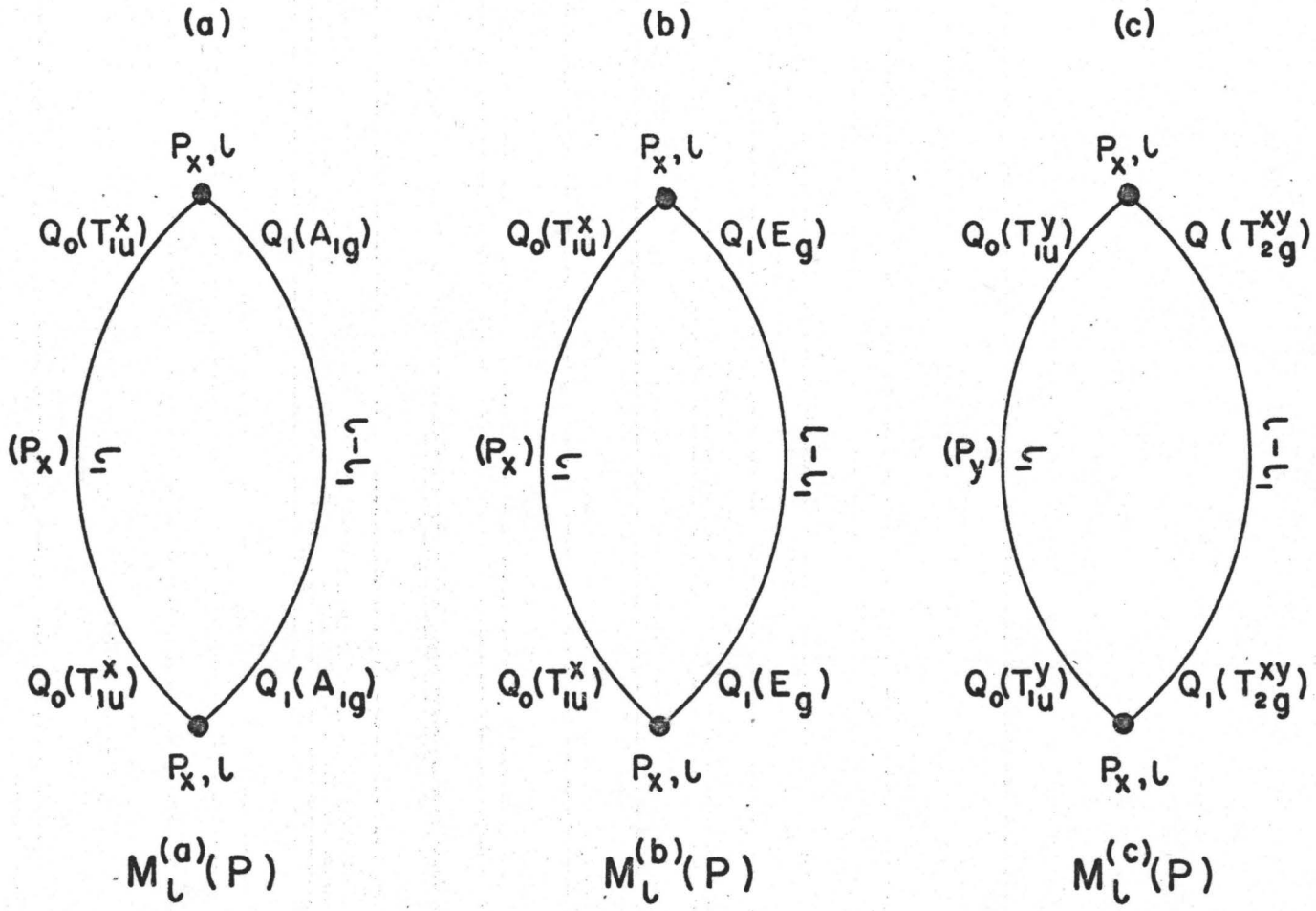

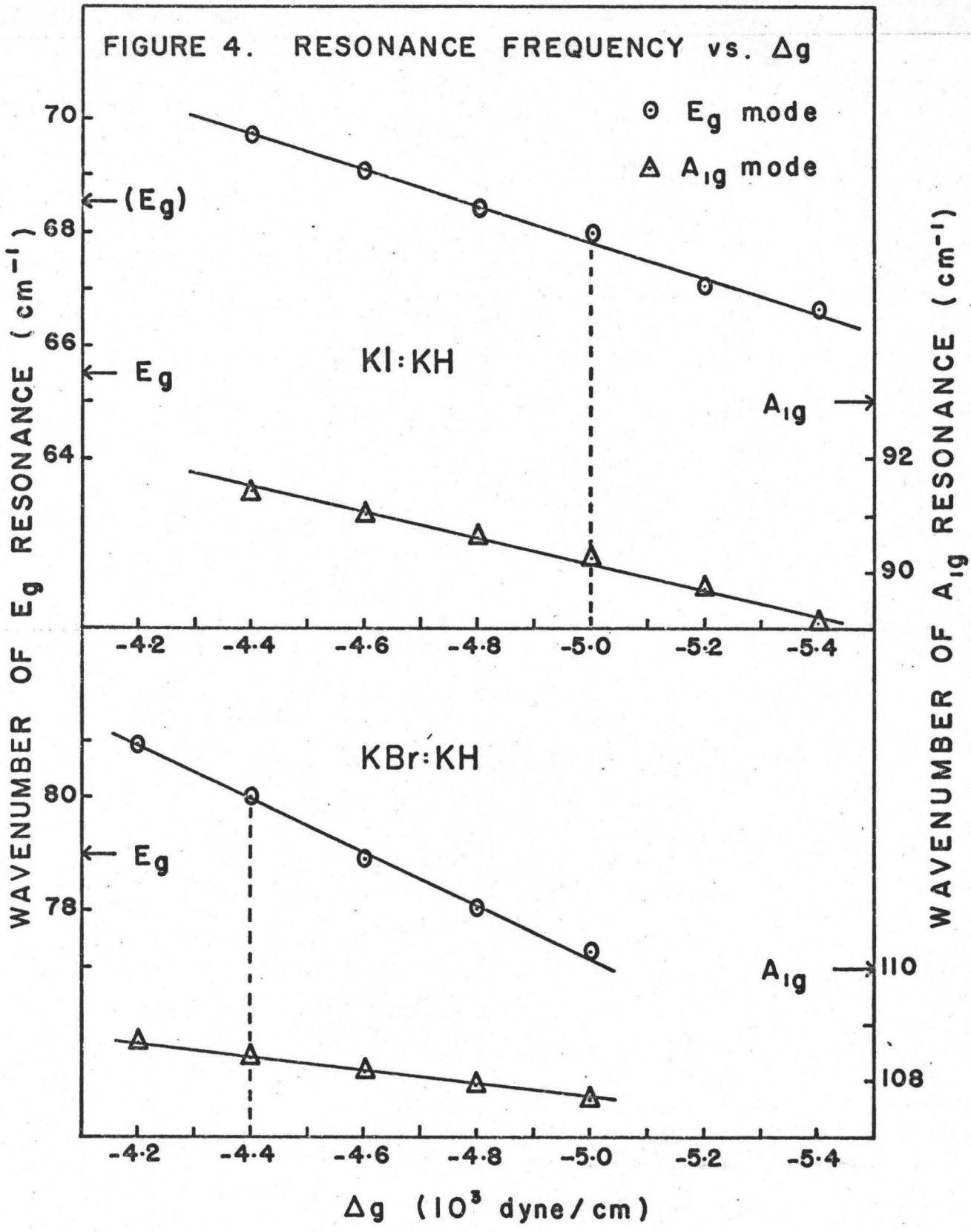
FIGURE 4. RESONANCE FREQUENCY vs. Δg
⊙ Eg mode
△ A1g mode
KI:KH
KBr:KH
(Eg)
Eg
A1g
WAVENUMBER OF Eg RESONANCE (cm⁻¹)
WAVENUMBER OF A1g RESONANCE (cm⁻¹)
70
68
66
64
92
90
80
78
110
108
-4·2
-4·4
-4·6
-4·8
-5·0
-5·2
-5·4
Δg (10³ dyne/cm)

FIGURE 5. SIDEBAND COMPONENTS FOR KI:KH

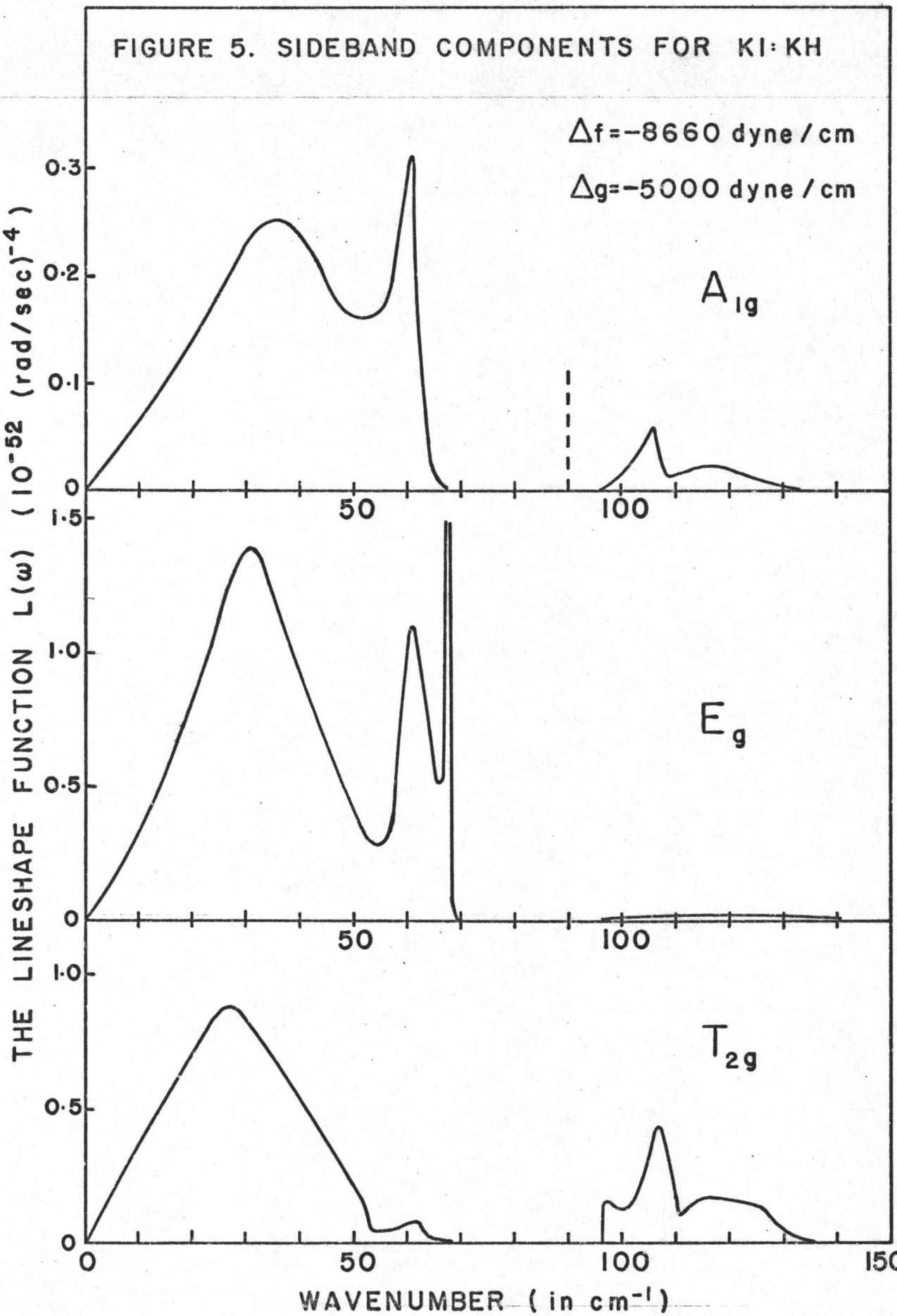

FIGURE 6. SIDEBAND COMPONENTS FOR KBr:KH

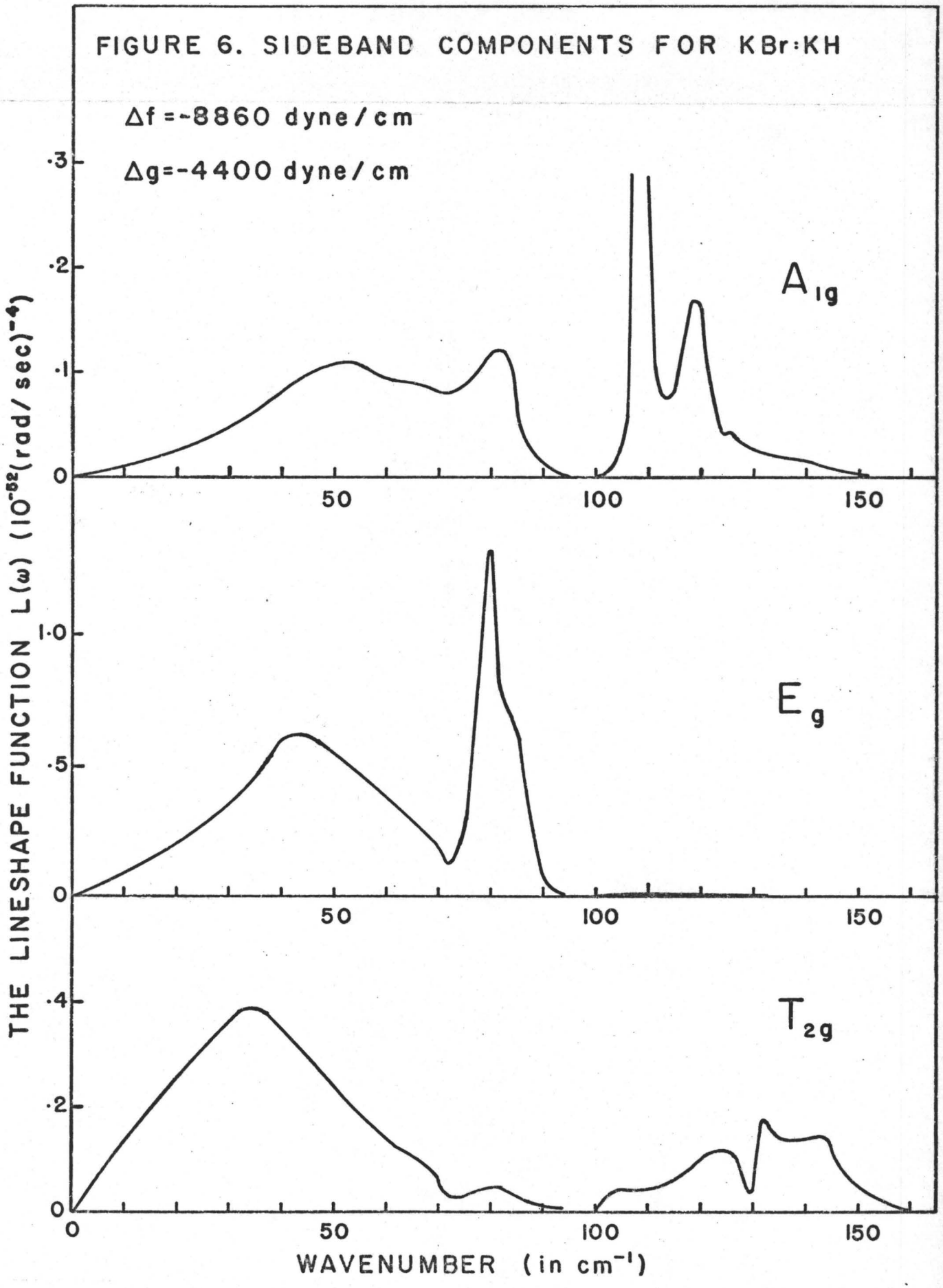

FIGURE 7. THE RESONANCE DENOMINATORS $D(A_{1g})$ AND $D(E_g)$

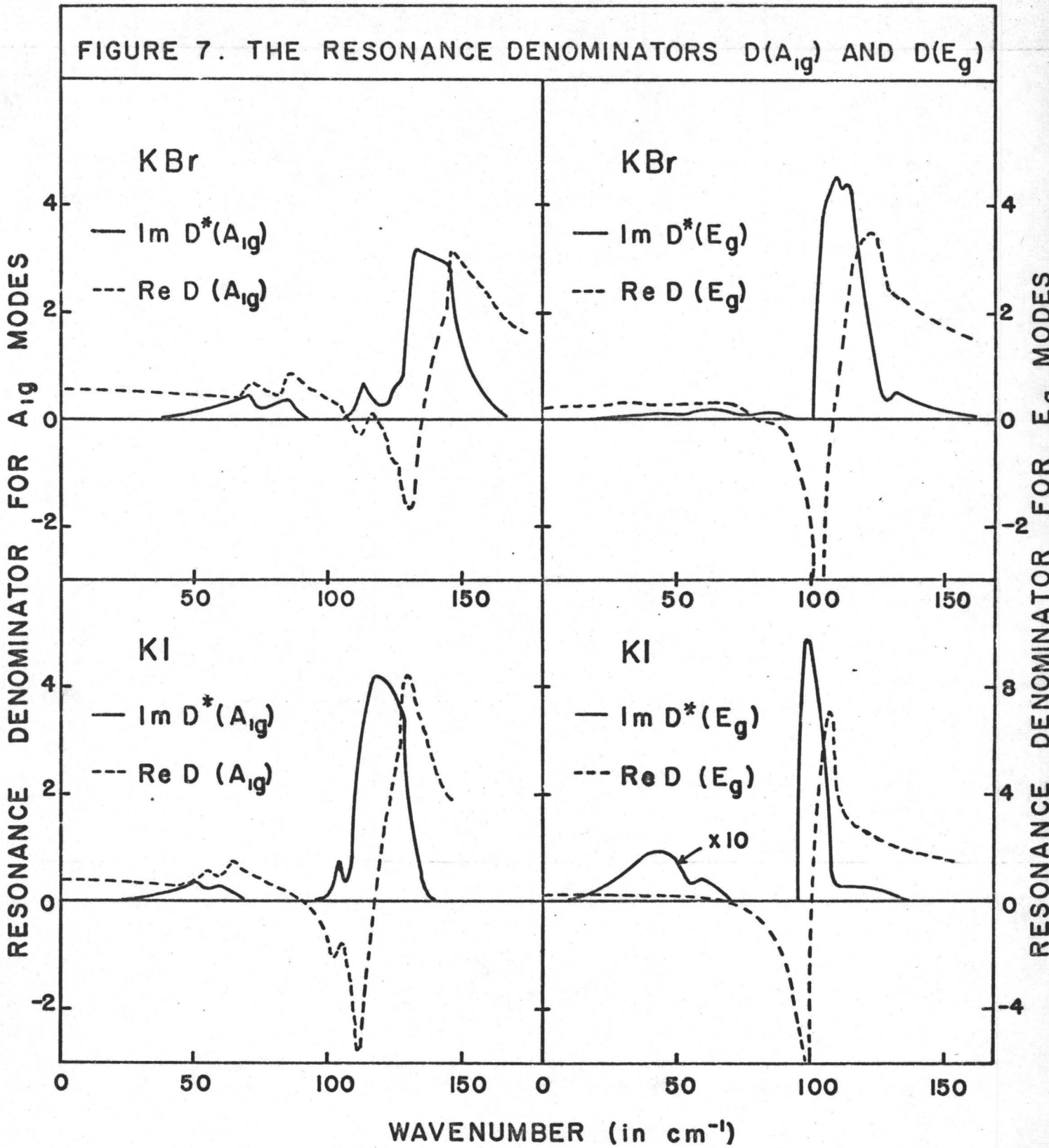

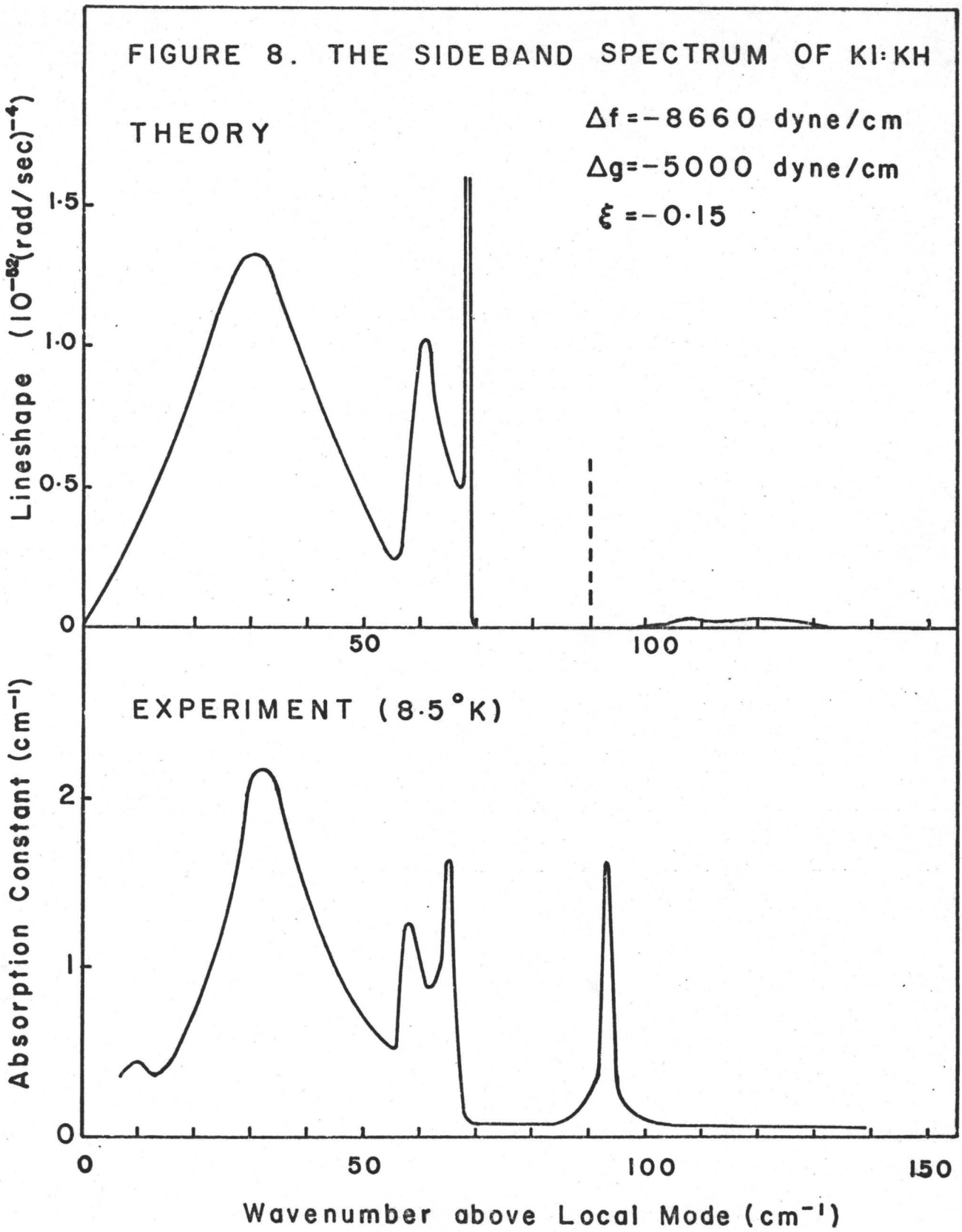

FIGURE 8. THE SIDEBAND SPECTRUM OF KI:KH

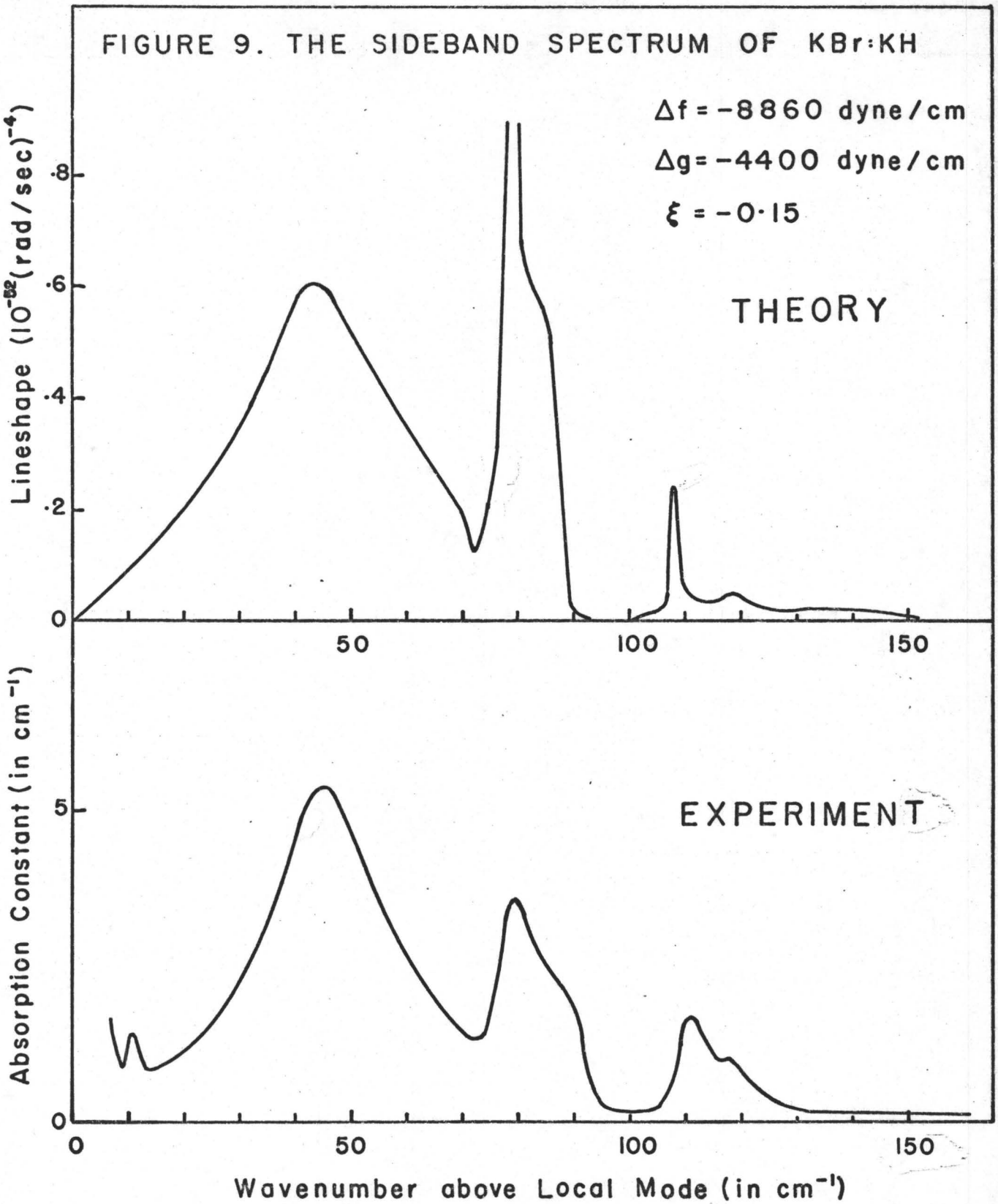
FIGURE 9. THE SIDEBAND SPECTRUM OF KBr:KH
Δf = -8860 dyne/cm
Δg = -4400 dyne/cm
ξ = -0·15
THEORY
Lineshape (10^{-82}(rad/sec)$^{-4}$)
·8
·6
·4
·2
0
50
100
150
EXPERIMENT
Absorption Constant (in cm^{-1})
5
0
0
50
100
150
Wavenumber above Local Mode (in cm^{-1})

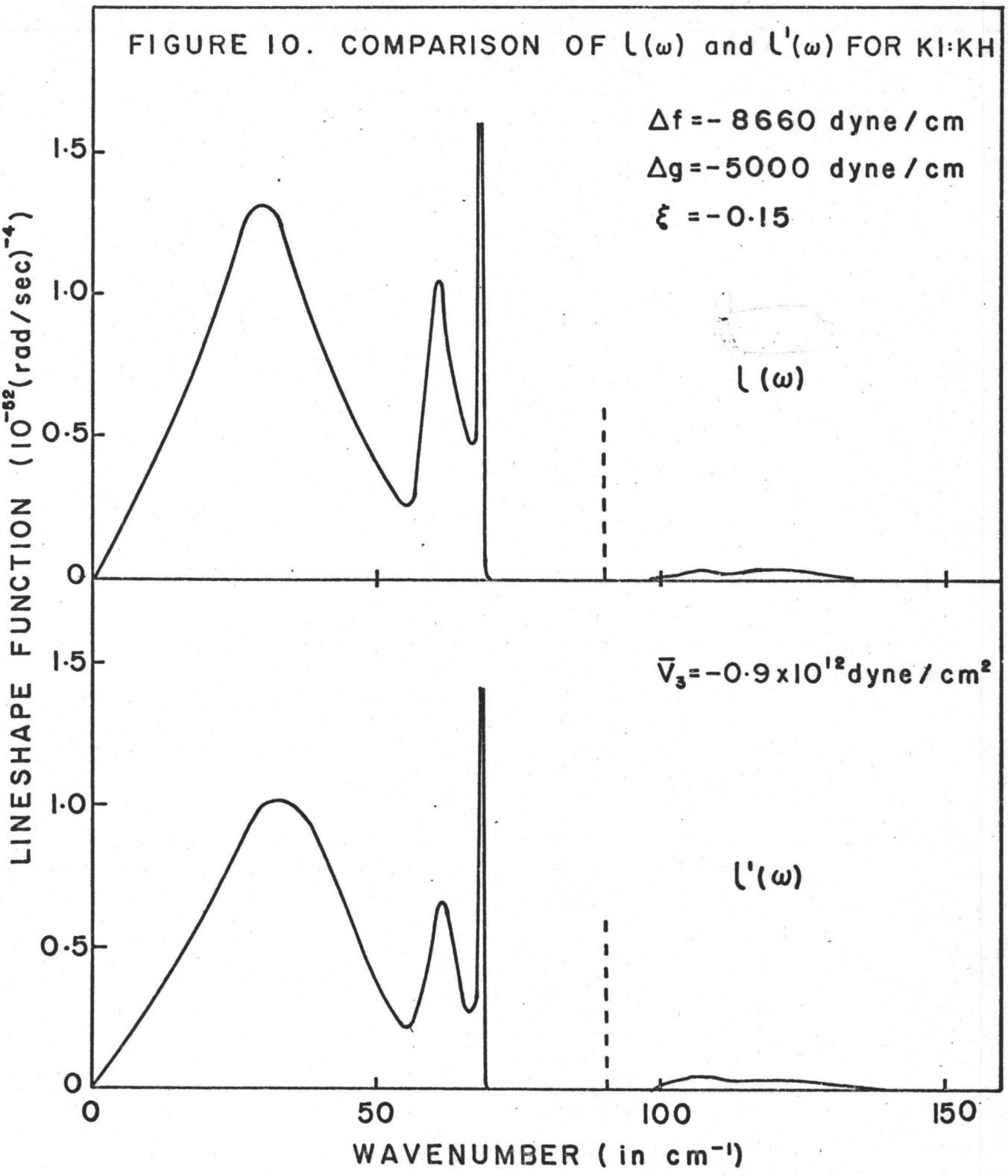
FIGURE 10. COMPARISON OF L(ω) and L'(ω) FOR KI:KH
Δf = - 8660 dyne / cm
Δg = - 5000 dyne / cm
ξ = - 0·15
L (ω)
$\bar{V}_3 = -0{\cdot}9 \times 10^{12}$ dyne / cm²
L'(ω)
LINESHAPE FUNCTION (10^{-52} (rad/sec)$^{-4}$)
1·5
1·0
0·5
0
0
50
100
150
WAVENUMBER (in cm^{-1})

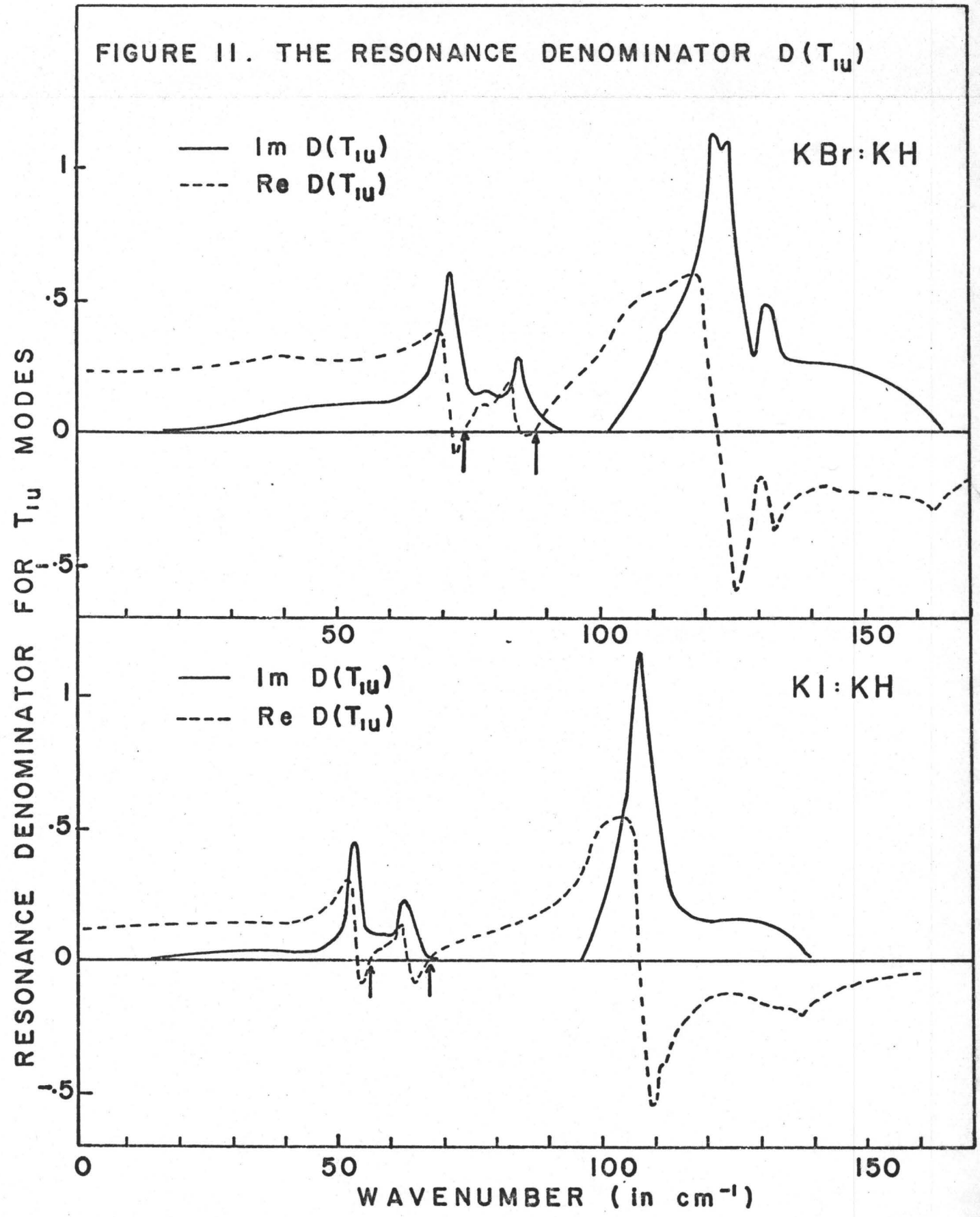
FIGURE II. THE RESONANCE DENOMINATOR D(T1u)
Im D(T1u)
Re D(T1u)
KBr:KH
KI:KH
RESONANCE DENOMINATOR FOR T1u MODES
1
.5
0
-.5
50
100
150
0
WAVENUMBER (in cm-1)

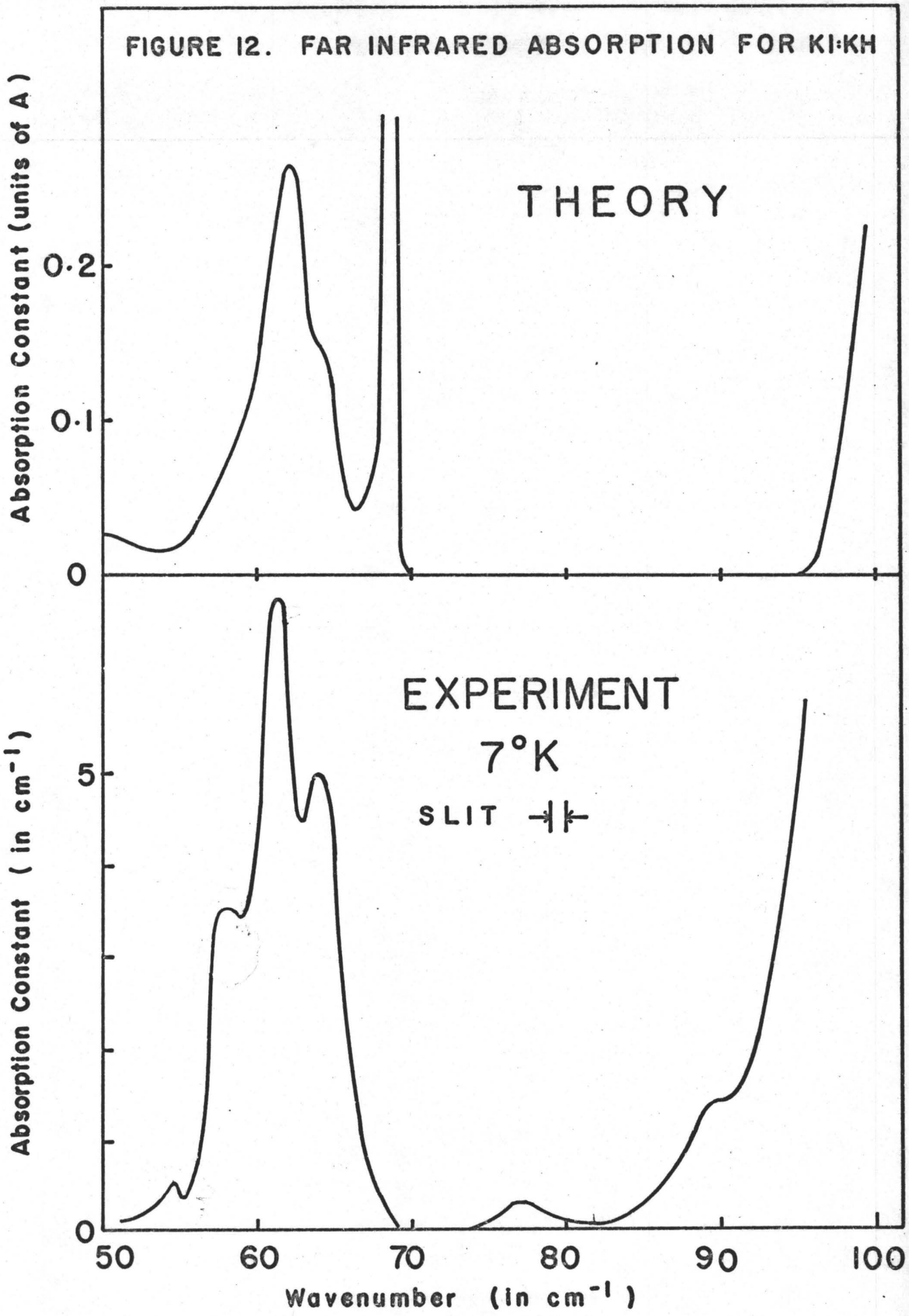
FIGURE 12. FAR INFRARED ABSORPTION FOR KI:KH
THEORY
EXPERIMENT
7°K
SLIT
Absorption Constant (units of A)
Absorption Constant (in cm⁻¹)
0·2
0·1
0
5
0
50
60
70
80
90
100
Wavenumber (in cm⁻¹)

FIGURE 13. FAR INFRARED ABSORPTION FOR KBr:KH

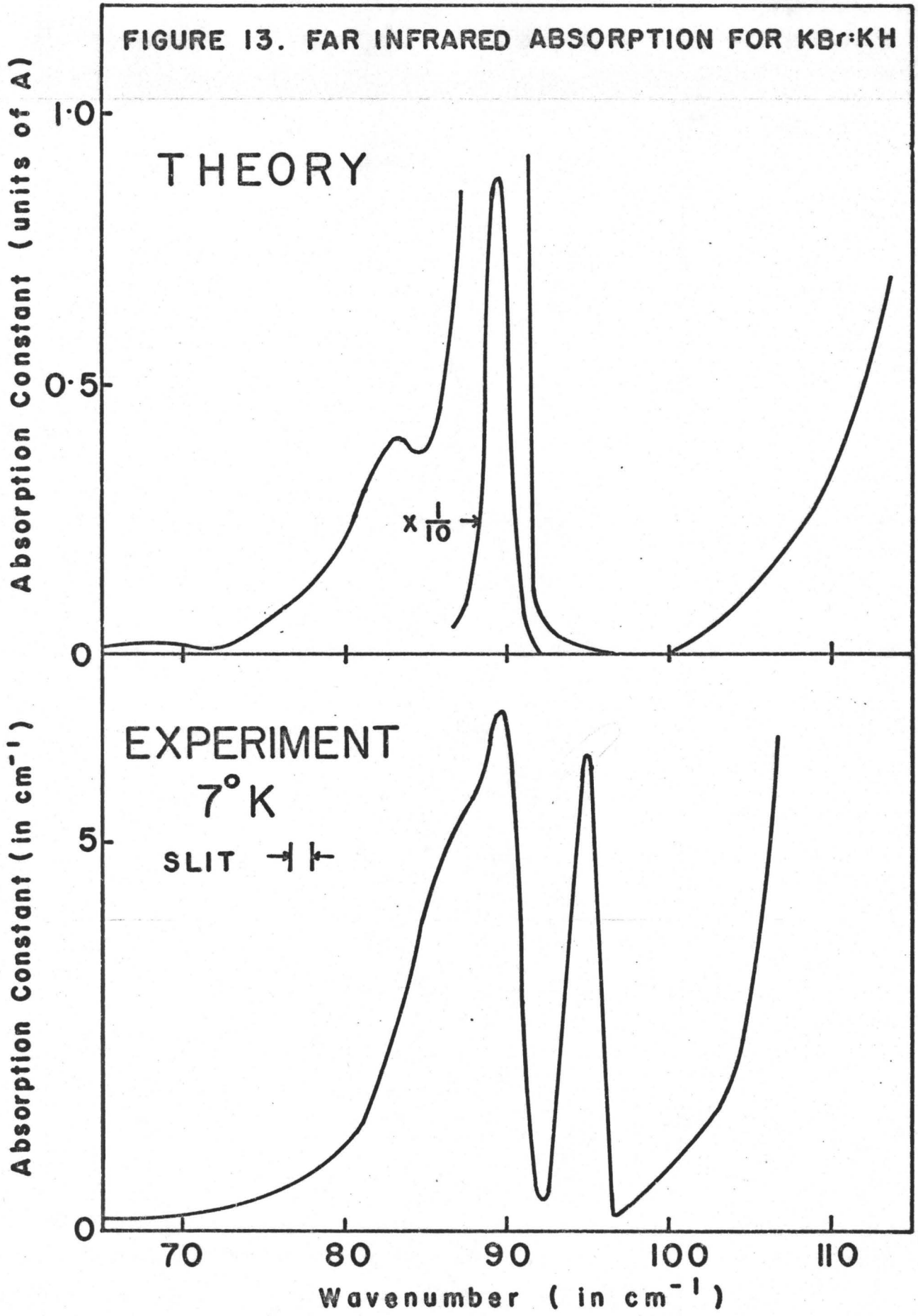

FIGURE 14. TOTAL DENSITIES OF STATES

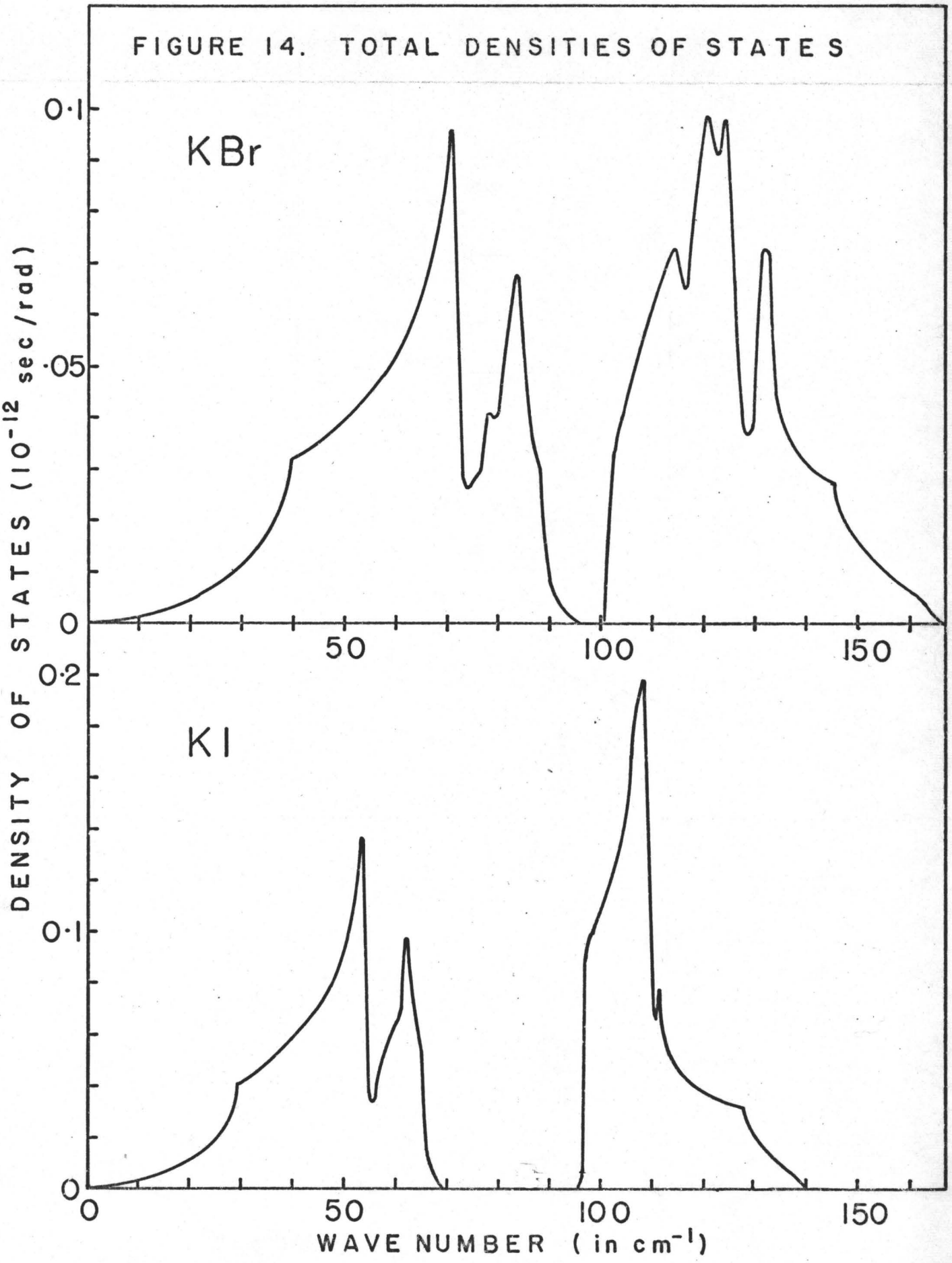

FIGURE 15. PROJECTED DENSITIES OF STATES FOR KI:KH

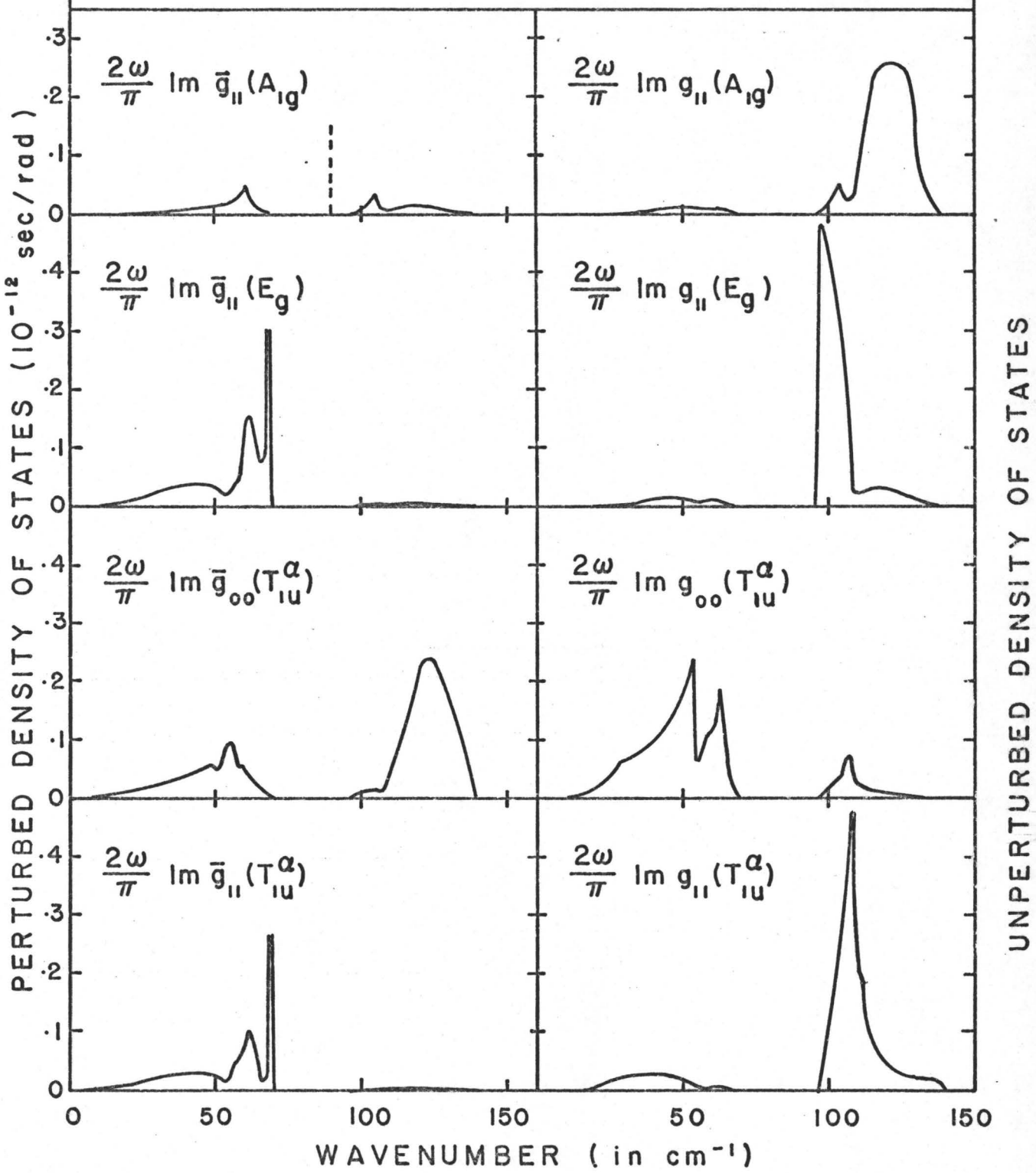

FIGURE 16. PROJECTED DENSITIES OF STATES FOR KBr:KH

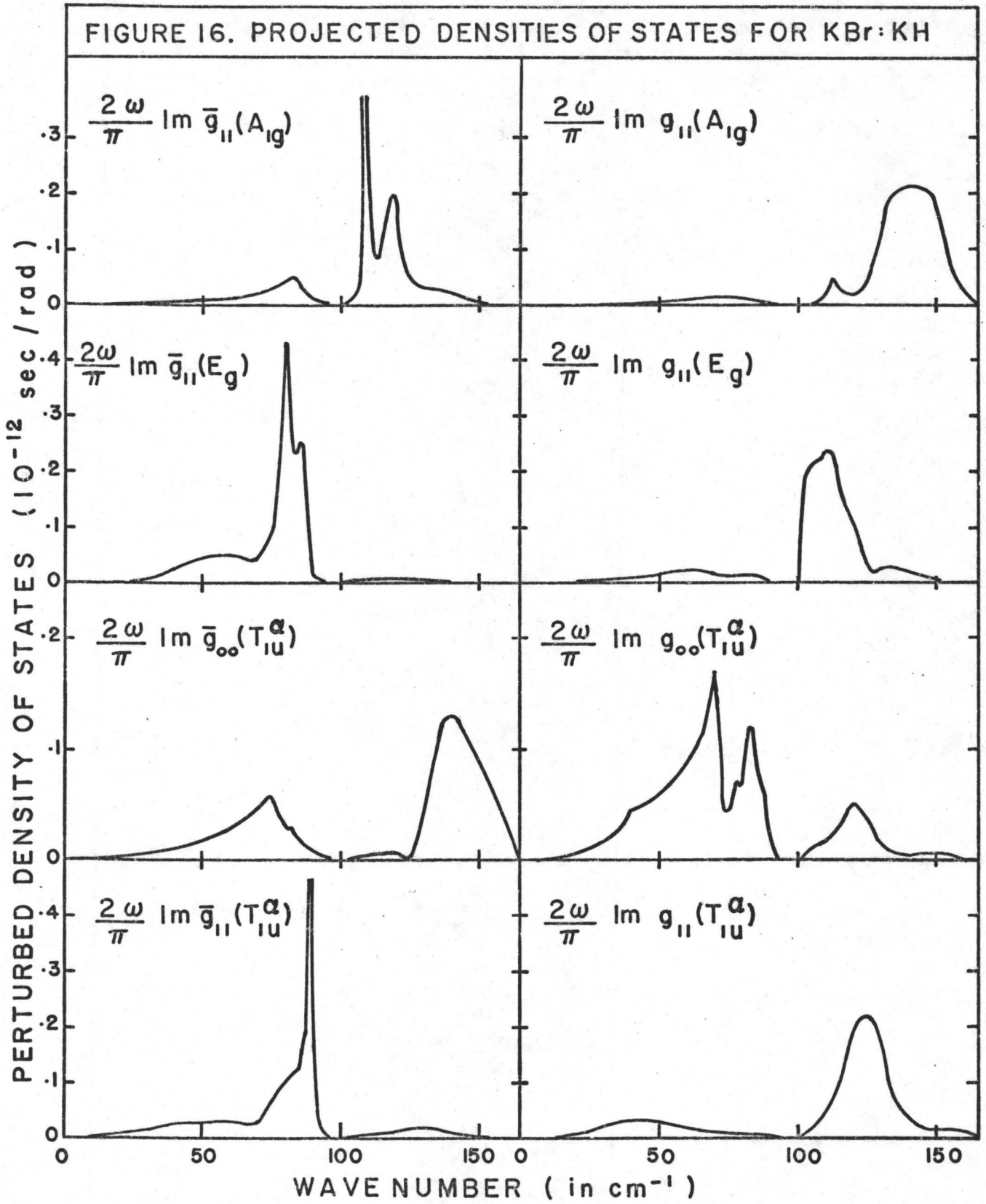

FIGURE 17. DIAGRAM CONTRIBUTING TO $M_l(p_A)$

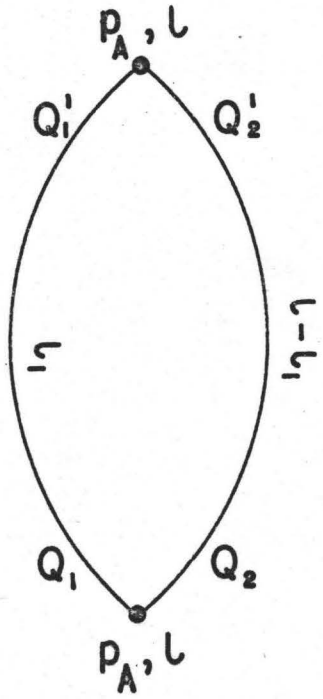

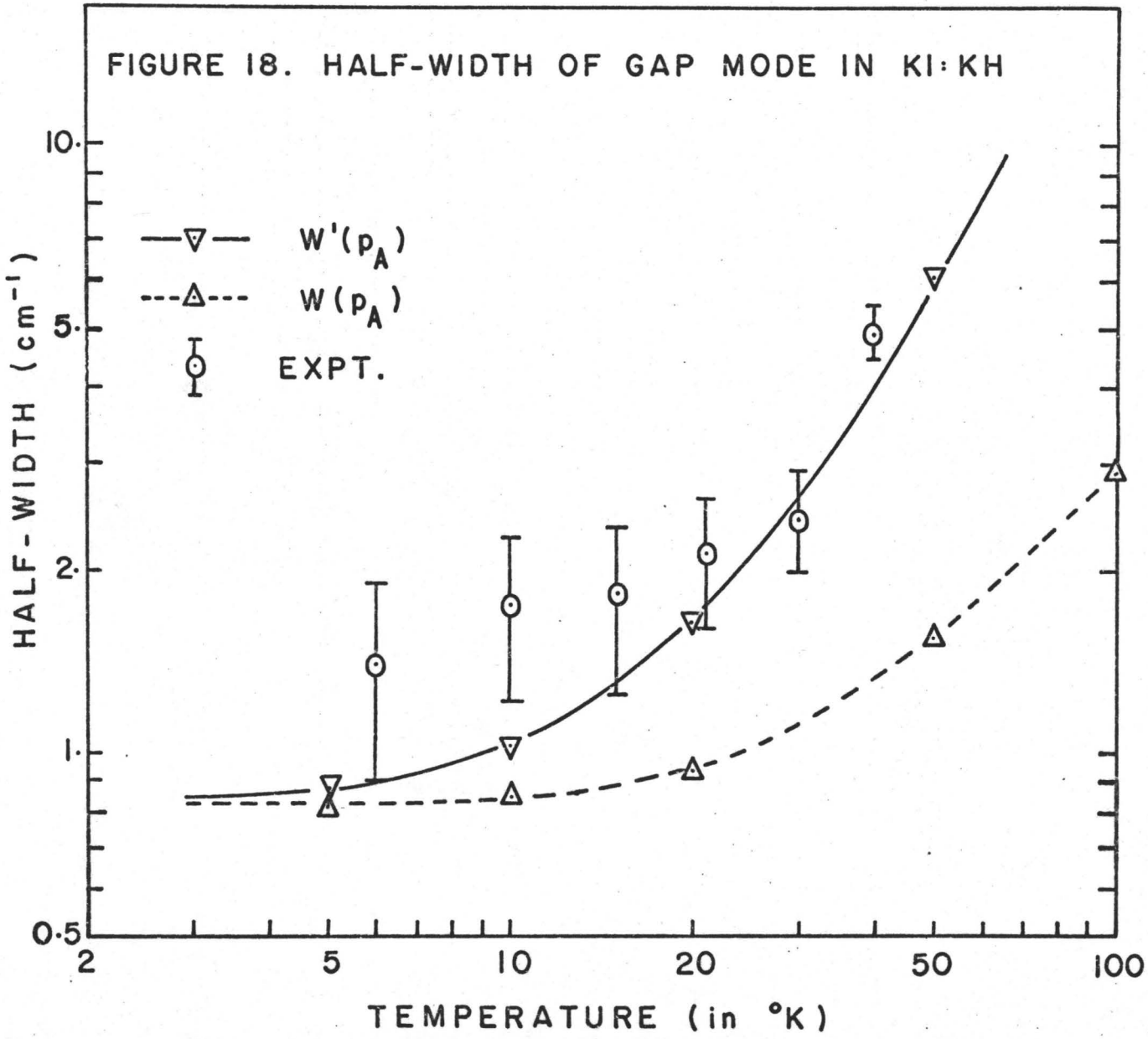
FIGURE 18. HALF-WIDTH OF GAP MODE IN KI:KH
W'(p_A)
W(p_A)
EXPT.
HALF-WIDTH (cm⁻¹)
10
5
2
1
0.5
2
5
10
20
50
100
TEMPERATURE (in °K)

FIGURE 19. DIAGRAMS CONTRIBUTING TO $M(P_x)$

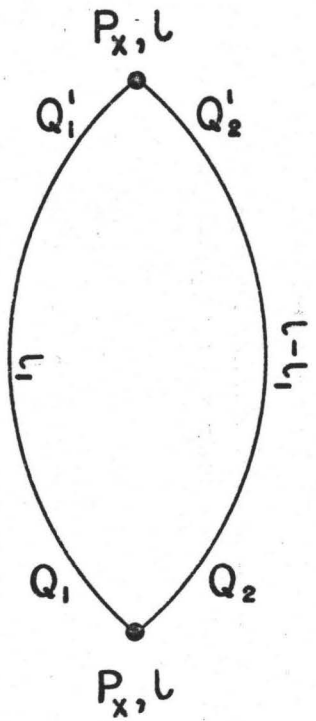

$M_l^{II}(P_x)$

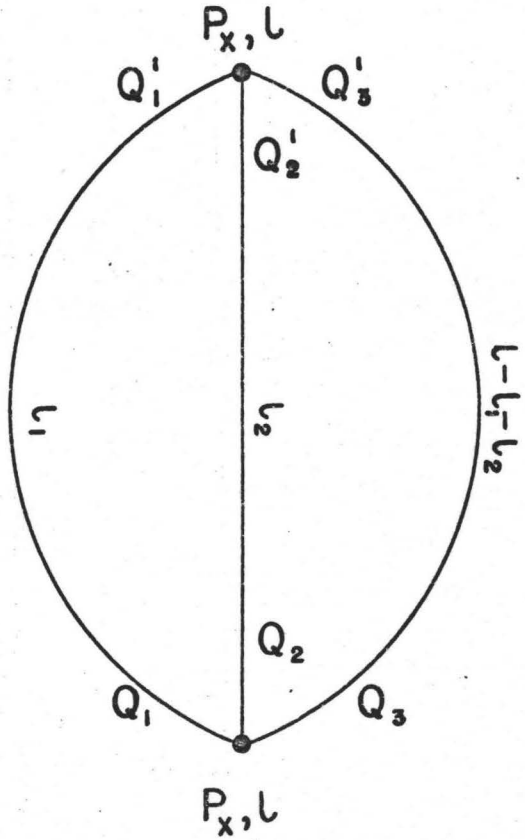

$M_l^{III}(P_x)$

FIGURE 20. THE SCATTERING MECHANISM

(a) CONTRIBUTING PROCESSES

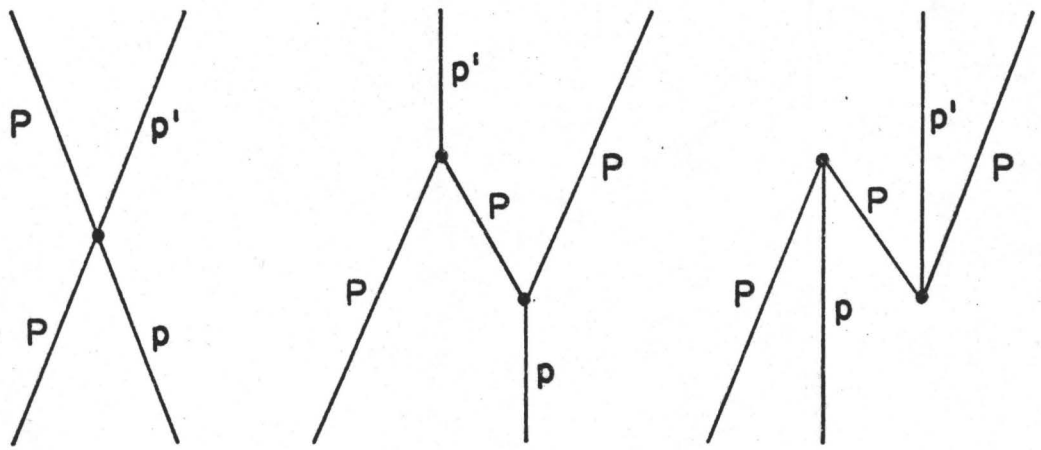

(b) DIAGRAM

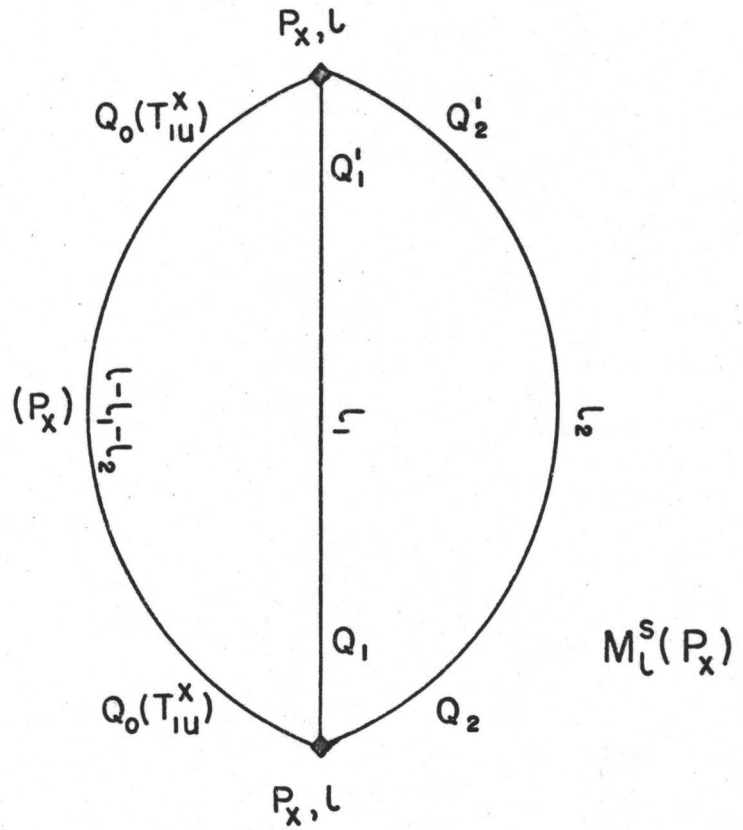

FIGURE 21. HALF-WIDTH OF U-CENTRE LOCAL MODE IN KBr

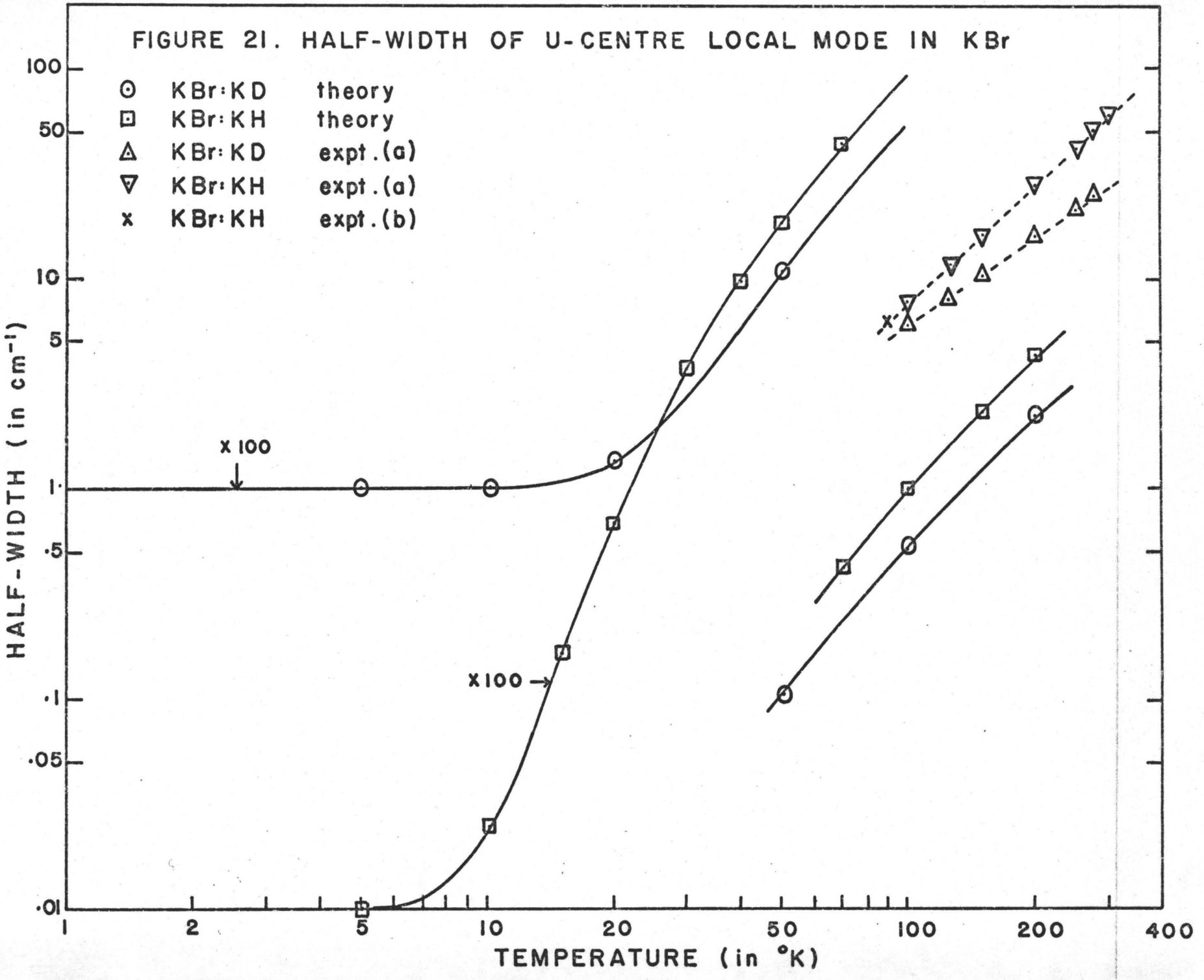

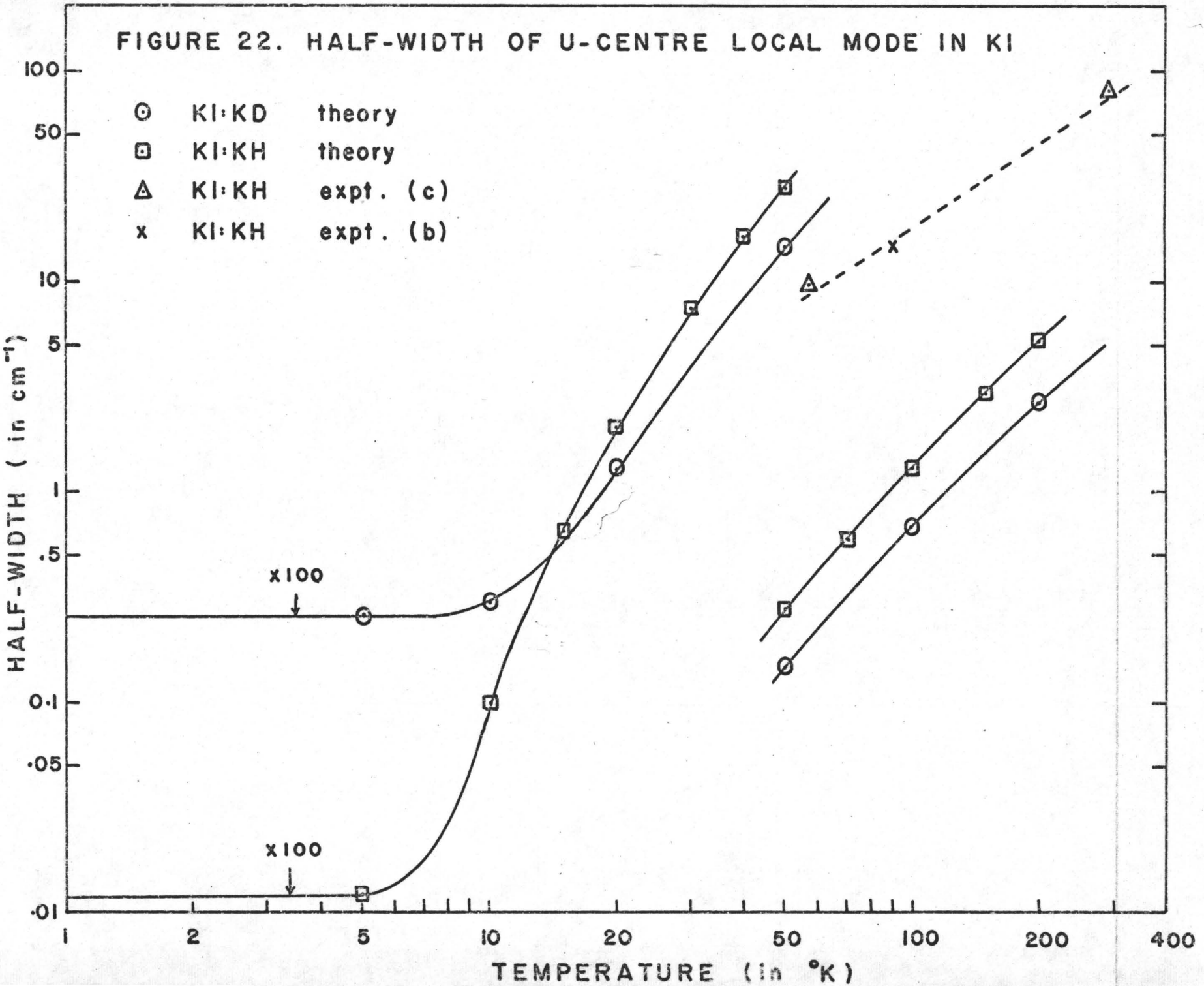
FIGURE 22. HALF-WIDTH OF U-CENTRE LOCAL MODE IN KI
KI:KD theory
KI:KH theory
KI:KH expt. (c)
KI:KH expt. (b)
HALF-WIDTH (in cm⁻¹)
100
50
10
5
1
.5
0.1
.05
.01
x100
x100
1
2
5
10
20
50
100
200
400
TEMPERATURE (in °K)